Centralised Offshore Hydrogen Production

Techno-Economic Optimisation and Assessment of the Benefit of Aggregated Power Supply

MSc Thesis Sustainable Energy Technology

Simon Hammecher

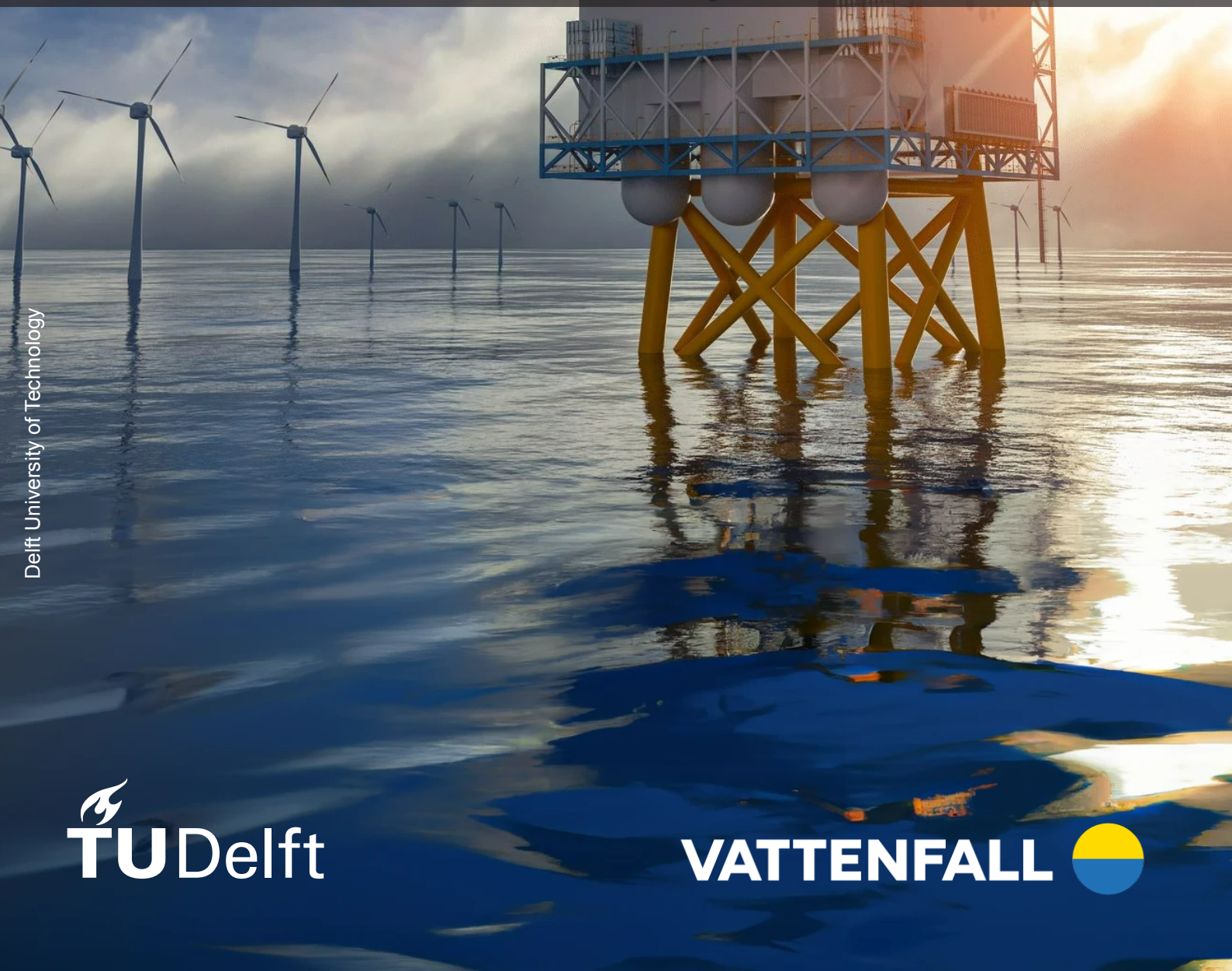

Delft University of Technology

TU Delft

VATTENFALL

Centralised Offshore Hydrogen Production
Techno-Economic Optimisation and Assessment of the Benefit of Aggregated Power Supply

by

Simon Hammecher

Simon Hammecher 4499565

Supervisor:	Dr. ir. M. Zaayer (Committee)
Vattenfall Supervisors:	ir. P. J. M. Bussemakers (Committee)
	ir. O. Partenie
Institution:	Delft University of Technology
Place:	Faculty of Electrical Engineering, Mathematics and Computer Science, Delft

Cover Image: Taken and adapted from [1]

TU Delft

VATTENFALL

Acknowledgements

I gratefully acknowledge the support and guidance of my supervisors, Michiel Zaayer from the TU Delft, and Matthijs Bussemakers and Octavian Partenie from Vattenfall, who have made this thesis possible. Their mentorship, devotion, and feedback have been invaluable in enriching my knowledge of hydrogen and offshore wind energy.

Michiel, your guidance throughout the project and the feedback on my work and report were phenomenal. You were always available to discuss new ideas and help me along the way during the research. Your feedback on my report was very elaborate and helped me structure my story. I learned a lot from you.

Octavian, I would like to express my sincere appreciation for initially taking up this challenge with me. I have great memories of our conversations, both about hydrogen and our other many shared interests. I want to thank you for all the insights you have given me into the world of hydrogen. I learned a lot from you.

Matthijs, thank you for taking over halfway through the project. Together we made great strides in a world that was still unknown to you. Your critical feedback pushed me to think beyond my boundaries and has been instrumental in this process. I will remember the pleasant time we had in the office and our games of table football. I learned a lot from you.

I would like to thank Dominic von Terzi and Ad van Wijk for participating in the Thesis Committee, and I want to thank Wim Bierbooms for being present feedback during the midterm presentation.

Furthermore, I would like to extend my gratitude to all of my colleagues at Vattenfall, particularly the System Design team, who made this a memorable and exciting time. I am especially grateful to Mads, Kenneth, Georgios, Robin, Ernst, Jan-Willem, Peter, Petr, Hans, Micheal, Søren, Simon and Emile for their input on the techno-economic model, and to Jason and Carlos for their input on the dynamic model. Furthermore, I would like to thank Þorkell and Helena for their endless time for discussions.

Finally, I want to acknowledge the unwavering love and support of my friends, family, and Willemijn, who have been a constant source of encouragement. I am deeply grateful for your support, which has been my driving force throughout my academic and personal career.

Simon Hammecher
Amsterdam, March 2023

Abstract

Green hydrogen is expected to play a crucial role in the energy transition as it can be utilised for both storage purposes and as fuel for hard-to-abate sectors. One of the possible configurations for producing green hydrogen is by means of a central offshore hydrogen production platform powered by offshore wind energy. Producing hydrogen offshore facilitates the possibility to eliminate parts of the expensive electrical infrastructure present in conventional offshore wind farms and could result in lower losses.

In collaboration with Vattenfall, this study provides a thorough examination of centralised offshore hydrogen production. The study addresses both the techno-economic feasibility of the centralised configuration and the effects of aggregating the power supplied by individual offshore wind turbines.

In Part I, the study presents a comprehensive techno-economic analysis of different electrolysis technologies, the optimal hydrogen production unit capacity, and compressor output pressure. The outcomes reveal that an optimal levelised cost of hydrogen can be achieved by reducing the hydrogen production unit capacity compared to the offshore wind farm capacity. Moreover, increasing the hydrogen pressure above the minimum pressure required to overcome the pipeline pressure drop, reduces the levelised cost of hydrogen further. The study reveals a small preference for hydrogen production based on proton exchange membrane electrolysis, in comparison to hydrogen production based on alkaline electrolysis.

In Part II, the focus is shifted towards hydrogen production solely, influenced by power fluctuations. By using historical offshore wind turbine power output data, it was found that aggregating the power output significantly reduces the normalised power output fluctuations, compared to a decentralised offshore configuration. However, the reduced power fluctuations did not result in a higher hydrogen yield, attributed to the inter-array cable losses of the centralised configuration. Nevertheless, a significant reduction in the number of switches of operational mode and the number of turn-offs of the stacks was observed. Reducing the number of switches and turn-offs will reduce the process of stack degradation.

The study concludes that centralised offshore hydrogen production facilitates the possibility to produce hydrogen at a competitive levelised cost of hydrogen. Furthermore, the reduction of the power fluctuations will benefit this configuration due to the deceleration of the stack's degradation process.

Contents

Preface i

Abstract ii

Nomenclature vii

List of symbols ix

Glossary xi

List of Figures xii

List of Tables xiv

1 Introduction 1
- 1.1 Background . . . 1
- 1.2 Problem analysis . . . 3
- 1.3 Research question and sub-research questions . . . 3
- 1.4 Methodology . . . 3
  - 1.4.1 Techno-economic analysis . . . 4
  - 1.4.2 Dynamic analysis . . . 4
- 1.5 Report outline . . . 4

2 System description and component selection 6
- 2.1 Wind turbines and wind farm description . . . 7
  - 2.1.1 Conventional offshore wind farm . . . 7
  - 2.1.2 Dedicated offshore wind farm . . . 7
- 2.2 Electrolyser description and selection . . . 8
  - 2.2.1 Electrolyser introduction and selection criteria . . . 8
  - 2.2.2 Direct seawater electrolysis . . . 9
  - 2.2.3 Alkaline Electrolysis . . . 9
  - 2.2.4 Proton Exchange Membrane Electrolysis . . . 10
  - 2.2.5 Solid Oxide Electrolysis . . . 10
  - 2.2.6 Anion exchange membrane electrolysis . . . 11
  - 2.2.7 Conclusion on electrolyser technologies . . . 11
- 2.3 Electrical equipment description . . . 12
- 2.4 Water treatment equipment description . . . 12
  - 2.4.1 Water pumps . . . 13
  - 2.4.2 Desalination . . . 13
  - 2.4.3 Deionization . . . 13
- 2.5 Gas conditioning equipment description . . . 13
- 2.6 Compressors description . . . 14
- 2.7 Superstructure description . . . 14
- 2.8 Substructure description . . . 15
- 2.9 Foundation description . . . 15
- 2.10 Hydrogen transmission description . . . 15
- 2.11 Transport, installation and commissioning description . . . 16
  - 2.11.1 Substructure installation . . . 16
  - 2.11.2 Foundation installation . . . 16
  - 2.11.3 Topside transport and installation . . . 16
  - 2.11.4 Commissioning . . . 16
  - 2.11.5 Decommissioning . . . 17

2.12 Other activities description . . . 17
2.13 Overview of preliminary design choices . . . 17

I Techno-economic analysis 18

3 Model set-up and modelling 19
3.1 Techno economic model overview . . . 19
3.2 Economic modelling . . . 20
3.2.1 Levelized costs of hydrogen . . . 20
3.2.2 Net present value . . . 20
3.2.3 Economies of unit scale . . . 21
3.3 Hydrogen production modelling . . . 21
3.3.1 Model type choice . . . 21
3.3.2 Hydrogen production model . . . 21
3.4 Wind farm modelling . . . 24
3.4.1 Offshore wind farm performance . . . 24
3.4.2 Offshore wind farm costs . . . 24
3.4.3 Offshore wind farm model constants . . . 24
3.5 Stack modelling . . . 25
3.5.1 Stack performance . . . 25
3.5.2 Stack costs and mass . . . 26
3.5.3 Stack model constants . . . 27
3.6 Electrical equipment modelling . . . 27
3.6.1 Electrical equipment performance . . . 27
3.6.2 Electrical equipment costs and mass . . . 28
3.6.3 Electrical equipment model constants . . . 28
3.7 Water treatment modelling . . . 28
3.7.1 Sea water pumps performance . . . 29
3.7.2 Desalination and deionization performance . . . 29
3.7.3 Water treatment costs . . . 30
3.7.4 Water treatment model constants . . . 30
3.8 Gas conditioning equipment modelling . . . 30
3.8.1 Gas conditioning equipment performance . . . 30
3.8.2 Gas conditioning costs . . . 31
3.8.3 Gas conditioning model constants . . . 31
3.9 Compressor modelling . . . 31
3.9.1 Compressor performance . . . 31
3.9.2 Compressor costs and mass . . . 32
3.9.3 Compressor model constants . . . 32
3.10 Superstructure modelling . . . 32
3.10.1 Superstructure costs and mass . . . 33
3.10.2 Superstructure model constants . . . 33
3.11 Substructure modelling . . . 33
3.11.1 Substructure costs and mass . . . 34
3.11.2 Substructure model constants . . . 35
3.12 Foundation modelling . . . 36
3.13 Hydrogen transmission modelling . . . 37
3.14 Transport, installation and commissioning modelling . . . 38
3.14.1 Transport modelling . . . 39
3.14.2 Installation modelling . . . 39
3.14.3 Commissioning modelling . . . 40
3.14.4 Decommissioning . . . 40
3.14.5 Transport, installation and commissioning model constants . . . 40
3.15 Other CAPEX modelling . . . 41

4 Case study, results and discussion **43**
4.1 Background case study . . . 43
4.1.1 Maritime condition . . . 43
4.1.2 Wind conditions and wind farm power curve . . . 44
4.1.3 Other case parameters . . . 45
4.2 Preliminary sizing results . . . 45
4.2.1 Optimum hydrogen production . . . 46
4.2.2 Optimum cost . . . 47
4.2.3 Optimum mass . . . 49
4.2.4 Optimum levelised cost of hydrogen . . . 50
4.2.5 optimum NPV . . . 51
4.3 Optimal compressor output pressure . . . 52
4.4 Analysis at optimal installed capacity . . . 55
4.4.1 Hydrogen production . . . 55
4.4.2 Costs . . . 56
4.5 Sensitivity analysis . . . 57
4.5.1 Sensitivity of obtained LCOH PEME-based system . . . 58
4.5.2 Sensitivity of obtained LCOH system AE-based system . . . 59
4.5.3 Sensitivity of obtained sizing PEME-based system . . . 60
4.5.4 Sensitivity of obtained sizing AE-based system . . . 61
4.6 Uncertainty analysis . . . 61
4.7 Discussion Part I . . . 62
4.7.1 Optimal HPU capacity . . . 62
4.7.2 Statistical model . . . 63
4.7.3 Mass data . . . 63
4.7.4 Transport and installation . . . 63
4.7.5 Assumed lifetime . . . 63
4.7.6 Assumed dynamic response . . . 63
4.8 Summary Part I . . . 63

II Dynamic analysis **65**

5 Power fluctuations theoretical background **66**
5.1 Power fluctuations and hydrogen production . . . 66
5.2 Fluctuations of wind turbines output power . . . 66
5.3 Power fluctuations in large offshore wind farms . . . 67
5.4 Time-series model description . . . 69
5.4.1 Electrolyser operation state . . . 69
5.4.2 Model assumptions . . . 70
5.5 Model modification for centralised production . . . 70
5.5.1 Efficiency curve . . . 70
5.5.2 Start up time and down time . . . 71
5.5.3 Inter-array cable losses . . . 72
5.6 Applied control strategy . . . 72

6 Case study, Results and Discussion **74**
6.1 Specific wind farm . . . 74
6.2 Specific data set . . . 75
6.3 Time-series data preparation . . . 75
6.3.1 Gabs in received data . . . 75
6.3.2 Difference in sampling interval . . . 75

6.4 Power output analysis . . . 76
6.5 System operation results . . . 80
6.5.1 Time-series visualisation . . . 81
6.5.2 Hydrogen production . . . 83
6.5.3 Switching operational modes . . . 84
6.5.4 Turn-offs . . . 85
6.6 Discussion . . . 85
6.6.1 Centralised integrated system . . . 85
6.6.2 Energy storage element . . . 86
6.6.3 Data set choice . . . 86
6.7 Summary Part II . . . 86

7 Conclusion and recommendations 88
7.1 Conclusion . . . 88
7.2 Recommendations . . . 89

References 96

A Appendix Techno-economic analysis 97
A.1 Cost modelling superstructure . . . 97
A.1.1 Topside primary steel . . . 97
A.1.2 Topside grating . . . 97
A.1.3 Cladding . . . 98
A.1.4 Topside coating . . . 98
A.1.5 Total topside structure . . . 98
A.1.6 Data input . . . 98
A.2 Total CAPEX and OPEX curves . . . 99
A.3 LCOH curve per technology . . . 99
A.4 Monte-Carlo method . . . 101

B Times series appendix 102
B.1 Original lay-out offshore wind farm . . . 102
B.2 Distance inter-array cable sections . . . 103
B.3 Output per wind turbine . . . 104

Nomenclature

Abbreviation	Meaning
AC	Alternating current
AE	Alkaline electrolysis
AEME	Anion exchange membrane electrolysis
AG	Air gab
AHP	Annual hydrogen production
CAPEX	Capital expenditure
COHP	Centralised offshore hydrogen platform
COM	Compressor
DC	Direct current
DI	Deionization
DSE	Direct seawater electrolysis
EEQ	Electrical equipment
ELE	Electrolyser stacks
OEL	End of life
EPCm	Engineering, Procurement, Construction and management
FLH	Full load hours
GCE	Gas conditioning equipment
HER	Hydrogen evolution equation
HHV	Higher heating value
HLV	Heavy lifting vessel
HPU	Hydrogen production unit
HVAC	Heating, ventilation and air conditioning
IAC	Inter-array cables
LCOH	Levelised cost of hydrogen
LV	Low voltage
MEA	membrane-electrode assembly
MV	Medium Voltage
NPV	Net present value
OER	Oxygen evolution reaction
OPEX	Operational expenditure
OWF	Offshore wind farm

PEME	Proton exchange membrane electrolysis
PS	Primary steel
RO	Reverse osmosis
SOE	Solid oxide electrolyser
SOL	Start of life
SoP	State of performance
SLR	Sea level rise
SP	Selling price
SS	Storm surge
ST	Settlement depth
SSCV	Semi-Submersible crane vessel
TIC	Transport, installation, and commissioning
WACC	Weighted average cost of capital
WC	Wave crest
WTE	Water treatment equipment
WTG	Wind turbine generator

List of symbols

Symbol	Definition	unit
A	Surface	[m^2]
A	Availability	[%]
c	Specific costs	[€/unit]
C	CAPEX	[€]
f_{OPEX}	OPEX factor	[-]
g	Gravitational constant	[m/s^2]
h	Water head	[m]
I	Current	[A]
k	Specific mass	[kg/kg]
L_t	Life time	[Years]
m	Mass	[kg]
M_W	Molecular weight	[g/mol]
n_{rep}	Number of replacements	[-]
n_{stage}	Number of stages	[-]
n_{trips}	Number of trips	[-]
$\dot{m}$	Mass flow	[kg/s]
O_t	Operational time	[h]
p	Specific power	[W/W]
P_e	Electrolyser capacity	[W]
P	Pressure	[Bar]
P_i	Instantaneous power	[W]
P_r	Installed capacity	[W]
P_{pump}	Pump power rating	[W]
Q	Quantity	[W]
r	Compression ratio	[-]
R	Recovery rate	[%]
R	Resistance	[Ω]
S_f	Scaling factor	[-]
T	Temperature	[K]
V	Volume	[m^3]
Z	Compressibility factor	[-]

δ	Degradation	[-]
γ	Specific heat ratio	[-]
η_{ELE}	Stack efficiency	[-]
η_m	Mechanical compressor efficiency	[-]
η_n	Isentropic compressor efficiency	[-]
η_{OWF}	Conversion efficiency	[-]
μ	Friction factor	[-]
ρ	Density	[kg/m^3]
σ_{cool}	Cooling requirement	[kg/kg]

Glossary

A variety of terms is used to refer to groupings of components and aspects throughout the report. The following section elaborates on which components are grouped and their respective name. Attempts are made to use terminology that appeals to readers imagination.

Hydrogen production unit
The hydrogen production unit (HPU) consits of all components directly related to the production and processing of hydrogen at the platform. This therefore exists out of the water pumps, desalination and deionization equipment, electrical equipment, electrolyser stacks, gas conditioning equipment, and compressors.

Centralised offshore hydrogen platform
The centralised offshore hydrogen platform (COHP) consists out of the all hydrogen production unit equipment, together with the superstructure, substructure and foundation.

Hydrogen transmission system
Once the hydrogen is produced at the platform, the hydrogen will be transported to shore. This is done using the hydrogen transmission system.

Dedicated offshore wind farm
The dedicated wind farm refers to all the components needed to supply electricity to the centralised offshore hydrogen platform. This includes the turbines with all internal equipment and the inter array cables.

Offshore wind-hydrogen system
The wind-hydrogen system refers to all components needed to convert the incoming wind speed, to delivering hydrogen to shore. These are the dedicated offshore wind farm, the centralised offshore hydrogen platform and the hydrogen transmission system.

Offshore wind-hydrogen project
The offshore hydrogen project refers to the total energy system, the installation of the centralised offshore hydrogen platform and the other non-material project aspects.

List of Figures

1.1 Onshore (left), centralised offshore (center), and decentralised offshore (right) hydrogen production. . . . 1
1.2 LCOH for different scenarios over time. Adopted from [16]. . . . 2
1.3 Graphical readers guide. The two parts are presented in grey, and the recommended readings are in blue. . . . 5

2.1 Overview of an offshore wind hydrogen system and project aspects. . . . 6
2.2 Schematic representation of a conventional wind farm. . . . 7
2.3 Schematic representation of an offshore wind-hydrogen system. . . . 7
2.4 Efficiency curve of a PEME-based system, taken from [24]. . . . 9
2.5 Simplified electrical infrastructure of the COHP . . . 12
2.6 Simplified water infrastructure of the COHP for both a PEME-based (top) and AE-based system (bottom). . . . 13

3.1 Visualisation of the relations of all system components and project aspects. . . . 20
3.2 Flowchart used to determine hydrogen production per wind speed bin, ovals represent inputs and outputs, squares represent actions and diamonds represent logic. . . . 23
3.3 Visualisation of the state of performance of the stacks over time, for different replacement strategies. AE-based system at HPU capacity of 950 MW. . . . 26
3.4 Pipeline diameter versus hydrogen pressure. . . . 37
3.5 Transmission CAPEX for different output pressures. . . . 38
3.6 Transport and installation CAPEX for different topside and substructure masses. . . . 40

4.1 Intended location. . . . 43
4.2 Representation of a wind farm power curve and wind speed distribution, provided by Vattenfall. . . . 44
4.3 Load duration curve of the offshore wind farm. . . . 45
4.4 Annual load duration curves of the COHP for different installed HPU capacities. . . . 46
4.5 Annual hydrogen production per installed HPU capacity for a PEME- and AE-based system 47
4.6 Total and specific CAPEX for a PEME- and AE-based system over installed HPU capacities for a 60 bar compressor output pressure. . . . 48
4.7 Total and specific COHP OPEX for a PEME- and AE-based system over installed HPU capacities. . . . 49
4.8 Mass of the topside and substructure for the PEME- and AE-based system. . . . 49
4.9 LCOH curves with 10 percent CAPEX difference. . . . 50
4.10 NPV of a PEME-based system for different assumed hydrogen selling prices. . . . 51
4.11 NPV of an AE-based system for different assumed hydrogen selling prices. . . . 52
4.12 LOCH for a PEME-based system versus installed HPU capacity and compressor output pressure. . . . 53
4.13 LOCH for a PEME-based system versus installed HPU capacity and compressor output pressure. . . . 54
4.14 Annual hydrogen production of both technologies. The minimum amount of stack replacements. . . . 55
4.15 CAPEX of all COHP project aspects of both the PEME- and AE-based system at optimal installed HPU capacity. . . . 56
4.16 Breakdown of the OPEX . . . 57
4.17 Tornado LCOH sensitivity chart of the main categories of a PEME-based system. . . . 59
4.18 Tornado LCOH sensitivity chart of the main categories of an AE-based system. . . . 59
4.19 Tornado sizing sensitivity chart of the main categories of a PEME-based system. . . . 60

4.20 Tornado sizing sensitivity chart of the main categories of an AE-based system. 61
4.21 PEME- and AE- based system Monte Carlo Method simulation. Based on an input variance of $\pm 10\%$. 100.000 simulations for both technologies. 62

5.1 Van der Hoven Spectrum (1957) as drawn by Alan Davenport. Taken and adapted from [84]. 67
5.2 Normalised wind turbine power output versus wind speed. Made with historical data provided by Vattenfall. 68
5.3 Time series power output of an individual wind turbine versus offshore wind farm. 68
5.4 Efficiency curve of the centralised and decentralised configuration. 71
5.5 Power losses in inter-array cable sections. Distances between wind turbines and COHP are not proportional. 72

6.1 Time-series of the individual power output of four wind turbines of the offshore wind farm between 14 and 16 October 2022. 75
6.2 Visualisation of sampling at Nyquist rate (left) and the selected rate of 1 Hz. (right) . . . 76
6.3 Normalised power fluctuation of an individual wind turbine (blue) and the offshore wind farm (yellow) for a 1-minute, 5-minute, and 10-minute average power output. The number of fluctuations decreases as result of increases in averaging time of the output power. 77
6.4 Maximum fluctuation versus number of wind turbines for different time-steps. Data created using 5.000 combinations of wind turbines. 79
6.5 Standard deviation of normalised power fluctuations versus number of wind turbines for different time-steps. Data created using 5.000 combinations of wind turbines. 79
6.6 Incoming power profile (top), power consumption per electrolyser (middle), and operational mode (bottom) for a decentralised configuration. Power rating on y-axis left out intentionally due to confidentiality. 81
6.7 Incoming power profile (top), power consumption per module (middle), and operational mode (bottom) for decentralised configuration. Power rating on y-axis left out intentionally due to confidentiality. 82
6.8 Total hydrogen production for the centralised and decentralised configuration for different control strategies. 83
6.9 Number of operational switches for the centralised and decentralised configuration. . . 84
6.10 Number of turn-offs for the centralised and decentralised configuration. 85

A.1 CAPEX and OPEX for PEME-based and AE-based system 99
A.2 LCOH for the PEME-based system. 99
A.3 LCOH curve for the AE-based system. 100

B.1 Original layout of the offshore wind farm.[*Confidential*] 102
B.2 Standard deviation of power fluctuation over 5 minutes per WTG.[*Confidential*] 104
B.3 Maximum power fluctuation over 5 minutes per WTG.[*Confidential*] 104
B.4 Number of switches of operational state per WTG.[*Confidential*] 104

List of Tables

2.1 Compression of different electrolysis technologies. 11
2.2 Overview of preliminary design choices. 17

3.1 Input and output parameters overview of the hydrogen production submodel. 21
3.2 Input and output parameters overview of the offshore wind farm submodel. 24
3.3 Model constants of the offshore wind farm submodel 25
3.4 Input and output overview of the stack submodel 25
3.5 Model constants of the stack submodel. 27
3.6 Input and output overview of electrical equipment submodel. 27
3.7 Model constants of the electrical equipment submodel. 28
3.8 Input and output overview of the water treatment equipment (WTE) submodel. 28
3.9 Model constants of the WTE submodel. 30
3.10 Input and output overview of the gas conditioning equipment (GCE) submodel. 30
3.11 Model constants of the gas conditioning equipment submodel. 31
3.12 Input and output overview of the compressor (COM) submodel 31
3.13 Model constants of the compressor submodel. 32
3.14 Input and output overview of superstructure submodel. 33
3.15 Model constants of the superstructure submodel. 33
3.16 Input and output overview of the substructure submodel. 34
3.17 Model constants of the substructure submodel. 36
3.18 Input and output overview of foundation submodel 36
3.19 Model constants of the foundation submodel 36
3.20 Input and output overview of the transmission submodel 37
3.21 Model constants of the transmission submodel 38
3.22 Input and output overview of the transport, installation, and commissioning (TIC) submodel 38
3.23 Methods of transport and installation. 39
3.24 Model constants for the transport, installation, and commissioning CAPEX submodel. . 41
3.25 Model constants of the other soft CAPEX submodel 41
3.26 Model constants of the soft CAPEX submodel. 42

4.1 Maritime conditions at the designated location. 44
4.2 Values at minimum LCOH for both systems. 51
4.3 Explanation of the different categories. 58

5.1 Comparison of energy consumption for a small-scale and large-scale electrolysis system [68]. 71

6.1 Maximum normalised power fluctuation. 77
6.2 Standard deviation of the normalised power fluctuation. 78

A.1 Topside structure constants and prices 98
A.2 Input parameters or categories covered by the Monte-Carlo uncertainty analysis 101

B.1 Distance per cable section. [*Confidential*] 103

1 Introduction

This chapter will introduce the topic of this study. Section 1.1 will provide background information and the rationale for interest in this topic. Then, Section 1.2 presents the problem analysis. The research questions and methodology are presented in Section 1.3 and Section 1.4, respectively. Finally, the structure of the report is presented in Section 1.5.

1.1. Background

The Paris Agreement of 2015, signed by 196 nations, set the ambitious target of limiting global warming to below 2 degrees Celsius, relative to pre-industrial levels [2]. An important aspect contributing to realising this goal is the energy transition, implying the abandoning fossil-fuelled processes. Electrification will be a key component of this transition for many sectors. Certain sectors, known as the hard-to-abate sectors, may face challenges in electrifying. Examples of hard-to-abate sectors and processes are heavy transport, iron and steel production, aviation, and the production of feedstock for fertilisers [3]. These sectors and processes required a different form of energy than electricity. Additionally, while fossil fuels offer the advantage of easy storage, achieving low-cost and high-efficiency electricity storage remains a significant challenge. A solution to both these problems could be the use of green hydrogen. The demand for this green hydrogen is expected to increase by 7% annually till 2050 [4]. One of the methods to produce green hydrogen is through electrolysis, by coupling of a renewable energy source to an electrolyser.

In recent years, there has been a substantial increase in the use of sustainable energy sources, with offshore wind energy emerging as one of the fastest-growing renewable energy sources. Production costs for offshore wind energy have dropped dramatically in recent decades, a trend that is expected to continue [5]. Since the costs of hydrogen produced via electrolysis are highly reliant on the costs of electricity, large-scale hydrogen production using offshore wind is currently being investigated. Multiple configurations are proposed in literature. The three main configurations are decentralised and centralised offshore hydrogen production, and onshore centralised hydrogen production, as presented in Figure 1.1.

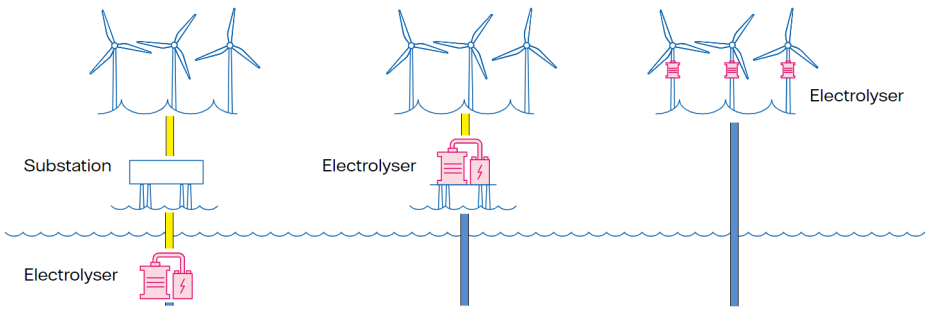

Figure 1.1: Onshore (left), centralised offshore (center), and decentralised offshore (right) hydrogen production.

In both offshore configurations, the electricity produced by the offshore wind farm (OWF) is converted into hydrogen offshore, to be then transported via pipelines to shore. In the decentralised offshore topology, all wind turbine generators (WTGs) are equipped with their own electrolyser. The centralised offshore configuration employs a large central platform, referred to as the centralised offshore hydrogen platform (COHP), that houses all hydrogen production unit (HPU) equipment. In the onshore centralised topology, electricity produced by the OWF is transported to shore using conventional electrical infrastructure, where electrolysis then takes place [6]. All three configurations have their advantages and might be used in a future energy system.

First pilots are currently set up to demonstrate the feasibility of producing hydrogen using wind-powered electrolysers in offshore conditions. The PosHYdon project will equip an existing oil platform with a 1 MW electrolyser to produce hydrogen at sea. Through this project, an attempt will be made to understand the practical effects of hydrogen production in such offshore conditions [7]. The Brande Hydrogen project seeks to test the effects of a variable power source on the electrolyser. This is done by directly connecting a 400 kW electrolyser to a 3 MW onshore WTG. The objective of this pilot is to gain insight into the degradation process of the electrolysers under variable power [8]. Vattenfall has indicated it will have an offshore hydrogen turbine operational by 2025, the so-called Hydrogen Turbine 1 project [9]. The pilots will provide crucial insights needed to scale up these technologies and ultimately produce hydrogen offshore cost-effectively at large scale.

Some of the main drawbacks of conventional offshore wind electricity production are the high costs for and losses occurring during the transportation of the produced energy to shore. The cost and losses due to transport will increases given the assumption that future OWFs are to be built further offshore [10]. Producing hydrogen locally offshore could offer a solution since submarine pipelines for hydrogen transport are cheaper and result in lower losses than submarine electrical cables, when transporting an equal amount of energy [11].

Moreover, the centralised production of offshore hydrogen could provide multiple advantages. The large system brings multiple possibilities to reduce the costs for the produced hydrogen. The size of the total system offers room for large individual components and system integration, instead of the use of modular electrolysers seen in decentralised topologies [12]. The use of larger components is more cost-efficient [13, p. 72]. Furthermore, the large platform could offer room for facilities to ease maintenance [14]. A final possible benefit stems from the aggregation of the power produced by the spatially distributed WTG, resulting in a more consistent power supply to the platform [15], which potentially benefits hydrogen production.

For the centralised offshore configuration to be a success, it needs to compete with other methods of producing green hydrogen. Direct competitors are the decentralised and onshore configurations, both powered by offshore wind energy. Other competitors are electrolysis powered by onshore wind, solar, or hydropower energy [3]. The costs of producing renewable hydrogen, addressed as the levelised costs of hydrogen (LCOH), currently is still between 3 to 8 €/kg [16], as presented in Figure 1.2.

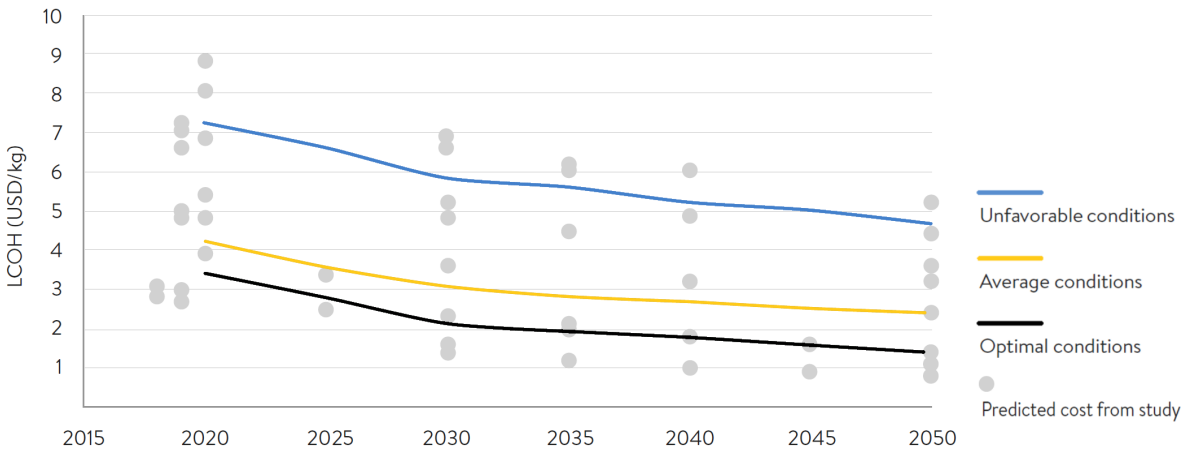

Figure 1.2: LCOH for different scenarios over time. Adopted from [16].

1.2. Problem analysis

To date, research on the integration of renewable energy sources with electrolysers has been performed. The conceptual phase for onshore large-scale electrolyser systems has now passed [17]. Besides, the difficulties associated with offshore operations are not a novelty since experience is gained from either the oil and gas industry or the offshore wind industry. Recently, there has been a surge in interest in investigating the viability of offshore hydrogen generation.

However, detailed information about the specifications of centralised offshore hydrogen platforms is scarce, as this is a relatively new concept that companies are presently investigating and there isn't much public information accessible. Companies are hesitant to share technical specifics to keep any potential edge, which means that the potential advantages of centralised offshore hydrogen production and other critical issues are still lesser known. Therefore, there is a scientific gap regarding the techno-economic feasibility and potential benefits of centralised offshore hydrogen production.

1.3. Research question and sub-research questions

The primary objective of this study is to have a thorough understanding of centralised offshore hydrogen production, by establishing its performance and feasibility, and identifying possible advantages. The main research question is formulated as followed:

"What is the techno-economic viability of centralised offshore green hydrogen production for projected performances and costs of 2030, and how beneficial is its smoother power input on electrolyser dynamics?"

To divide the work into several parts, multiple sub-questions are raised. Answering these sub-questions will contribute to answering the main research question. The sub-questions are as follows:

1: "Which electrolyser technology is most suitable for centralised offshore hydrogen production?"

Several electrolysis technologies are available, each with its advantages and disadvantages. The choice of electrolysis technology also affects the auxiliary equipment. To produce hydrogen in the most competitive method, it is necessary to use the most appropriate electrolysis technology and associated systems.

2."What are the optimal installed hydrogen production unit capacity and electrolyser capacity in relation to the installed offshore wind capacity?"

Not all power supplied to the COHP can be used as feed-in for the stacks. Losses occur while transferring the power from the WTG to the platform and the auxiliary equipment demands a share of the supplied power. Besides, an OWF operates at its rated capacity only part of the time. Given the high cost associated with installed hydrogen production unit capacity, it is worth investigating the effects of undersizing the hydrogen production unit capacity relative to the installed wind capacity. This will however affect the total produced hydrogen. It is necessary to determine which phenomena all influence the optimal installed capacity. A differentiation will be made for optimisation for either the lowest LCOH or the highest net present value (NPV).

3: "Does the damping of power fluctuation due to aggregation of power output benefit hydrogen production in a centralised configuration"

Aggregating the power of the individual wind turbine generators could provide a more consistent power supply to the COHP. The reduction in power fluctuations is likely to benefit hydrogen production and the lifetime of the hydrogen-producing system.

1.4. Methodology

Different approaches are required to answer the sub-questions. The first two sub-questions are answered using a techno-economic model, the third sub-question is answered using a dynamic model. The reason for this dichotomy and explanation of the setup of the models is explained in this section in more detail.

1.4.1. Techno-economic analysis

To answer the sub-questions related to Part I, both the hydrogen yield and associated system costs are relevant, hence a techno-economic model is adopted. In order to optimise for the two different objectives, being the minimum LCOH and maximum NPV, the total system will be examined from a holistic point of view. This is done as the optimisation of one of the components of the system will not guarantee the optimal result.

To maintain structure and oversight in this complex problem, a Model-Based System Engineering approach will be used. This implies that the entire system will be first broken down into all its different components. These components will be defined and the physical parameters on which these components depend will be examined. This includes presenting the different design choices for each component. Once the individual components are clearly defined, their interactions will be identified to assemble the entire system. This will be done based on literature research.

Models exist for some of the components and these are either used directly or modified to use those for its intended purpose. In the absence of models, relationships, as found in literature, will be used. Model inputs will come from a variety of sources. Some of the required data is present within Vattenfall and others can be found in literature. In the case of a lack of publicly available data, assumptions are made where no information was available, based on experts' view. Once the complete model is finished, a case study will be performed in order to evaluate the different configuration and installed capacities.

1.4.2. Dynamic analysis

For answering the sub-question related to Part II, only the production of hydrogen is relevant. To address this sub-question, a more detailed investigation into hydrogen production is required. This requires a dynamic model that simulates the production of hydrogen and the status of the system at short intervals to understand the effect of power fluctuations. An existing power-to-hydrogen time-series model will be used to answer this question. As this model was originally constructed for decentralised offshore hydrogen production, it necessitates modifications to make it suitable for its novel application.

A case study will be performed based on historical power output data. Since no benchmark values to evaluate the obtained results of the centralised offshore configuration are available, its performance is compared to a decentralised offshore configuration. First, the effects of aggregating power supply will be identified, by evaluating the power output of the OWF and the WTGs. Then, the power-to-hydrogen time-series model will be used to evaluate the differences in hydrogen-related performances.

1.5. Report outline

The purpose of this section is to guide the reader to through this report and to direct to the sections of interest. Figure 1.3 presents a graphical readers-guide of the report. As presented in Section 1.4, the sub-questions are answered using two different models. These models are addressed in two separate parts. Both parts follow a similar structure, beginning with a chapter outlining the model and its specifications. The second chapter presents the results according to a performed case study.

Before delving into the specific models, Chapter 2 provides an overview of the relevant components and aspects related to centralised offshore hydrogen production. Readers familiar with such systems could be directed to Section 2.13, where an overview of the preliminary design choices for this study are presented, as presented in blue in Figure 1.3. Hereafter, the two parts are presented.

Part I focuses on the techno-economic analysis, where both the total produced hydrogen and costs are relevant. Here, efforts are made to determine the optimal installed HPU capacity for different objectives and to quantitatively evaluate the different electrolysis technologies. Chapter 3 outlines the techno-economic model and sub-models. Then, Chapter 4 presents the results, case study, and summary of Part I. Part II narrows down on hydrogen production only and examines the effect of power fluctuations on hydrogen production, using the time-series-based model. The phenomenon of power fluctuations and the model used are described in Chapter 5. Then, the case study, results, and summary of Part II are presented in Chapter 6. A summary per part is supplied for readers only interested in one of the two parts, as presented in blue in Figure 1.3. The information found in these summaries suffices to read the conclusion. The summary of Part I is found in Section 4.8, and the summary of Part II in Section 6.7.

The report concludes with Chapter 7. Here, an overarching conclusion is drawn based on the results

of both parts and recommendations for future work are presented.

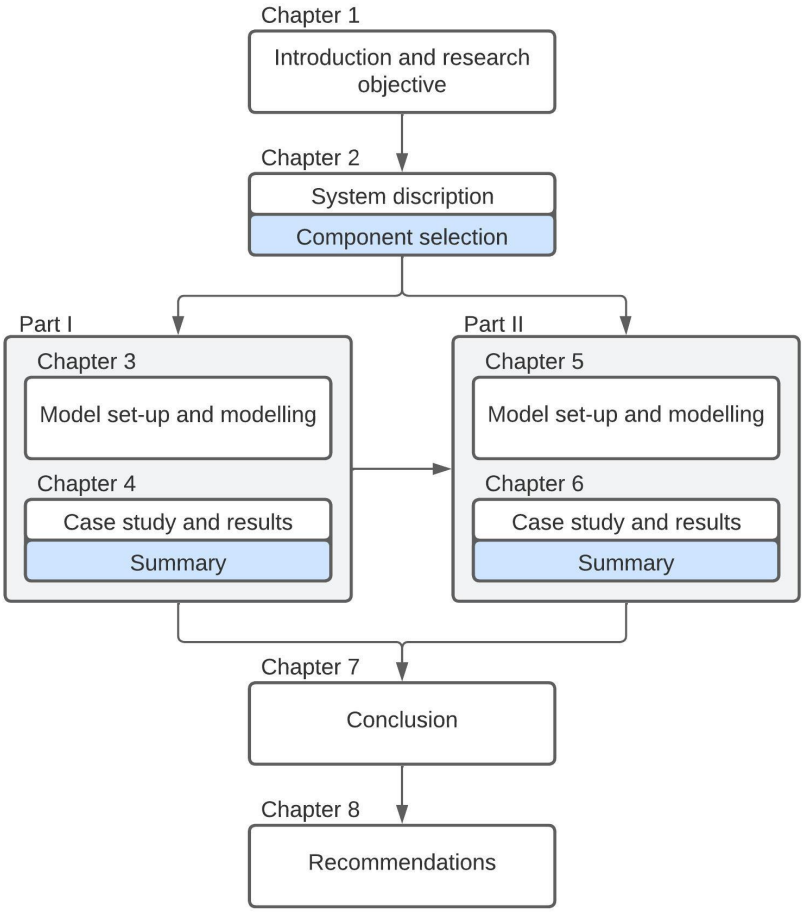

Figure 1.3: Graphical readers guide. The two parts are presented in grey, and the recommended readings are in blue.

2

System description and component selection

The following chapter introduces all the components relevant to the offshore wind-hydrogen system, aspects of the offshore wind-hydrogen project, and which design choices are possible. An overview of all components and aspects considered in this work is presented in figure 2.1. Readers familiar with components of such offshore wind-hydrogen system can jump to section 2.13, where the preliminary design choices for the COHP are presented.

First, the dedicated offshore wind farm, powering the COHP, is elaborated on in section 2.1. Subsequently, the components of the hydrogen production unit (HPU) are introduced, starting with the electrolysers in section 2.2. Then, the electrical equipment is presented in section 2.3. Next, the water treatment equipment and gas conditioning equipment are presented in sections 2.4 and 2.5. The final component of the HPU, the compressors, is presented in section 2.6. Besides the components of the HPU, the COHP consists of the superstructure, substructure, and foundation, which are presented in sections 2.7, 2.8 and 2.9 respectively. The produced hydrogen will be transported to shore using the hydrogen transmission system, presented in 2.10. Besides the previously mentioned physical components, such offshore wind-hydrogen project consists of procedures and aspects. First, the transport, installation, and commissioning of the COHP is introduced in section 2.11, and finally, to make it a complete offshore wind-hydrogen project, the Other activities are presented in section 2.12.

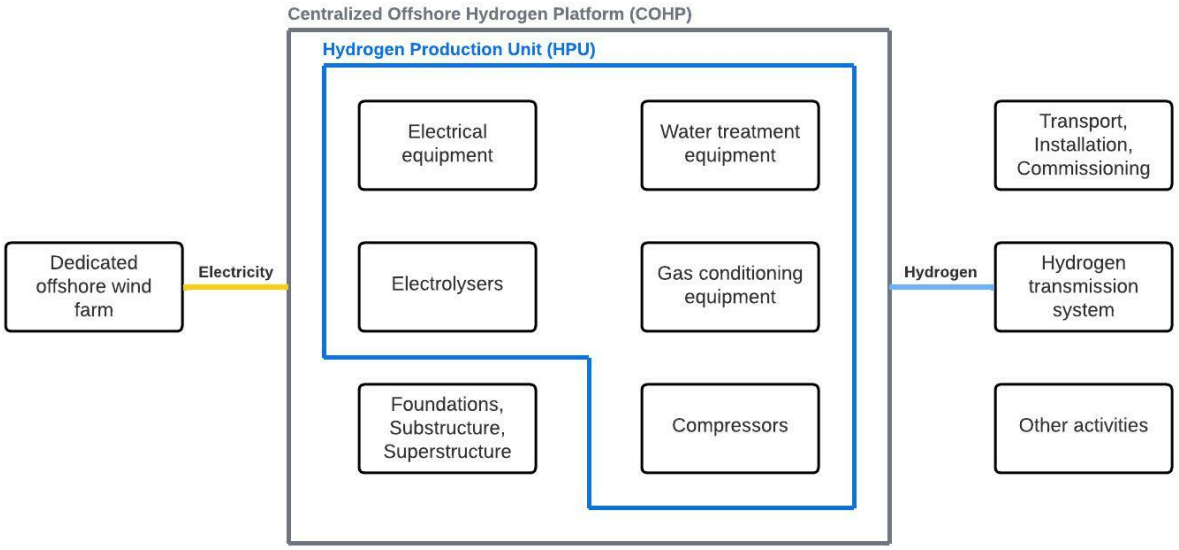

Figure 2.1: Overview of an offshore wind hydrogen system and project aspects.

2.1. Wind turbines and wind farm description

The following section is related to the dedicated offshore wind farm, powering the COHP. In the wind farm, electricity is generated by converting kinetic energy into rotational energy, and rotational energy into electrical energy. First, in section 2.1.1, a conventional offshore wind farm with all its components is presented followed by section 2.1.2, presenting the components of a dedicated offshore wind farm. This section addresses which components of a traditional offshore wind farm are redundant, and the aspects of the offshore wind farm performance that needs to be taken into account.

2.1.1. Conventional offshore wind farm

Figure 2.2 presents a schematic representation of a conventional wind farm. Besides the wind turbines ①, it consists of the inter-array cables (IAC) ②, which transfer the produced electricity to the offshore substation ③. At the offshore substation, the voltage of the produced electricity is increased to lower the losses caused by cable resistance [18]. Subsequently, the electricity is transported to the shore via the export cables ④. Finally, onshore, the voltage is increased once more at the onshore substation ⑤ before the electricity is delivered to the grid ⑥.

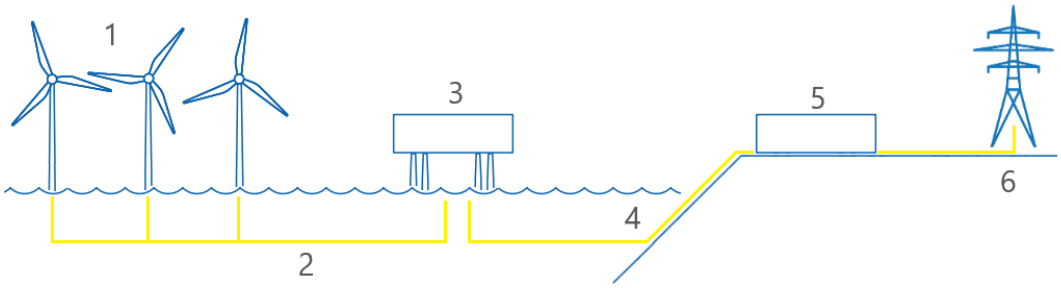

Figure 2.2: Schematic representation of a conventional wind farm.

2.1.2. Dedicated offshore wind farm

In the offshore wind-hydrogen system, the energy carriers are transported to shore in the form of molecules rather than electrons, hence the system looks different from a conventional wind farm. The hydrogen system is schematically represented in figure 2.3. In the hydrogen system, similar to a traditional wind farm, electricity is generated using wind turbines ①. This electrical energy is transported via the IAC ② to the COHP ③ where the electricity is converted into hydrogen. The produced hydrogen is transported to shore via the hydrogen transmission system ④. Onshore, the hydrogen is delivered directly to industrial offtakers ⑤ or fed into the hydrogen backbone ⑥.

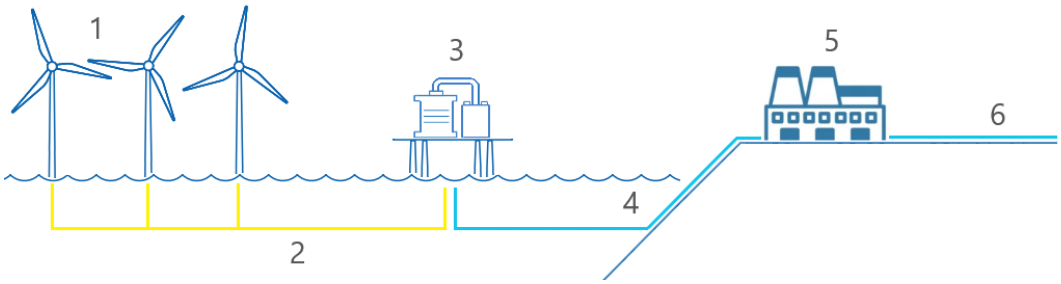

Figure 2.3: Schematic representation of an offshore wind-hydrogen system.

Superfluous in the hydrogen system are the offshore substation, the export cable, and the onshore substation. This saves on the material costs of these components, as well as on installation, transportation, and development costs. However, these components are replaced by the COHP and hydrogen transmission system and their respective costs. Losses caused by cable resistance and conversion in substations are replaced by hydrogen conversion losses and pressure drop [11].

Several aspects of the farm's performance must be taken into account. Wind turbines use wind energy to generate, hence the wind passing the turbine must have less energy than the wind upstream of the turbine. As a result, the wind downstream of a wind turbine is slower and more turbulent. This downstream wind is known as the turbine's wake. As the wind flow moves downstream, the wake will expand and gradually restore to free stream conditions. When a wake meets the swept region of a downwind turbine, the downwind turbine is said to be shadowed by the wake-producing turbine [19].

Over the life of the wind farm, the performance of the wind farm decreases. Both in rated power and annual yield. Wind turbines are subjected to a variety of stresses over their lifetime, which can cause wear and tear on numerous components. This can involve damage to the blades, gearbox, generator, and other components. As a result, the turbine's performance may gradually deteriorate as these components erode. Besides, its performance may degrade if it is not maintained properly. For example, rotor blades that are not cleaned regularly may become less efficient. The decrease of the wind farms' conversion efficiency, combined with the decrease in annual availability, causes the annual yield to decrease as well [20]. It is essential to lessen the impact on performance and extend the lifetime of the turbine by resolving these concerns through regular small maintenance and large maintenance campaigns [21].

The 33 kV IAC continues to be the industry standard for offshore wind farms today. However, a trend toward 66 kV IAC is justifiable given the expanding surface area of future wind farms and the increase of individual turbine power rating. Less array cabling, the possibility of transmitting up to twice as much power, fewer related power losses, and capital cost savings, in terms of both cable cost and installation, are potential advantages of employing a 66 kV IAC [18].

2.2. Electrolyser description and selection

The following section is dedicated to the electrolysers. A general introduction to what electrolysers are and how they work, together with the selection criteria is provided in section 2.2.1. Then, the five main electrolyser technologies are discussed in sections 2.2.2 to 2.2.6. Finally, in section 2.2.7 the electrolyser technologies considered feasible for centralised offshore hydrogen production are presented.

2.2.1. Electrolyser introduction and selection criteria

The electrolysers are considered to be the core of the system. During the electrolysis process, electric direct current (DC) is applied to water, generating high purity hydrogen and oxygen. Although different electrolyser technologies are based on slightly different electrochemical reactions, all electrolyser types have an anode and cathode, separated by an electrolyte [22]. At the cathode, the hydrogen evolution reaction (HER) takes place and at the anode, the oxygen evolution reaction (OER) takes place. The electrolyte enables charge carrier transport between the anode and the cathode [23].

In addition, the efficiency curve of an electrolyser is a well-known phenomenon. This efficiency curve is a representation of the system efficiency of an electrolyser and indicates the operation efficiency compared to the load given to the electrolyser. Figure 2.4 shows the system efficiency curve of a PEME-based system based on historical data. What can be seen is that the system operates most efficiently around 20% of the nominal load and efficiency decreases thereafter.

Water electrolysis can be categorised into five main technologies, distinguished by the type of electrolyte used. Direct seawater electrolysis (DSE), Alkaline electrolysis (AE), Proton exchange membrane electrolysis (PEME), Solid oxide electrolysis (SOE), and Anion exchange membrane electrolysis (AEME) are evaluated on their feasibility for centralised offshore hydrogen production.

These five different electrolyser technologies can be compared on an inordinate number of different criteria. Therefore, only those criteria that have a significant impact on the intended application are considered. Concerning the general operation of the electrolyser, the following are examined: the type of electrolyte in the system, whether or not precious metals are used, the feedstock used, the operating temperatures, and finally the pressure under which the produced hydrogen exits the electrolyser. Furthermore, the performance of the technology is assessed by the efficiency and degradation of the stacks and with respect to cost, the capital expenditure (CAPEX) and operational expenditure (OPEX) are evaluated. Finally, the size and weight of different technologies are considered. It should be mentioned that currently many developments are taking place in the field of electrolyser technologies. Therefore the values mentioned in literature are not always representative or up to date. Also, these theoretical values may differ from the performance actually obtained by manufacturers.

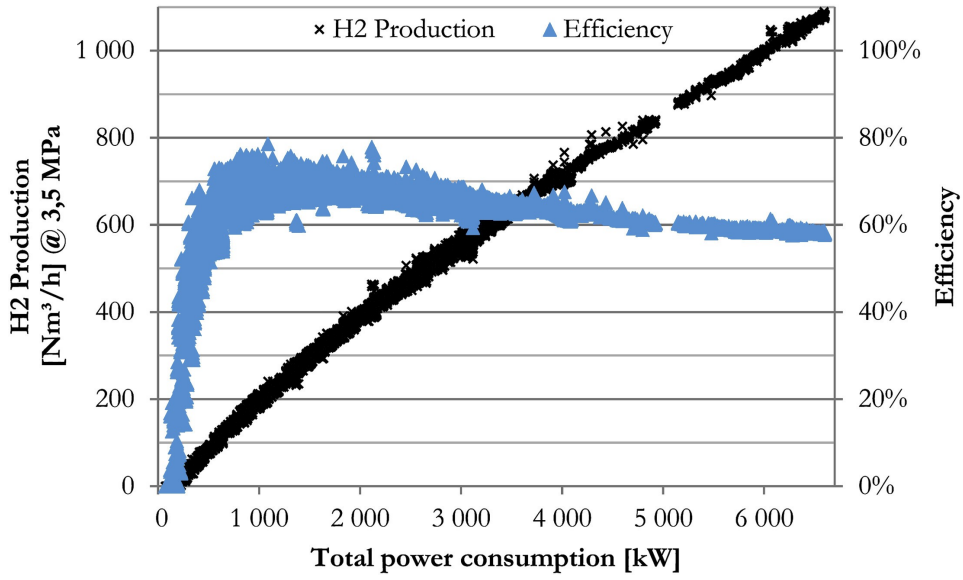

Figure 2.4: Efficiency curve of a PEME-based system, taken from [24].

2.2.2. Direct seawater electrolysis

DSE uses seawater as both electrolyte and feedwater. The reaction taking place during this water splitting process is depicted in equation 2.1. This process is widely known in the chemical industry as the Chlor-alkali process [25]. Traditionally, during the Chlor-alkali process, the formation of hydrogen is seen as a byproduct, as this process focuses on the production of sodium chloride. A water splitting system based on DSE omits the use of water desalination and purifying equipment. This results theoretically in a smaller required space and fewer components, which could lead to a lower overall CAPEX and OPEX [26]. The pressure of the hydrogen produced in a chloralkali process ranges usually around 200 bar [27].

$$\begin{aligned} Anode: &\quad 2Cl^-_{(aq.)} \rightarrow Cl_{2(g)} + 2e^- \\ Cathode: &\quad 2H_2O_{(l)} + 2e^- \rightarrow H_{2(g)} + 2OH^-_{(aq.)} \\ Overall: &\quad 2NaCL_{(aq.)} + 2H_2O_{(l)} \rightarrow Cl_{2(g)} + H_{2(g)} + 2NaOH_{(aq.)} \end{aligned} \tag{2.1}$$

The downsides of this water splitting technology are the high concentrations of chlorine produced during the process, the short lifetime due to high unavoidable impurities in the seawater, and frequently required maintenance [28]. Also, no commercial examples that rely on this technology for dedicated hydrogen production currently exists [29]. Taking into account that the CAPEX, OPEX, and specific power consumption of seawater desalination are marginal compared to those of water splitting, the benefits of direct seawater splitting are thus insignificant.

2.2.3. Alkaline Electrolysis

AE is the most well-understood and mature water splitting technology. It has been widespread commercially available for decades and therefore currently the most cost-effective electrolyser technology available [22][14]. The water splitting reaction that occurs in the electrolyser is presented in equation 2.2. In the process, an alkaline solution of KOH or NaOH is used as electrolyte. As feedstock, desalinated water is used with a maximum conductivity of 5 µS/cm [30]. Historically, this type of electrolyser was run at near-constant power while linked to the grid. Due to recent advancements, better compatibility with fluctuating power input is realised although the system experiences relatively slow dynamic response [11]. Due to the avoidance of precious materials, alkaline electrolysis is characterised by low CAPEX when compared to other electrolyser methods [22].

$$\begin{aligned} Anode: &\quad 2OH^-_{(aq.)} \rightarrow \frac{1}{2}O_{2(g)} + H_2O_{(l)} + 2e^- \\ Cathode: &\quad 2H_2O_{(l)} + 2e^- \rightarrow H_{2(g)} + 2OH^-_{(aq.)} \\ Overall: &\quad H_2O_{(l)} \rightarrow \frac{1}{2}O_{2(g)} + H_{2(g)} \end{aligned} \tag{2.2}$$

Downsides of an AE-based system are the relatively low current densities resulting in a large required footprint, the use of the alkaline fluid as electrolyte requires complex maintenance because of its corrosive nature [23], and the aforementioned relative slow dynamic response.

Assumed is that, due to the maturity of the technology, slower technological progress will be made compared to other electrolyser technologies. Where previous AE systems produced hydrogen at an atmospheric pressure, current AE systems are capable of producing hydrogen at an output pressure of 30 bar [11].

In the majority of papers comparing AE with other electrolyser technologies for offshore application, the AE-based system does not emerge as the most promising, due to its lower dynamics, relatively large footprint [11] and more frequent maintenance [29]. However, these papers do not mention that the central character of the COHP may be able to compensate for these disadvantages, as highlighted by [14].

2.2.4. Proton Exchange Membrane Electrolysis

PEME is one of the fastest developing electrolyser technologies and is relatively new compared to AE. PEME-based systems make use of a solid electrolyte, instead of a liquid one as used in the previous electrolyser technologies. The system uses deionized water as feedstock with a maximum conductivity of 1 µS/cm [30]. The absence of liquid electrolyte enables a more compact design and therefore lower footprint [31]. The compact design is realised by the zero-gab architecture. This zero-gab concept is realised by a membrane-electrode assembly (MEA) which is a single piece containing all the necessary components of a cell in a three layer sandwich. On the one hand, PEME is more expensive than the alternatives because of this costly MEA component. However, the MEA requires no maintenance for the duration of the electrolysers lifetime [29]. Other benefits of using the MEA include the ability for faster dynamics and shorter cold-starts compared to AE-based systems, both qualities required for coupling to an intermittent power source. Finally, the produced hydrogen is often at higher pressures compared to AE [6].

$$\begin{aligned} Anode: &\quad H_2O_{(l)} \rightarrow \frac{1}{2}O_{2(g)} + 2H^+_{(aq.)} + 2e^- \\ Cathode: &\quad 2H^+_{(aq.)} + 2e^- \rightarrow H_{2(g)} \\ Overall: &\quad H_2O_{(l)} \rightarrow \frac{1}{2}O_{2(g)} + H_{2(g)} \end{aligned} \tag{2.3}$$

Downsides of this emerging technology are the higher CAPEX than its direct competitor. This is due to the usage of noble metals such as Pt, Ir, or Ru in the cathode and anode [31]. Another disadvantage of the PEME-systems is the relativity shorter lifetime due to faster degradation [22]. Nevertheless, the PEME technology is considered highly suitable due to its compact design, fast dynamic responses, and low maintenance costs. Also, the relatively high CAPEX costs are expected to decrease in the future due to the expansion of production scale [14][29].

2.2.5. Solid Oxide Electrolysis

SOE is one of the more recently developed technologies and is still in a pre-commercial phase. It can be categorised as a high-temperature electrolyser, as superheated steam is used as feedstock. As electrolyte, a ceramic membrane is used. Temperatures vary between 700 °C and 1000°C [29] which promises a higher efficiency than both PEME and AE [14]. Another benefit of this electrolyser technology is that it does not make use of precious metals [11].

$$\begin{aligned} Anode: &\quad O^{2-}_{(g)} \rightarrow \frac{1}{2}O_{2(g)} + 2e^- \\ Cathode: &\quad H_2O_{(g)} + 2e^- \rightarrow H_{2(g)} + O^{2-}_{(g)} \\ Overall: &\quad H_2O_{(g)} \rightarrow \frac{1}{2}O_{2(g)} + H_{2(g)} \end{aligned} \tag{2.4}$$

To avoid thermal cracks developing in the components, cool-downs and heat-ups must be carried out utter slowly. Direct coupling to an intermittent energy source like offshore produced wind energy is therefore a considerable challenge. Furthermore, when used in maritime environments, the main issue with this technology is finding an external source of high temperature that can maintain the SOE at operational temperature continually [29].

2.2.6. Anion exchange membrane electrolysis

AEME is the newest electrolyser technology aiming for combining the benefits of AE and PEME. The system's reaction is presented in equation 2.5. The system operates with an electrolyte consisting of low concentrations of alkaline, thus a less corrosive environment than in an AE-based system [31]. The AEME weak alkaline operating conditions are suitable with inexpensive electrode materials, which are mostly based on nickel and cobalt, and can be similar to those used in classic AE. They also make it possible to use membranes that are less expensive than those used in PEME stacks [23]. Hydrogen output pressures are reported to be up to 35 Bar [32].

$$\begin{aligned} Anode: &\quad 4OH^-_{(aq.)} \rightarrow O_{2(g)} + 2H_2O_{(l)} + 4e^- \\ Cathode: &\quad 4H_2O_{(g)} + 4e^- \rightarrow 2H_{2(g)} + 4OH^-_{(aq.)} \\ Overall: &\quad 2H_2O_{(l)} \rightarrow 2H_{2(g)} + O_{2(g)} \end{aligned} \tag{2.5}$$

The small size of the cells and the moderate temperatures (25-70 °C) are further benefits of AEME technology. Due to all of these factors, the AEME technology has emerged as a promising option that satisfies the requirements of inexpensive integrated components and straightforward operation [31]. However, the AEME technology is still in laboratory stage and lacks large scale production [22].

2.2.7. Conclusion on electrolyser technologies

Five different electrolysis technologies were considered, each with varying degrees of feasibility when employed for centralised offshore hydrogen generation. Table 2.1 presents the most important characteristics of the different electrolysis technologies.

Technology	DSE	AE	PEME	SOE	AEME
Temperature	Low	Low	Low	High	Low
Efficiency	Moderate	Moderate	Moderate	High	Moderate
Output pressure	High	Low	High	Low	Medium
Maturity	Low	High	Moderate	Moderate	Low
CAPEX	High	Low	Moderate	High	High
OPEX	High	Moderate	Low	Moderate	Low
Size	Low	High	Low	Moderate	Low
Lifetime	Low	High	Moderate	High	Low

Table 2.1: Compression of different electrolysis technologies.

Not all technologies will be considered for the remainder of this study. DSE will not be considered feasible because of its low maturity for the sole purpose of hydrogen production and high production of

chlorine. SOE requires high operating temperatures that are technically difficult to achieve and maintain in offshore conditions. Also, achieving these high temperatures would require a too large fraction of the total energy available which has negative effects on the efficiency of the system. The intermittent nature of wind energy could lower the lifetime of this technology significantly. For these reasons, SOE is not considered a feasible option for this study. AEME, although theoretically promising, is at an immature technology stage, which results in excessive capital expenditure and is therefore excluded from the rest of this study. Both the AE and PEME technologies are at a relatively mature technological stage. The compact design and fast dynamics of the PEM system are accompanied by higher CAPEX. The AE technology, on the other hand, is cheaper but has its disadvantages like the larger associated mass and slower dynamics. Both technologies are promising and therefore considered in this study.

2.3. Electrical equipment description

The IAC delivers medium voltage (MV), alternating current (AC) to the COHP, which has to be converted to be usable by the components of the HPU unit. This conversion happens in several steps by switchgear, transformers, rectifiers, and passive and active reactive power compensation equipment [33][34]. Together with the electrical cables present at the platform, these components are referred to as the electrical equipment. Figure 2.5 presents a simplified overview of what the electrical infrastructure of the COHP will look like, adapted from the work of ISPT for an onshore centralised hydrogen production plant [35].

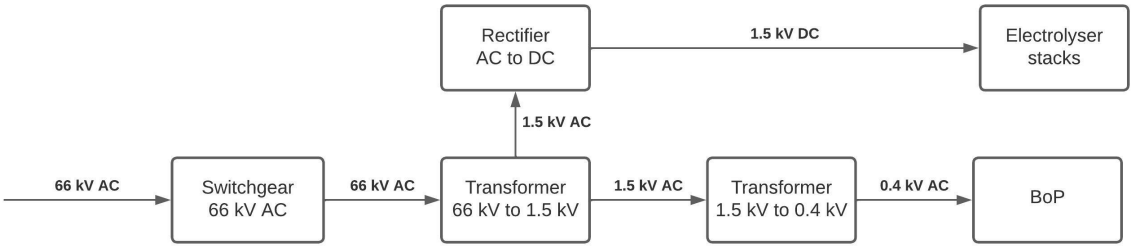

Figure 2.5: Simplified electrical infrastructure of the COHP

The system's switchgear is used to distribute energy to various loads and pieces of equipment while also controlling the flow of electricity to guarantee that the right voltage and frequency are applied. It has several safety features like circuit breakers and fuses that may be used to stop the flow of electricity in the case of a failure or overload. Transformers are used to step down the voltage of electricity received from the IAC grid to a level that is suitable for the HPU components while the rectifiers are used to convert AC power into DC.

The equipment in the HPU can be divided into two groups, depending on their requirement for AC or DC power. The first group, which consists only of the electrolysers, requires low voltage (LV), DC. The other group, the remaining equipment of the HPU, requires an LV, AC power.

2.4. Water treatment equipment description

The water treatment equipment of the HPU is responsible for preparing the water needed for all water-related operations. In the proposed offshore wind-hydrogen system, seawater will be used as both a feedstock for electrolysis and as a cooling agent. Due to the efficiencies of the electrolysers, portions of the power supplied to the stacks will be converted into heat. Also, the compressors and desalination and deionization equipment require cooling [35]. Given the high concentration of stacks at the platform, it is necessary to have adequate cooling facilities in place. Using the abundant seawater as a cooling agent for the electrolysers is a logical solution.

The water infrastructure for both the PEME- and AE-based system are presented in figure 2.6. Both consist of water pumps and desalination equipment and, depending on the chosen electrolysis technology, deionization equipment. As stated previously in section 2.2, both technologies require different qualities of feedwater, and therefore different water treatment equipment. In an AE-based system,

desalinisation of the incoming seawater would suffice while in a PEME-based system, additional deionization of the feedwater is required.

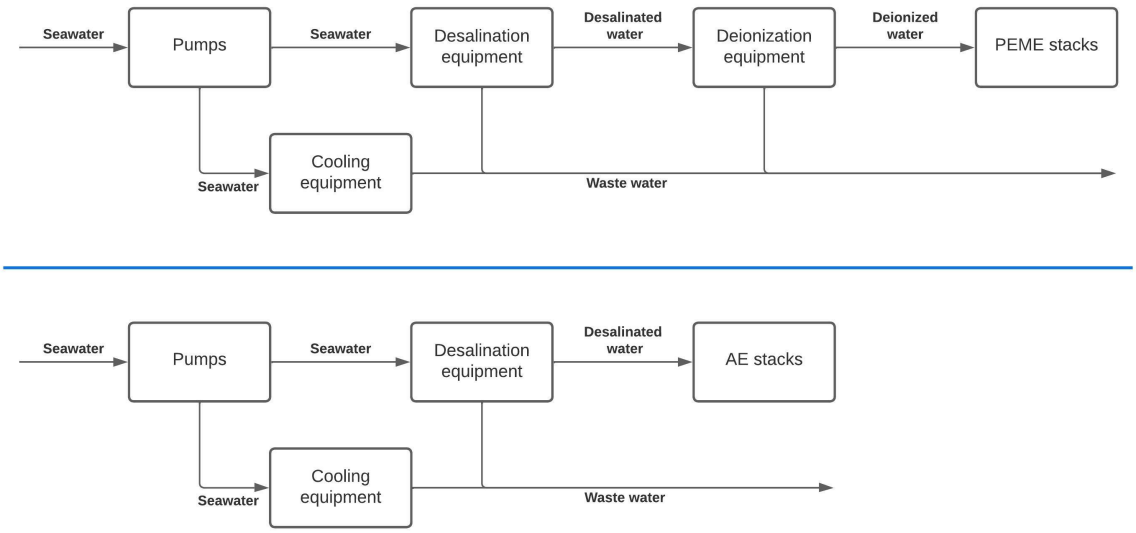

Figure 2.6: Simplified water infrastructure of the COHP for both a PEME-based (top) and AE-based system (bottom).

2.4.1. Water pumps

To facilitate the use of seawater for both feedwater and cooling at the COHP, pumps are necessary to elevate the seawater from sea level to the platform. The capacity of these pumps should be sufficient to meet the demand for seawater at the platform at its maximum capacity. It is recommended to use separate pumps for the feedwater and the cooling water, to ensure that the necessary flow rates can be maintained for both purposes. The volumetric intake of seawater and the electric output of the turbine must be coordinated to ensure that the seawater supply can meet the demand for electrolysis and cooling.

2.4.2. Desalination

One commonly used method for seawater desalination is reverse osmosis (RO), in which seawater is forced through a membrane with small pores. The pores are small enough to allow water molecules to pass through but too small for salt and other dissolved minerals. As a result, the purified water is collected on one side of the membrane, while the salt and other minerals are left behind on the other side [36]. It is important to note that the RO process has a certain recovery rate, which represents the fraction of the seawater that is converted into desalinated water. This recovery rate is influenced by various factors, such as the seawater quality, the feedwater quality requirements, and the membrane separation efficiency [37].

2.4.3. Deionization

The higher purity requirements of the feedwater for a PEME-based stack compared to an AE-based stack, necessitates the use of additional water purification, known as deionization. This is a procedure designed to remove ions and other impurities from the desalinated water to meet the requirements of the PEME-based stacks [38]. Once again, a fraction of the incoming desalinated water is lost due to the recovery rate of the deionization equipment [37].

2.5. Gas conditioning equipment description

The gas conditioning equipment of the HPU consists of a series of components that process the hydrogen, oxygen, and water produced by the electrolysers to increase the purity of the hydrogen and partially prepare it for transmission. This involves separating the hydrogen from traces of impurities,

deoxidising, and drying the gases to remove moisture to avoid the presence of liquids in the downstream systems. The specific components of the gas conditioning equipment will depend on the type of electrolysis technology used. A PEME-based system typically requires hydrogen gas/liquid separators, oxygen gas/liquid separators, deoxidisers, and dryers, while an AE-based system also requires lye recirculating equipment [35].

The hydrogen produced by a PEME-based stack is typically at higher pressures than hydrogen produced by an AE-based stack, which means that the gas conditioning equipment must be resistant to these higher pressures. As a result, the gas conditioning equipment in a PEME-based system may be more expensive than that of an AE-based system [13, p. 38]. However, the AE-based system requires an additional lye circulation system, which increases the total number of pieces of equipment required [35].

2.6. Compressors description

The final step in the HPU is executed by the compressors. The compressors increase the pressure of the hydrogen to the desired level. There are various types of compressors, but the majority of compressors used today are either positive displacement or dynamic compressors [39]. Positive displacement compressors work by trapping a specific amount of gas and pushing it into the discharge pipe. Dynamic compressors employ a spinning impeller to transmit kinetic energy from the motor to the gas. The impeller drafts the gas and increases its velocity as it revolves, propelling the gas to the discharge point. The compressor type employed depends on the mass flow rate of the hydrogen gas and the desired compression ratio. Anticipating on the high expected maximum hydrogen flow rate, so-called reciprocating piston and centrifugal compressors are deemed suitable [40].

Reciprocating piston compressors are suited for applications requiring moderate flow rates and high pressure. These compressors are positive displacement devices that compress and displace gases using a piston and cylinder arrangement, with the piston's motion being powered by a crankshaft. The cylinder has two automated valves, one for gas suction and one for gas release. Reciprocating compressors are used in petrochemical facilities and oil refineries, and they are able to realise high pressures, especially when employed in a multi-stage design [39].

Centrifugal compressors are dynamic compressors, often employed in applications requiring high flow rates and moderate compression ratios. They compress the gas with a revolving impeller with radial blades, which raises the velocity of the gas and transforms the kinetic energy into pressure. These compressors are frequently used to pressurise air and natural gas in petrochemical facilities, refineries, gas collection, and transmission pipelines. However, the compression ratio of a centrifugal compressor is determined by the molecular weight of the gas being compressed, and because hydrogen has a low molecular weight, high impeller tip speeds are required. Due to material strength limits and hydrogen embrittlement occurring, this can be challenging [39][41].

Due to the challenges arising using a dynamic compressor for hydrogen compression, it is decided to only consider reciprocating piston compressors for this study. The power requirements of the compressors are dependent on the compression step. Increasing the number of compression steps, and therefore decreasing the size of a single step, decreases the overall power consumption of the compressors but increases the complexity of the compressor. Anticipated is on a significant difference between the instantaneous power requirements of the compressors for the PEME- and the AE-based system, due to the difference in stack hydrogen output pressure.

2.7. Superstructure description

The superstructure is a steel structure, often consisting of several decks, that supports and houses all the equipment. Besides, it consists of the gratings and claddings where the gratings act as floors, and the claddings act as walls. Some of the functional areas on the platform may require specific operating temperatures and conditions. The heating, ventilation, and airconditioning (HVAC) system is responsible for protecting the equipment from harsh offshore conditions and maintaining the required operating temperatures. This ensures that the equipment is able to function properly [42].

In addition to the steel structure and HVAC equipment, the topside of a COHP may also include components such as cranes, emergency shutdown systems, and fire protection systems. Cranes are often used to move heavy equipment and materials on and off the platform and may include both fixed and mobile cranes. Emergency shutdown systems are critical for ensuring the safety of the platform

and its personnel and may include a variety of sensors and alarms to detect potential hazards. Fire protection systems may include sprinkler systems, fire extinguishers, and other measures to protect against the risk of fire on the platform [43][44].

2.8. Substructure description

The substructure rests below the surface of the seawater and supports the topside. These substructures can either be mounted to the seabed or floating [45]. Jacket foundations, floating substructures, and concrete gravity based substructures are the most widely used substructures, both in the offshore wind industry, and oil and gas industry [46].

Jacket foundations consist of a vertical steel structure, which is attached to the seabed. The jacket consists of primary steel, which serves as the major structural support, and secondary steel, which is used for features like boat landings and external access ladders [34]. The jacket includes anodes and coating to protect the steel from corrosion and wear [33]. Jacket substructures have been installed up to depths of around 400 meters in the oil and gas industry, however, at such depths alternatives might be cheaper nowadays [45].

Concrete gravity based substructures are constructed from concrete and reinforced by steel. They rest on the seafloor and withstand sliding and overturning through friction between the structure and the soil. These substructures are typically used in water depths similar to that of jacket based structures, but are in general less frequently used than jacket substructures [45].

Floating substructures, as the name implies, are intended to float on the surface of the water. These substructures are often employed for platforms located at larger water depths, where installing a bottom fixed structure would become technically challenging and cost-inefficient [45].

Anticipating on an expected water depth below 50 meters at the COHP site, the use of a jacket foundation or a gravity-based structure is deemed appropriate. Based on Vattenfall's experience with jacket foundations, it is decided to utilise a jacket as substructure for the COHP.

2.9. Foundation description

Foundations connect the jacket substructure to the seabed and provide the necessary support. Several different types of foundations can be used for offshore substructures. The most commonly used are piles and suction caissons.

Piles are long, slender structures that are driven or bored into the ground to provide support for a structure. Piles are generally able to transfer loads more efficiently than suction caissons, due to their large surface and ability to penetrate deep into the seabed [47].

Suction buckets are another type of foundation used for offshore substructures. Suction caissons are generally easier and faster to install than piles. However, they have a lower load capacity compared to piles [47].

Anticipating on the large mass of the substructure and topside of the COHP, it has been decided to use piles as foundation type of the platform [48].

2.10. Hydrogen transmission description

After the hydrogen is produced, processed, and compressed at the COHP, the hydrogen will be transported to shore. Different transportation methods exist for hydrogen transportation. The most commonly used methods are shipping and pipelines. The most promising transmission method for a specific case depends on hydrogen flow rate and distance [49]. Transmission using ships often requires temporary hydrogen storage at the location of production, while pipelines can be run continuously. Also, the use of existing pipeline infrastructure is promising [50].

Below a distance of 3,000 km, the use of pipelines is the most cost-efficient option [49]. It is assumed that the distance between the COHP and the offtake location onshore is smaller than this threshold. Furthermore, it is highly site-specific whether an already existing pipeline can be reused for hydrogen transmission. For these reasons, only the use of a new pipeline for hydrogen transmission is considered in this study.

2.11. Transport, installation and commissioning description

Once the components of the COHP have been constructed onshore, they remain to be transported, installed, and commissioned at the designated location. The transport, installation, and commissioning activities are closely related, hence they are treated simultaneously.

2.11.1. Substructure installation

Two main methods for substructure installation can be distinguished, the lift method and the launch method. Lift installation involves the use of a heavy lift vessel. Once at the site, the substructure is lifted and placed onto the seabed, where it is secured in place using piles or other foundation elements. This method is often used for smaller substructures or those with relatively low weight, as it requires a vessel with a high lifting capacity [51].

The substructure is launched into the sea using a launch barge and buoyancy tanks during launch installation. The substructure is upended at its designated place once afloat. This technique is frequently utilised for bigger or heavier substructures [51].

2.11.2. Foundation installation

Two installation methods are common for piles, pre-pilling and post-pilling. These methods are distinguished by the relative moment the piles are installed in reference to the installation of the substructure as the names suggest.

2.11.3. Topside transport and installation

In the oil and gas industry, three types of topside installation methods are commonly used. These are single lift installation, modular installation, and float over [42].

Using the single lift installation method, the topside is installed at its jacket at once using a heavy lift vessel. The lifting capacities of these crane vessels have increased parallel to the increasing platform dimensions and mass [52]. Installing the topside at once decreases commissioning time. The capacity and availability of crane vessels are the primary restrictions placed on the single lift installation method. Only a small number of crane vessels have a lifting capacity of more than 5000 tonnes [52].

In the modular installation approach, the topside structure is installed in sections onto its substructure. This approach is often used when the weight of the topside exceeds the lifting capacity of a single crane vessel. One advantage of this approach is that the weight of the sections being lifted is reduced, allowing for the use of smaller capacity installation lift vessels, which are more readily available and generally have lower associated costs. However, this approach also has the disadvantage of higher commissioning costs due to the need for offshore connections between the various sections. These additional offshore costs can be significant, as offshore labour is generally more expensive than onshore labour [53].

The float-over method is a technique used in the oil and gas industry for installing offshore structures when the weight of the topside exceeds the available crane lifting capacity [52]. The topside is placed on a barge and docked between the legs of the jacket. By ballasting the barge, the topside can be lowered and connected to the substructure. One advantage of the float-over method is that it allows for the integrated installation of the topside, which reduces the offshore commissioning period. However, this method has a limited operational weather window, which can impact workability [54]. If it is chosen to use a float-over installation, this should be taken into account during the design of the substructure to allow for docking.

It is assumed that a regardless of single lift and modular installation method is used, the topside can be installed on a similar substructure. Because of this reason, only single lift and modular installation is chosen to be considered for this study.

2.11.4. Commissioning

Once all components of the COHP are installed at the designated location, the platform must be connected to the IAC to receive the incoming electricity and to the export pipeline to discharge the hydrogen produced. In addition to these connection activities, all equipment must be tested to verify their proper functioning.

2.11.5. Decommissioning

At the end of the project's lifetime, the COHP requires to be decommissioned. This includes the dismantling of the topside from the substructure and removal of the substructure of the seabed. Both these structures require to be transported to shore once dismantled. The methods used for removal during decommissioning are related to the methods used during the installation.

2.12. Other activities description

The other activities are activities related to refers to the non-physical costs associated with a project. Three main other activities are distinguished. First, the engineering, procurement, construction, and management (EPCm). This cost factor includes all the costs made during the designing, engineering, and acquisition of goods and services from external sources. Owner costs are costs made for in the form of permits, licensing fees, and training of staff. Finally, contingency costs are expenses incurred proactively for a usage that might not materialise [35].

2.13. Overview of preliminary design choices

During the first stages of this study, a preliminary design was made. Table 2.2 outlines the potential design choices for the COHP, as discussed in this chapter, and distinguishes between those that are and those that are not considered for the remainder of this study. Additionally, the table indicates the corresponding section in which each design choice is elaborated on.

Aspect	Considered	Not considered	Section
Electrolysis	AE, PEME	DSE, AEME, SOE	Section 2.2
Compressors	Reciprocating piston	Centrifugal	Section 2.6
Substructure	Jacket	Gravity based, Floating	Section 2.8
Foundation	Piles	Suction caissons	Section 2.9
Transmission	New pipeline	Reusing pipeline, Shipping	Section 2.10
Installation	Single lift, Modular	Float-over	Section 2.11

Table 2.2: Overview of preliminary design choices.

Part I

Techno-economic analysis

3

Model set-up and modelling

The following chapter addresses the modelling of the different components and aspects. First, in section 3.1, a visualisation of the techno-economic model is presented, illustrating the relation between all different submodels. Then, in Section 3.2, the economic modelling methods are given and in Section 3.3, the hydrogen production model is presented. After the main model is discussed in the first three sections, the aspect-bound submodels are each presented in their own section. All submodels are addressed according to the same structure. First, the input and output parameters are presented in a table. The input parameters are divided into case-dependent, variable, and fixed parameters. Hereafter, the modelling methods to derive the outputs from the inputs are shown and finally the case-independent, fixed parameters, are given.

The submodels are presented in the following sequence. First, the wind farm submodel is discussed in Section 3.4. Subsequently, the HPU unit submodels are addressed, starting with the stacks in Section 3.5. Hereafter, the electrical equipment, water treatment equipment, gas conditioning equipment, and compressors are presented in Sections 3.6, 3.7, 3.8 and 3.9, respectively. The super-, substructure, and foundation submodels are discussed in Section 3.10, 3.11, and 3.12. The final submodel related to a material component is the hydrogen transmission submodel, addressed in 3.13. Finally, the submodels related to the activities are presented. Section 3.14 presents the transport, installation and commissioning submodel, and the submodel related to the other activities is discussed in Section 3.15.

3.1. Techno economic model overview

Figure 3.1 illustrates the interrelationships between the various submodels. Each block represents a submodel, which is described in more detail later in this chapter. Six different relationships are depicted, distinguished by colour. The purple (dotted) line represents the inputs. The blue (dash-dotted) line represents hydrogen production including the efficiencies, mass flows, losses, and availabilities of the different subsystems. The green (long-dashed) and orange (short-dashed) lines represent the CAPEX and OPEX, respectively. The red (dash-dot-dotted) line represents mass and the black (solid) represents the totals.

Submodels represented by square blocks refer to material components, which have specific mass, dimensions, CAPEX, OPEX, and performance characteristics. Ovals are used for non-material concepts, which only affect the overall system CAPEX. Diamonds represent system totals. The model is structured in this way to allow for the assessment of the impact of different design choices, taking into account the interdependencies between the components.

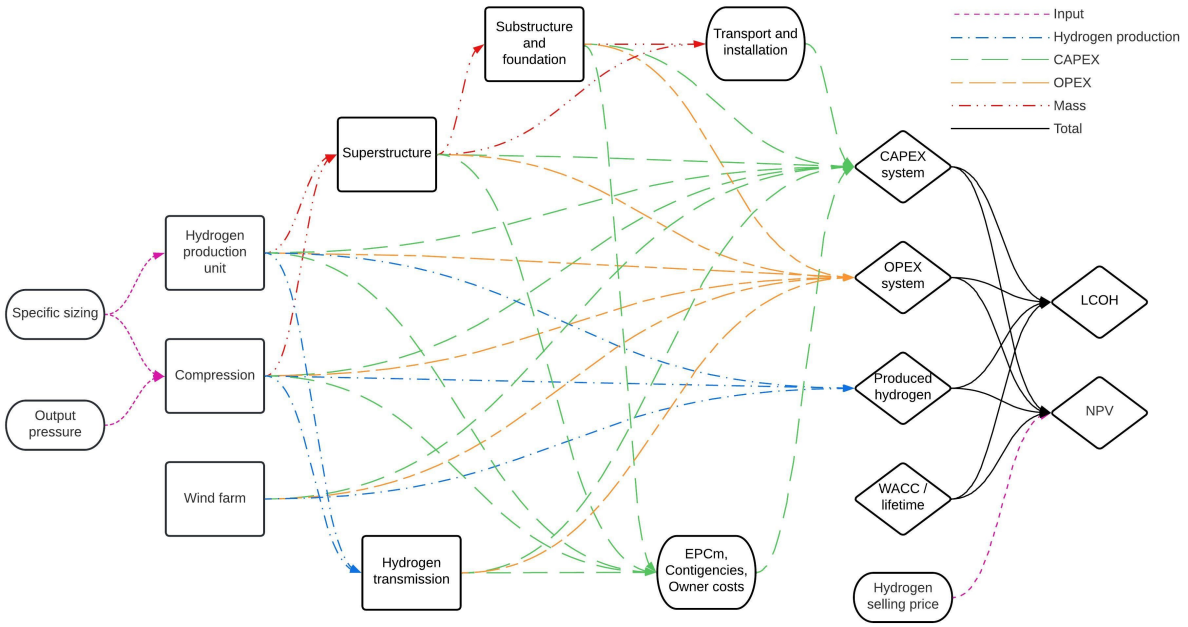

Figure 3.1: Visualisation of the relations of all system components and project aspects.

3.2. Economic modelling

The following section is related to economic modelling. First, Subsection 3.2.1 addresses the equation used to calculate the LCOH. Next, Subsection 3.2.2 is dedicated to the net present value (NPV). Finally, Subsection 3.2.3 addresses the economies of unit scale.

3.2.1. Levelized costs of hydrogen

Once all the CAPEX, OPEX, and system performances are determined, the LCOH is calculated according to Equation 3.1. The LCOH measures the average cost of generating one kilogram of hydrogen over the project's lifetime and takes into account the time value of money.

$$LCOH = \frac{\sum_{y=0}^{Lt}(CAPEX_{tot}(y) + OPEX_{tot}(y)) \cdot (1 + WACC)^{-y}}{\sum_{y=0}^{Lt} AHP(y) \cdot (1 + WACC)^{-y}} \tag{3.1}$$

Here, $CAPEX_{tot}(y)$ represents the capital expenditure in year y of the total wind-hydrogen system. The OPEX of the total wind-hydrogen system in year y, is represented by $OPEX_{tot}(y)$. The hydrogen production during a given year is represented by $AHP(y)$. Finally, the weighted average cost of capital (WACC) is denoted by $WACC$. For simplicity, it is assumed that all initial investments are done in year 0. The total lifetime of the project is depicted by Lt.

3.2.2. Net present value

The Net Present Value (NPV) is a measure of the value of a series of future cash flows. It is determined by applying the WACC to the predicted future cash flows to determine their present value. This approach is often used to assess a project's viability and prospective profitability. The NPV is calculated by subtracting the total system CAPEX of the first year from the sum of the cash flows over all operational years, according to Equation 3.2. In this equation, SP_{H_2} is the hydrogen selling price.

$$NPV = \left[\sum_{y=0}^{Lt} \frac{AHP(y) \cdot SP_{H2} - (OPEX_x(y) + CAPEX_x(y))}{(1 + WACC)^y}\right] - CAPEX_x(0) \tag{3.2}$$

3.2.3. Economies of unit scale

It is assumed that the total installed capacity or quantity of a given component affects the price per unit of installed capacity or quantity. This phenomenon is referred to as economies of unit scale [55]. The cost of a certain capacity or quantity of a given component, affected by the economies of unit scale, is determined according to Equation 3.3.

$$C_{new} = C_{ref} \cdot \left(\frac{Q_{new}}{Q_{ref}} \right)^{S_f} \tag{3.3}$$

Here, C_{ref} represent the reference costs and Q_{ref} the reference quantity. C_{new} presents the costs of the new quantity, presented by Q_{new}. The new quantity or size is scaled according to a scaling factor S_f. Each material component of the COHP has its scale factor. A scale factor closer to one implies fewer economies of unit scale.

3.3. Hydrogen production modelling

The model to calculate hydrogen production from kinetic energy is elaborated on in the following section. First, the choice to use a model based on statistical data instead of time series data is discussed in Subsection 3.3.1. Then, in Subsection 3.3.2 the hydrogen production model is presented.

3.3.1. Model type choice

Models to convert incoming energy to produced hydrogen can be differentiated by the type of data used as input. There are models that work based on time series data versus models that work based on statistical probability data. Translated to the context of this project, that is the wind speed observed at a given interval versus the annual probability of a given wind speed.

A time series model allows for an interval-by-interval analysis of the system performance. This enables the examination of the effects of changes in power input and the system's response to these fluctuations. Additionally, the system efficiency at each point in time, influenced by the load, can be obtained using such model.

It is crucial to select a wind data set that is representative of the entire lifetime of a project to accurately perform a techno-economic analysis. Using a data set that only spans a short period, may result in biased results due to potentially favourable or unfavourable conditions during that time. Instead, a data set with a duration that accurately reflects the chosen location should be used. While a multi-year time series data set may be a better representation, the use of such a data set requires a large amount of computing power. The solution to this would be to use the multi-year data set, sampled at larger intervals. However, this has the consequence that the results obtained no longer reflect what was initially the reason for choosing a time-series model. Besides, the use of an integrated system in the COHP necessitates a more complex control strategy compared to the use of modular stacks. Such control strategy influences the behaviour of the system, and therefore the obtained results, and is currently not known. For these reasons, it is decided to use a hydrogen production model based on statistical data of wind speed occurrences. Statistical data ensures that representative data of a long period can be used, without adverse consequences in terms of simulation duration.

3.3.2. Hydrogen production model

Table 3.1 presents the input and output parameters of the hydrogen production model.

Case parameter	Variable parameter	Fixed parameter	Output
Wind speed distribution	OWF availability	Higher heating value	Hydrogen mass flow
Power curve	OWF efficiency	COHP availability	Annual H_2 production
WTE consumption	Stack SoP	Stack efficiency	
GCE consumption	IAC losses	Electrical losses	
COM consumption			

Table 3.1: Input and output parameters overview of the hydrogen production submodel.

The annually produced hydrogen by the COHP is calculated according to the flowchart as presented in Figure 3.2. The model is run over all wind speed bins, starting with the first bin. The wind speed U_{bin} of the respective bin is fed to the model in the "wind speed" input block. The wind speed is used to calculate the wind farm power using the farm representing deterministic power curve $f_{OWF}()$. This implies that the losses due to wake effects are accounted for. By considering the year-dependent offshore wind farm performance $\eta_{OWF,y}$, year-dependent offshore wind farm availability $A_{OWF,y}$ and power losses in the IAC cables P_{IAC}, the instantaneous power as delivered to the platform $P_{i,OWF}$ is determined, Equation 3.4.

$$P_{i,OWF} = f_{OWF}(U_{bin}) \cdot A_{OWF,y} \cdot \eta_{OWF,y} - P_{IAC} \tag{3.4}$$

The instantaneous offshore wind farm power delivered to the platform is compared to the installed HPU capacity $P_{r,HPU}$, as presented Equation 3.5. If the installed HPU capacity is larger than the instantaneous delivered offshore wind farm power, the power used by the HPU, $P_{i,HPU}$, equals the instantaneous delivered offshore wind farm power. However, if the HPU capacity is lower than the instantaneous delivered offshore wind farm power, the power used by the HPU is equal to the installed HPU capacity. As a result, there is a power surplus. This power surplus is equal to the instantaneous offshore wind farm power, minus the installed HPU capacity. By multiplying the surplus power by the annual hours of the respective wind speed bin, the bin-specific amount of surplus power is calculated.

$$P_{i,HPU} = \begin{cases} P_{i,OWF}, & \text{if } P_{i,OWF} < P_{r,HPU} \\ P_{r,HPU}, & \text{if } P_{i,OWF} \geq P_{r,HPU} \end{cases} \tag{3.5}$$

The next step is to determine what part of the power instantaneously delivered to the HPU will be used as feedstock for the stacks $P_{i,ELE}$ and what part will be used to operate the other components of the system, through iteration. The auxiliary power consumption is subtracted from the power delivered to the HPU to calculate the power intended for the stacks, according to Equation 3.6.

$$P_{i,ELE} = P_{i,HPU} - P_{i,EEQ} - P_{i,WTE} - P_{i,GCE} - P_{i,COM} \tag{3.6}$$

Here, the losses occurring in the electrical equipment are denoted by $P_{i,EEQ}$. The power consumed by the water treatment equipment, gas conditioning equipment, and compressors are denoted by $P_{i,WTE}$, $P_{i,GCE}$, and $P_{i,COM}$, respectively. The massflow of hydrogen, $\dot{m}_{H2}$, is calculated according to Equation 3.7.

$$\dot{m}_{H2} = \frac{P_{i,ELE} \cdot \eta_{ELE,HHV}}{HHV} \tag{3.7}$$

Here, $\eta_{ELE,HHV}$ denotes the stack higher heating efficiency and HHV the hydrogen higher heating value. It was decided to use a load-independent stack initial stack efficiency. The small difference in efficiency at peak efficiency and nominal capacity suggests that the choice to exclude load-dependent efficiency will not affect the results obtained. This is supported by the almost linear relationship between hydrogen output and power input, as observed in Figure 2.4. Using a load-independent value for initial stack efficiency is a method found in comparable techno-economic studies where the time-specific system response is less of influence [6][14][56]. The massflow of hydrogen delivered by the stacks is multiplied by the annual probability of the respective wind speed bin, Π_{bin}, to calculate nominal annual hydrogen production per wind speed bin, $AHP_{nom,bin}$, Equation 3.8.

$$AHP_{nom,bin} = \Pi_{bin} \cdot 8760 \cdot \dot{m}_{H2} \tag{3.8}$$

To calculate the real annual hydrogen production per wind speed bin $AHP_{real,bin}$, the nominal annual hydrogen production per wind speed bind is multiplied by the COHP availability, A_{COHP}, and decreasing stack performance $SoP_{ELE}(y)$, Equation 3.9.

$$AHP_{real,bin} = AHP_{nom,bin} \cdot A_{COHP} \cdot SoP_{ELE}(y) \tag{3.9}$$

Once the hydrogen production of a respective wind speed bin in a given year is calculated, the wind speed and annual probability of the next wind speed bin are fed to the model and the process is repeated.

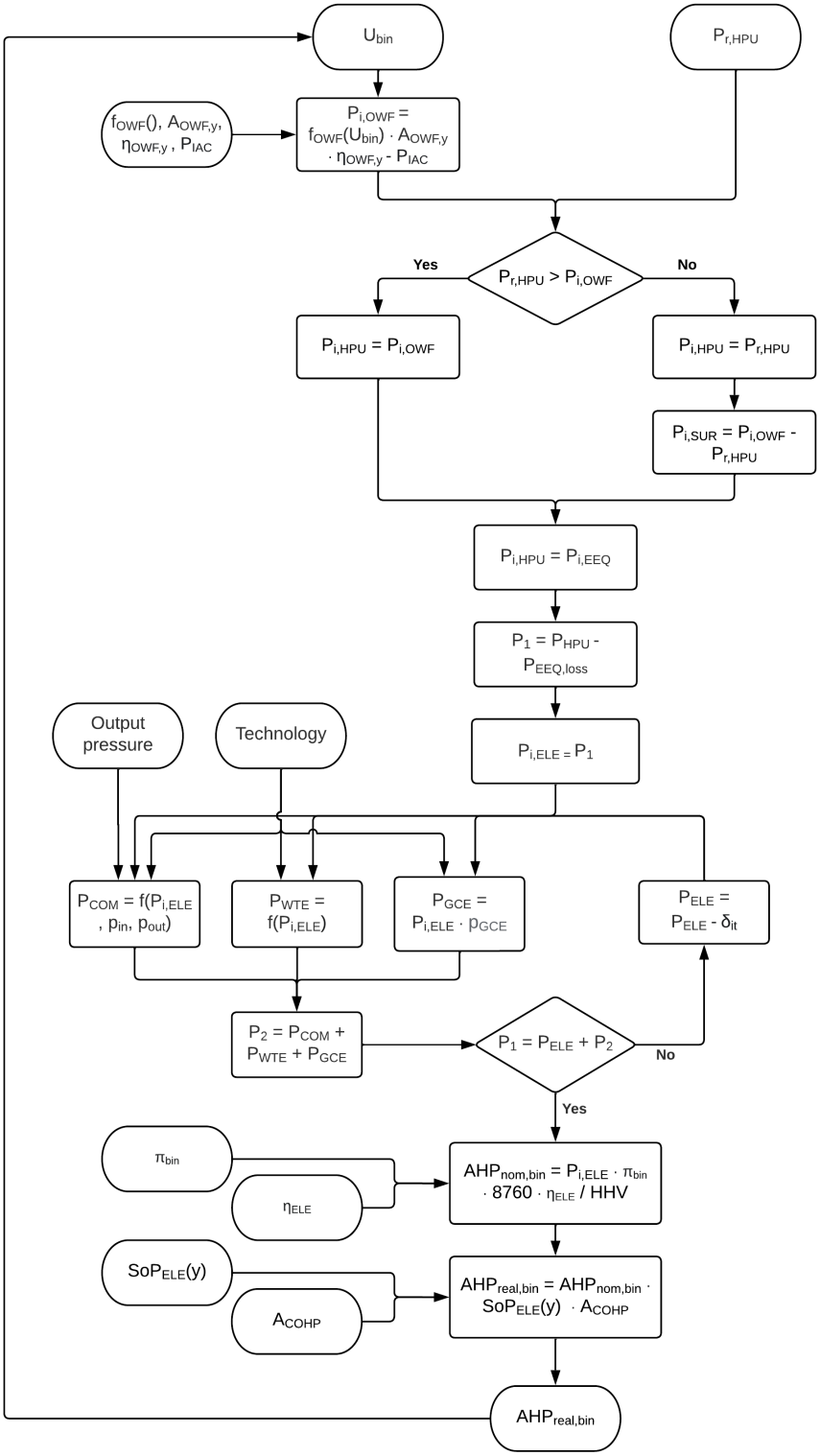

Figure 3.2: Flowchart used to determine hydrogen production per wind speed bin, ovals represent inputs and outputs, squares represent actions and diamonds represent logic.

3.4. Wind farm modelling

Table 3.2 presents the input and output parameters for the offshore wind farm submodel.

Case parameter	Variable parameter	Fixed parameter	Output
Installed capacity	Year of operation	Annual degradation	OWF availability
		Decrease availability	OWF efficiency
		Specific CAPEX	OWF CAPEX
		OPEX factor	OWF OPEX

Table 3.2: Input and output parameters overview of the offshore wind farm submodel.

3.4.1. Offshore wind farm performance

Over the life of the wind farm, the performance of the wind farm decreases, both in annual yield and nominal power. Reasons for this are the decline in aerodynamic and mechanical efficiency, and decreasing availability [20]. Both the reduction in nominal power production and reduced annual availability of the wind farm are taken into account. The availability and conversion efficiency are taken as the average of the availability and conversion efficiency at the start and end of a given year and are assumed to be constant over that year. Furthermore, it is assumed that the conversion efficiency is constant for each wind speed and therefore each load.

Every 6th year there is a major maintenance campaign, increasing the performance of the wind farm. However, after this campaign, the initial conversion efficiencies are not reached, simply because of the ageing of the components [21]. It is chosen that only half of the lost conversion performance of the farm is recovered during such campaign. The conversion efficiency for a given year, $\eta_{OWF}(y)$, is calculated according to Equation 3.10.

$$\eta_{OWF}(y) = \eta_{OWF,0} \cdot (1 - \eta_{OWF,loss})^y \tag{3.10}$$

Here, $\eta_{OWF,0}$ is the initial offshore wind farm performance and $\eta_{OWF,loss}$ the annual offshore wind farm performance degradation. The availability of the wind farm for a certain year is calculated according to Equation 3.11.

$$A_{OWF}(y) = A_{OWF,0} \cdot (1 - A_{OWF,loss})^y \tag{3.11}$$

Here, $A_{OWF,0}$ is the initial offshore wind farm availability and $A_{OWF,loss}$ annual loss in offshore wind farm availability [21].

3.4.2. Offshore wind farm costs

The offshore wind farm CAPEX, C_{OWF}, is assumed to be a linear relationship between the installed offshore wind farm capacity, $P_{r,OWF}$, and the specific offshore wind farm costs, c_{OWF}, according to Equation 3.12. The offshore wind farm CAPEX is made up of all initial costs related to the offshore wind farm, and therefore includes the installed cost WTG and the IAC. The annual offshore wind farm OPEX is calculated according to Equation 3.13 using the OPEX factor, $f_{OPEX,OWF}$.

$$C_{OWF} = P_{r,OWF} \cdot c_{OWF} \tag{3.12}$$

$$OP_{OWF} = C_{OWF} \cdot f_{OPEX,OWF} \tag{3.13}$$

3.4.3. Offshore wind farm model constants

Table 3.3 presents the fixed farm parameters.

Parameter	Symbol	Value	Unit	Source
Initial availability	$A_{OWF,0}$	X	%	[21]
Annual availability decrease	$A_{OWF,loss}$	X	%/year	[21]
Initial performance	$\eta_{OWF,0}$	100.0	%	[21]
Annual conversion degradation	$\eta_{OWF,loss}$	X	%/year	[21]
Specific costs	c_{OWF}	X	€/kW	[57]
OPEX factor	OP_{OWF}	3.2	%	[58]

Table 3.3: Model constants of the offshore wind farm submodel

3.5. Stack modelling

Table 3.4 presents the input and output parameters of the stack submodel.

Case parameter	Variable parameter	Fixed parameter	Output
Installed capacity	Operational time	Specific CAPEX	Stack SoP
	Annual energy	OPEX factor	Stack CAPEX
		Stack efficiency	Stack OPEX
		Degradation	Stack mass
		Lifetime stack	Minimal replacements
		Scale factor	Replacement costs
		Replacement factor	

Table 3.4: Input and output overview of the stack submodel

3.5.1. Stack performance

With ageing, the performance of the stacks decreases, influencing the annual hydrogen production. The state of performance of the stacks is determined according to Equation 3.14.

$$SoP(y) = (1 - \delta_{ELE})^{Ot/1000} \tag{3.14}$$

Here, $SoP(y)$ is the state of performance of the stacks in year y, δ_{ELE} the degradation of per 1000 hours, and Ot the operational time of the stack. It is decided to let the degradation depend on the operational time instead of the total project time. This choice was made because literature is currently not unequivocal about whether what the reasons for this degradation are. The identified reasons for degradation stem from activities that are associated to operation like the impurities of the feed in water and high over-potentials [59]. The operational time of the stacks is calculated by summation of the full load hours (FLH) of the stacks of the previous years. The annual FLH of the stacks is determined according to Equation 3.15. The annual FLH of the stacks decreases due to the diminishing performance of the offshore wind farm. The state of performance is taken as the average of the state of performance at the start and at the end of the year, for a given year, and is assumed to be constant over that year.

$$FLH_{ELE}(y) = \frac{E_{ELE}(y)}{P_{r,ELE}} \tag{3.15}$$

Here, $E_{ELE}(y)$ represents the annual energy supplied to the stack. The calculation of the FLH is based on the annual energy supplied rather than the annual hydrogen production since the annual hydrogen production decreases due to the declining performance of the stacks. Because of these declining performances, the stacks will be replaced over time to revive the performance of the total wind-hydrogen system. The minimum number of times the stacks needs be replaced, n_{rep}, depends

on the annual FLH of the stacks and the predetermined lifetime of the stacks, Lt_{ELE}, as per Equation 3.16. The minus one is added to account for the initially installed stacks.

$$n_{rep} = \left\lceil \frac{\sum FLH_{ELE}(y)}{Lt_{ELE}} \right\rceil - 1 \tag{3.16}$$

It is not possible to replace the stack fewer times than the minimum number of replacements. However, it is possible to replace the stacks more often than the minimum number of replacements. Such a replacement strategy could be advantageous when the costs incurred during replacement are less than the cost of revenue due to the higher hydrogen production resulting from better-performing stacks.

It is decided to operate the different stacks for an equal number of years. The alternative would be to operate the stacks until they reach their maximum number of operational hours, before replacing them with new stacks. However, in most cases this would cause the stacks that would operate for the latter part of the project lifetime, to operate for a shorter time than the earlier installed stacks. This creates a more unfavourable distribution of the state of performance of the stacks. Because of this approach, the total degradation of a stack before replacement will depend on the total number of replacements and the FLHs of the stack, influenced by the installed HPU capacity. Figure 3.3 presents a visualisation of the stack state of performance over time for different replacement strategies. It must be noted that this graph is only a representation of the effect of the number of replacements and an example of the total degradation before stack replacement.

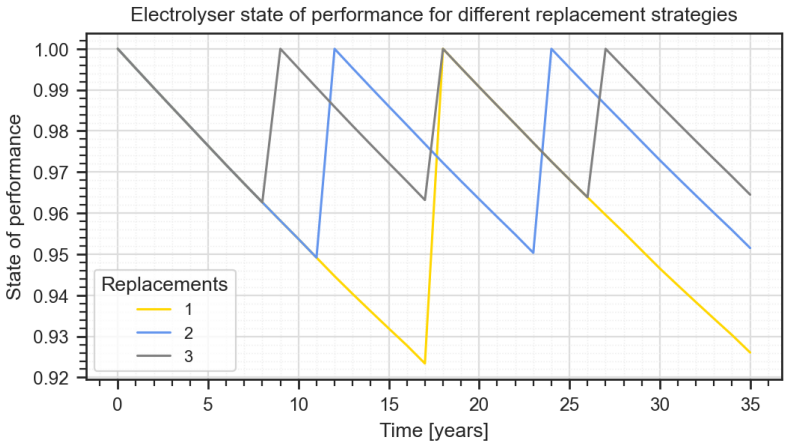

Figure 3.3: Visualisation of the state of performance of the stacks over time, for different replacement strategies. AE-based system at HPU capacity of 950 MW.

3.5.2. Stack costs and mass

The stack CAPEX is calculated trough a linear relation with the installed capacity, in Equation 3.17 and corrected for economies of unit scale by Equation 3.3. The stack CAPEX, C_{ELE}, is calculated according to Equation 3.17. Here, $P_{r,ELE}$ is the installed stack capacity and c_{ELE} is the specific stack costs. The annual stack OPEX is calculated according to Equation 3.18, using the OPEX factor $f_{OPEX,ELE}$.

$$C_{ELE} = c_{ELE} \cdot P_{r,ELE} \tag{3.17}$$

$$OP_{ELE} = C_{ELE} \cdot f_{OPEX,ELE} \tag{3.18}$$

The replacement of the stacks adheres costs. These replacement costs, C_{rep}, comprise both the cost of the uninstalled equipment and the activities to reinstall the new stacks.

$$C_{rep} = (C_{ELE} + C_{EPCm,stack} + C_{cont.,stack}) \cdot f_{rep} + C_{TIC,stack} \tag{3.19}$$

The stack CAPEX C_{ELE}, EPCm $C_{EPCm,stack}$, and contingencies $C_{cont.,stack}$ are corrected by the replacement factor, f_{rep}, to account for development and learning [6][60]. $C_{TIC,stack}$ represents the transportation, installation and offshore commissioning of the newly installed stacks.

The mass of the stacks is calculated according to Equation 3.20. Here, m_{ELE} is the mass of the stacks and k_{ELE} the specific mass of the stack.

$$m_{ELE} = k_{ELE} \cdot P_{r,ELE} \tag{3.20}$$

3.5.3. Stack model constants

Table 3.5 presents the fixed input parameters for the two different stack technologies. Publicly and internally available information regarding the mass of hydrogen production equipment is very limited. Therefore, it was not possible to assess the mass per installed capacity of the stacks individually. The specific mass shown in Table 3.5 represents the mass of the water treatment equipment, stacks, and gas conditioning equipment.

Parameter	Symbol	PEME value	AE value	Unit	Source
Specific costs	c_{ELE}	154	100	€/kW	[35]
OPEX factor	$f_{OPEX,ELE}$	2.0	4.0	%	[13]
Stack efficiency	η_{ELE}	80	80	%	[35]
Degradation	δ_{ELE}	0.12	0.10	%/1000h	[38]
Lifetime	Lt_{ELE}	75000	90000	h	[13] [61]
Scale factor	$S_{f,ELE}$	0.89	0.89	[-]	[62]
Replacement factor	C_{rep}	60.0%	60.0	[%]	[60]
Replacement activities	$C_{TIC,stack}$	40.0	40.0	M€	Estimate
Specific mass	k_{ELE}	5.65	11.30	kg/kW	[35] [63]

Table 3.5: Model constants of the stack submodel.

3.6. Electrical equipment modelling

Table 3.6 presents the input and output parameters for the electrical equipment (EEQ) submodel.

Case parameter	Variable parameter	Fixed parameter	Output
Installed HPU capacity	Instantaneous power	Power loss factor	EEQ losses
		Specific costs	EEQ CAPEX
		Scale factor	EEQ OPEX
		OPEX factor	EEQ mass
		Mass factor	

Table 3.6: Input and output overview of electrical equipment submodel.

3.6.1. Electrical equipment performance

The power losses occurring in the electrical equipment, $P_{EEQ,loss}$, are determined according to Equation 3.21. The power losses are assumed to be constant for each load.

$$P_{EEQ,loss} = P_{i,EEQ} \cdot p_{EEQ,loss} \tag{3.21}$$

Here, $P_{i,EEQ}$ represents the instantaneous power delivered to the electrical equipment and $p_{EEQ,loss}$ the electrical equipment power loss factor.

3.6.2. Electrical equipment costs and mass

The electrical equipment CAPEX, C_{EEQ}, is calculated according to Equation 3.22, by an assumed linear relation with the installed capacity and correction for the economies of unit scale by Equation 3.3. Here, $P_{r,EEQ}$ represents the installed electrical equipment capacity and c_{EEQ} the specific electrical equipment costs. The electrical equipment installed capacity is equal to the HPU capacity. The annual electrical equipment OPEX is calculated according to Equation 3.23, using the OPEX factor $f_{OPEX,EEQ}$.

$$C_{EEQ} = P_{r,EEQ} \cdot c_{EEQ} \tag{3.22}$$

$$OP_{EEQ} = C_{EEQ} \cdot f_{OPEX,EEQ} \tag{3.23}$$

The mass of the electrical equipment, m_{EEQ}, is calculated according to Equation 3.24. Here, $P_{r,EEQ}$ represents the installed capacity of the electrical equipment and k_{EEQ} the specific mass.

$$m_{EEQ} = P_{r,EEQ} \cdot k_{EEQ} \tag{3.24}$$

3.6.3. Electrical equipment model constants

The fixed input parameters for the electrical equipment submodel are presented in Table3.7. The fixed input parameters are indifferent to a PEME- or AE-based system.

Parameter	Symbol	Value	Unit	Source
Specific costs	c_{EEQ}	140	€/kW	[35]
OPEX factor	$f_{OPEX,EEQ}$	3.0	%	[6]
Specific mass	k_{EEQ}	5.65	kg/kW	[33]
Power loss factor	$p_{EEQ,loss}$	2.7	%	[35]
Scale factor	$S_{f,EEQ}$	0.75	[-]	[62]

Table 3.7: Model constants of the electrical equipment submodel.

3.7. Water treatment modelling

Table3.8 presents the input and output parameters of the water treatment equipment submodel.

Case parameter	Variable parameter	Fixed parameter	Output
Installed HPU capacity	Hydrogen mass flow	Pump efficiency	Pump power consumption
Avg. seawater elevation		Pump specific power	RO power consumption
Seawater density		RO specific power	DI power consumption
		DI specific power	WTE CAPEX
		Specific costs	WTE OPEX
		Scale factor	
		OPEX factor	
		In-deck height	
		Cool requirements	
		DI Recovery factor	
		RO Recovery factor	

Table 3.8: Input and output overview of the water treatment equipment (WTE) submodel.

3.7.1. Sea water pumps performance

Both the water used as feedstock and for cooling purposes will be pumped from sea level to the desired platform height. However, it is assumed that the water system used for cooling acts like a closed-loop system as the cooling water leaves the COHP again at sea level. Therefore, the static head is not taken into account when calculating the pump power consumption required for the cooling water, since these systems are largely unaffected by static pressure. A closed-loop exhibits only friction losses and thus only dynamic friction losses must be overcome. The instantaneous power required, $P_{i,pump,avg}$, to elevate the water from sea level to the level of its intended use and to overcome the internal friction losses, is calculated according to Equation 3.25.

$$P_{i,pump,avg} = \frac{\dot{m}_{feed} \cdot h_{pump,avg} \cdot g}{\eta_{pump}} + \mu_{cool} \cdot \frac{\dot{m}_{cool} \cdot h_{pump,avg} \cdot g}{\eta_{pump}} \tag{3.25}$$

Where $\dot{m}_{feed}$, is the mass flow rate of the feed-in water and $\dot{m}_{cool}$ the mass flow of the cooling water, h the head, g the gravitational constant, η_{pump} the pump efficiency, and μ_{cool} the internal friction fraction of the cooling system. This friction factor and the cooling pump power requirements are used as it is not possible to calculate the friction losses since this would require the actual design, but the design of the COHP is still in a conceptual phase. Since it is anticipated that the cool water pump requirements are small, it is deemed possible to use this assumption. As the feedwater requirements are significantly smaller than the cooling requirements, the feedwater friction losses are not taken into account. The mass flow of water to be pumped is determined according to Equation 3.27 and 3.26. A linear relationship is assumed between the cooling requirements and the production of hydrogen.

$$\dot{m}_{cool} = \dot{m}_{H_2} \cdot \sigma_{cool} \tag{3.26}$$

$$\dot{m}_{feed} = \frac{\dot{m}_{H_2} \cdot \sigma_{stoi}}{R_{RO} \cdot R_{DI}} \tag{3.27}$$

Here, R_{RO} and R_{DI} are the recovery factor of desalination and deionization equipment in percentage, σ_{cool} the mass flow of cooling water required per mass flow of hydrogen and σ_{stoi} the mass flow of pure water required per mass flow of hydrogen in an ideal reaction. According to the stoichiometric reaction, σ_{ideal} is equal to 8.94 $kg_{H2O/H2}$. The average seawater elevation, $h_{pump,avg}$, is calculated using the deck elevation $h_{elevation,avg}$, as will be seen in Equation 3.47.

$$h_{pump,avg} = h_{elevation,avg} + h_{in-deck} \tag{3.28}$$

3.7.2. Desalination and deionization performance

Dependent on the chosen stack technology, the seawater will be prepared. The use of reverse osmosis (RO) equipment produces water of high enough purity that it can be used directly as feed-in in an AE-based system. The instantaneous RO power consumption, $P_{i,RO}$, is calculated according to Equation 3.29.

$$P_{i,RO} = \frac{\dot{m}_{feed,fresh}}{\rho_{sw} \cdot \cdot R_{RO}} \cdot p_{RO} \tag{3.29}$$

Where $\dot{m}_{feed,fresh}$ is the mass flow of fresh water, ρ_{sw} the density of seawater, and p_{RO} the specific power consumption in. In case of a PEME-based system, extra deionization of the feed-in water is required. The instantaneous power consumption of the deionization equipment, $P_{i,DI}$, is calculated according to Equation 3.30.

$$P_{i,DI} = \frac{\dot{m}_{feed,pure}}{\rho_{fresh} \cdot R_{DI}} \cdot p_{DI} \tag{3.30}$$

Where $\dot{m}_{feed,pure}$ is the mass flow of desalinated water, ρ_{fresh} the density of the fresh water, and p_{DI} the specific power consumption of the deionization equipment.

3.7.3. Water treatment costs

The CAPEX of the complete WTE, C_{WTE}, is calculated according to Equation 3.34, by an assumed linear relation with the installed capacity and correction for the economies of unit scale by Equation 3.3. Here, c_{WTE} represents the specific WTE costs and $P_{r,ELE}$ the installed stack capacity. The OPEX of the WTE is calculated according to Equation 3.35, using the OPEX factor $f_{OPEX,WTE}$. The capacity of the WTE is equal to the installed stack capacity.

$$C_{WTE} = P_{r,ELE} \cdot c_{WTE} \tag{3.31}$$

$$OP_{WTE} = C_{WTE} \cdot f_{OPEX,WTE} \tag{3.32}$$

3.7.4. Water treatment model constants

The model constants of the WTE submodel are presented in Table 3.9.

Parameter	Symbol	PEME Value	AE value	Unit	Source
Costs per kW	c_{WTE}	59	48	€/kW	[35]
OPEX factor	$f_{OPEX,WTE}$	2.5	2.5	%	[6]
Scaling factor	S_f	0.6	0.6	[-]	[62]
Pump efficiency	η_{pump}	80.0	80.0	%	[64]
Fresh water density	ρ_{fresh}	1000	1000	kg/m^3	[65]
RO recovery rate	R_{RO}	50.0	50.0	%	[36]
RO specific power rate	p_{RO}	3.0	3.0	kWh/m^3	[36]
DI recovery rate	R_{DI}	90	-	%	[66]
DI specific power	p_{DI}	2.0	-	kWh/m^3	[66]
Cooling water requirements	σ_{cool}	2000	2000	kg_{SW}/kg_{H2}	[67]
Friction factor	μ	0.01	0.01	[-]	Estimate

Table 3.9: Model constants of the WTE submodel.

3.8. Gas conditioning equipment modelling

Table 3.10 presents the input and output parameters of the gas conditioning equipment submodel.

Case parameter	Variable parameter	Fixed parameter	Output
Installed capacity	Instantaneous power	Specific power	GCE power consumption
		Specific costs	GCE CAPEX
		Scale factor	GCE OPEX
		OPEX factor	

Table 3.10: Input and output overview of the gas conditioning equipment (GCE) submodel.

3.8.1. Gas conditioning equipment performance

The power required to operate the gas conditioning equipment, P_{GSE}, is calculated according to Equation 3.33. Here, $P_{i,ELE}$ is the instantaneous power delivered to the stacks and p_{GSE} the specific gas conditioning equipment power consumption. It is assumed that the specific power consumption of the gas conditioning equipment is constant for each load.

$$P_{i,GSE} = P_{i,ELE} \cdot p_{GSE} \tag{3.33}$$

3.8.2. Gas conditioning costs

The CAPEX of the gas conditioning equipment, C_{GCE}, is calculated according to Equation 3.34, by an assumed linear relation with the installed capacity and correction for the economies of unit scale by Equation 3.3. Here c_{GCE} represents the specific gas conditioning equipment costs and $P_{r,ELE}$ the installed stack capacity. The OPEX of the gas conditioning equipment is calculated according to Equation 3.35 using the OPEX factor $f_{OPEX,GCE}$. The capacity of the gas conditioning equipment is equal to the installed stack capacity.

$$C_{GCE} = P_{r,ELE} \cdot c_{GCE} \tag{3.34}$$

$$OP_{GCE} = C_{GCE} \cdot f_{OPEX,GCE} \tag{3.35}$$

3.8.3. Gas conditioning model constants

The fixed input parameters of the gas conditioning equipment submodel are presented in Table3.11.

Parameter	Symbol	PEME Value	AE value	Unit	Source
Specific power	p_{GCE}	0.9	1.0	%	[68]
Specific costs	c_{GCE}	45	40	€/kW$_{GCE}$	[35]
OPEX factor	$f_{OPEX,GCE}$	3.0	3.0	%	[6]
Scaling factor	S_f	0.68	0.73	[-]	[62]

Table 3.11: Model constants of the gas conditioning equipment submodel.

3.9. Compressor modelling

Table 3.12 presents the input and output parameters of the compressor submodel.

Case parameter	Variable parameter	Fixed parameter	Output
COM inlet pressure	Hydrogen massflow	Mechanical efficiency	COM power cons.
COM output pressure	Compression factor	Isentropic efficiency	COM CAPEX
		Specific costs	COM OPEX
		OPEX factor	COM mass
		Specific mass	
		Max. compression ratio	
		Molecular mass	
		Ideal gas constant	
		Hydrogen temperature	

Table 3.12: Input and output overview of the compressor (COM) submodel

3.9.1. Compressor performance

The instantaneous power requirement of the compressors is calculated according to Equation 3.36 [69].

$$P_{i,COM} = n_{stage} \cdot \dot{m} \cdot \frac{R \cdot T_1}{M_W} \cdot \frac{\gamma}{\gamma - 1} \cdot \frac{Z_1 + Z_2}{2} \cdot \frac{1}{\eta_s \cdot \eta_m} \cdot \left[\left(\frac{P_2}{P_1} \right)^{\left(\frac{\gamma - 1}{n_{stage} \cdot \gamma} \right)} - 1 \right] \tag{3.36}$$

Here, n is the number of stages, $\dot{m}$ is the mass flow, R the ideal gas constant, T_1 the temperature at the compressor inlet, M_W the molecular mass of hydrogen, γ the specific heat ratio, Z the hydrogen compression factor at suction (1) and discharge (2), η_n the isentropic compressor efficiency, η_m the mechanical losses of the driver, and P the pressure at the inlet (1) and outlet (2). The compression factors are determined using the CoolProp Python package [70]. The number of stages, n_{stage}, is determined according to the Equation 3.37.

$$n_{stage} = \left\lceil \frac{ln(r_{tot})}{ln(r_{stage})} \right\rceil \tag{3.37}$$

Here, r_{stage} is the maximum compression ratio per stage and r_{tot} the total compression ratio between input and output of the compressor. Further more, it is assumed that there are no hydrogen pressure losses between the stacks and the compressors.

3.9.2. Compressor costs and mass

The CAPEX of the compressors, C_{COM} is calculated according to Equation 3.38. Here, $P_{r,COM}$ is the maximum instantaneous power requirement of the compressors, occurring at the largest hydrogen mass flow. The specific costs of the compressors are denoted by c_{pump}. The annual OPEX is calculated according to Equation 3.39. The mass of the compressors is calculated according to Equation 3.40.

$$C_{COM} = P_{r,COM} \cdot c_{COM,1} + c_{COM,2} \tag{3.38}$$

$$OP_{COM} = C_{COM} \cdot f_{OPEX,COM} \tag{3.39}$$

$$m_{COM} = k_{COM} \cdot P_{r,COM} \tag{3.40}$$

The advantage of utilising equation 3.38 is that the CAPEX for the compressor is proportional to both changing the installed HPU capacity, as well as changing the compressor output pressure.

3.9.3. Compressor model constants

The model constants used in the compressor submodel are presented in 3.13.

Parameter	Symbol	Value	Unit	Source
Specific costs	$c_{COM,1}$	*X*	€/W_{COM}	[41]
Specific costs	$c_{COM,2}$	*X*	M€	[41]
OPEX factor	$f_{OPEX,COM}$	8.0	% of CAPEX	[69]
Mass constant	k_{COM}	*X*	g/W	[41]
Mechanical efficiency	η_m	80.0	%	[69]
Isentropic efficiency	η_s	98.0	%	[69]
Ideal gas constant	R	8.314	J/mol K	[69]
Maximum compression step	r_{stage}	*X*	[-]	[41]
H_2 temperature	T_{H_2}	313	K	[41]
Molecular mass	M_W	2.016	g/mol	[69]

Table 3.13: Model constants of the compressor submodel.

3.10. Superstructure modelling

Table 3.14 presents the input and output parameters of the superstructure submodel. A total of three input parameters is required to obtain three output parameters

Case parameter	Variable parameter	Model constants	Output
Equipment mass		Specific PS mass	Superstructure CAPEX
		Specific SS mass	Superstructure OPEX
		Dynamic load factor	Superstructure mass
		OPEX factor	

Table 3.14: Input and output overview of superstructure submodel.

3.10.1. Superstructure costs and mass

The primary and secondary steel mass is determined according to Equation 3.41 and Equation 3.42. These relations are adapted from the work of DNV [33]. A full detailed breakdown of superstructure costs can be found in Appendix A.1, where the costs for primary steel, grating, cladding, and coating are calculated independently. Since the costs for these components are linearly related to each other, it is possible to represent a simplified form. The DNV report states that the material mass assumptions are in an uncertainty range of $\pm$ 25% and does not mention the effect of dynamic load due to vibrations on the structure. Therefore, a vibration factor, $\epsilon_{dynamic}$, is added.

$$m_{ps,SPS} = m_{HPU} \cdot k_{ps} \cdot \epsilon_{dynamic} \tag{3.41}$$

Where m_{HPU} is the mass of all HPU equipment combined and k_{PS} the primary steel constant. The secondary steel mass of the superstructure is determined according to Equation 3.42

$$m_{ss,SPS} = m_{ps,SPS} \cdot k_{ss} \tag{3.42}$$

The CAPEX of the superstructure, C_{SPS}, is determined according to Equation 3.43. Here, c_{SPS} are the specific costs of the superstructure. The OPEX of the superstructure, OP_{SPS}, is calculated according to Equation 3.44. Here, $f_{OPEX,SPS}$ is OPEX factor.

$$C_{SPS} = c_{SPS} \cdot (m_{ps,SPS} + m_{ss,SPS}) \tag{3.43}$$

$$OP_{SPS} = C_{SPS} \cdot f_{OPEX,SPS} \tag{3.44}$$

3.10.2. Superstructure model constants

Table 3.15 presents the model constants[1] used to determine the mass and costs of the superstructure.

Parameter	Symbol	Value	Unit	Source
PS mass constant	k_{ps}	1.035	kg_{SS}/kg_{HPU}	Adapted from [33]
SS mass constant	k_{ss}	0.498	kg_{PS}/kg_{SS}	Adapted from [33]
Specific costs	c_{SPS}	5.376	k€ ton	Adapted from [33]
Dynamic load factor	$\epsilon_{dynamic}$	1.0	[-]	[72]
OPEX factor	$f_{OPEX,SPS}$	2.0	[%]	[14]

Table 3.15: Model constants of the superstructure submodel.

3.11. Substructure modelling

Table 3.16 presents the input and output parameters for the substructure submodel.

[1] Prices are expressed in January 2022 Euro's. Converted according to: $€_{2018}$ = 1.0635 $€_{2022}$ [71]

Case parameter	Variable parameter	Fixed parameter	Output
Superstructure mass		Specific costs	Substructure CAPEX
Storm surge height		Specific mass	Substructure OPEX
Mean sea level		Air gab	Substructure Mass
Wave crest height		Settlement depth	
Sea level rise			

Table 3.16: Input and output overview of the substructure submodel.

3.11.1. Substructure costs and mass

The substructure holds the topside at an adequate height above the sea surface. The substructure is attached to the seabed. The substructure consists of multiple components, the primary steel, secondary steel, anodes, and coating [42].

Primary steel

The primary steel is dependent on the mass of the topside and jacket height, H_{jacket}. The mass of the primary steel is estimated according to Equation 3.45.

$$m_{PS} = (k_{PS,1} \cdot m_{topside} + k_{PS,2}) \cdot H_{jacket} \tag{3.45}$$

Here, m_{PS} is the mass of the primary steel, $m_{topside}$ the mass of the topside, $k_{PS,1}$ and $k_{PS,2}$ the primary steel constants, and H_{Jacket} the jacket height. The jacket height is calculated according to Equation 3.46.

$$H_{Jacket} = MSL + H_{Elevation} \tag{3.46}$$

Here, MSL is the mean sea level, and $H_{elevation}$ is the elevation of the deck above the mean sea level. The deck elevation is calculated according to Equation 3.47 [73].

$$H_{Elevation} = \frac{H_T}{2} + H_{SS} + H_{WC} + H_{ST} + H_{AG} + H_{SLR} \tag{3.47}$$

Here, H_T is the height of the tide, H_{SS} the height of the storm surge, H_{WC} the height of the wave crest, H_{ST} the depth of settlement, H_{AG} the height of the air gab, and H_{SLR} an additional factor taken into account because of the expected sea level rise. The tide height, storm surge height, and wave crest height are location dependent. The total CAPEX related to the primary steel is determined by multiplying the primary steel mass by the fabricated steel price using Equation 3.48. Where C_{PS}, is the CAPEX of the primary steel and c_{PS} the costs per ton of fabricated primary steel.

$$C_{PS} = m_{PS} \cdot c_{PS} \tag{3.48}$$

Secondary steel

The secondary steel mass, m_{SS}, is dependent on the primary steel mass, according to Equation 3.49. Where $k_{SS,1}$, $k_{SS,2}$ and $k_{SS,3}$ are the primary mass constants. The total secondary steel CAPEX, C_{SS}, is determined according to Equation 3.52.

$$m_{SS} = m_{PS}^2 \cdot k_{SS,1} + m_{PS} \cdot k_{SS,2} + k_{SS,3} \tag{3.49}$$

$$C_{SS} = m_{SS} \cdot c_{SS} \tag{3.50}$$

Anode
The anode mass, m_{Anode}, is dependent on the primary mass, according to Equation 3.51. Where $k_{Anode,1}$ and $k_{Anode,2}$ are the anode mass constants. The anode CAPEX, C_{Anode}, is determined according to Equation 3.52. Where C_{Anode} is the CAPEX of the anode, and c_{Anode} the specific anode costs.

$$m_{Anode} = k_{Anode,1} \cdot m_{PS} + k_{Anode,2} \tag{3.51}$$

$$C_{Anode} = m_{Anode} \cdot c_{Anode} \tag{3.52}$$

Coating
The area to be coated, $A_{Coating}$, is dependent on the primary steel mass as presented in Equation 3.53. Here, $k_{Coating,1}$ and $k_{Coating,1}$ are the variable and fixed coating area parameters. The coating CAPEX, $C_{Coating}$, is determined according to equation 3.54. Here, $c_{Coating}$ are the specific coating costs.

$$A_{Coating} = k_{Coating,1} \cdot m_{PS} + k_{Coating,2} \tag{3.53}$$

$$C_{Coating} = A_{Coating} \cdot c_{Coating} \tag{3.54}$$

Substructure total CAPEX modelling
The total substructure CAPEX is determined by adding all the component's individual CAPEX according to Equation 3.55. The total substructure mass is by summation of the individual substructure components, according to Equation 3.56.

$$C_{SBS} = C_{PS} + C_{SS} + C_{Anode} + C_{Coating} \tag{3.55}$$

$$m_{SBS} = m_{PS} + m_{SS} + m_{Anode} \tag{3.56}$$

3.11.2. Substructure model constants

Table 3.17 presents the constants and prices[2] used in the substructure submodel.

[2]Prices are expressed in January 2022 Euro's. Converted according to: €$_{2018}$ = 1.0635 €$_{2022}$ [71]

Parameter	Symbol	Value	Unit	Source
Settlement dept	H_{ST}	0.1	m	[73]
Airgap	H_{AG}	1.5	m	[73]
Mass constant	$k_{ps,1}$	0.012	ton/(ton m)	[33]
Mass constant	$k_{ps,2}$	7.180	ton/m	[33]
Specific steel costs	c_{ps}	2280	€/ton	[33]
Mass constant	$k_{Sec,1}$	1E-7	ton/ton^2	[33]
Mass constant	$k_{Sec,2}$	0.002	ton/ton	[33]
Mass constant	$k_{Sec,3}$	91.69	ton	[33]
Specific steel costs	c_{Sec}	2850	€/ton	[33]
Mass constant	$k_{Anode,1}$	0.0095	ton/ton	[33]
Mass constant	$k_{Anode,2}$	7.5265	ton	[33]
Specific anode costs	c_{Anode}	137	€/ton	[33]
Mass constant	$k_{Coating,1}$	1.0662	ton/ton	[33]
Mass constant	$k_{Coating,2}$	597.3	ton	[33]
Specific coating costs	$c_{Coating}$	7410	€/ton	[33]

Table 3.17: Model constants of the substructure submodel.

3.12. Foundation modelling

Table 3.18 presents the input and output parameters of the foundation submodel.

Case parameter	Variable parameter	Fixed parameter	Output
Soil type	Substructure mass	Specific costs Specific mass	Pile CAPEX

Table 3.18: Input and output overview of foundation submodel

The pile mass is calculated according to Equation 3.57, as presented in the work of NREL [74]. An additional soil factor, f_{soil} is taken into account. The CAPEX of the piles is calculated according to 3.58.

$$m_{pile} = 8 \cdot m_{jacket}^{k_{pile}} \cdot f_{soil} \tag{3.57}$$

$$C_{pile} = m_{pile} \cdot c_{pile} \tag{3.58}$$

The fixed input parameters of the foundation submodel are presented in Table 3.19.

Parameter	Symbol	Value	Unit	Source
Specific costs	c_{pile}	2.132	k€/ton	[33]
Specific mass	k_{pile}	0.5574	kg/kg	[74]
OPEX factor	f_{OPEX}	2.0	% of CAPEX	[34]

Table 3.19: Model constants of the foundation submodel

3.13. Hydrogen transmission modelling

Table 3.20 presents the input and output parameters of the hydrogen transmission submodel.

Case parameter	Variable parameter	Fixed parameter	Output
Hydrogen input pressure		Material costs	Transmission CAPEX
Hydrogen offtake pressure		OPEX factor	Transmission OPEX
Distance to shore			
Max. H_2 mass flow			

Table 3.20: Input and output overview of the transmission submodel

A model present within Vattenfall will be used to assess the CAPEX, C_{HTS}, of the transmission system [75]. Given that the model is implemented rather than constructed, the equations used in the model are not provided. The input parameters are the inlet pressure at the start of the pipeline, required offtake pressure at the end of the pipeline, maximum hydrogen mass flow, and the distance to shore. The model calculates subsequently the required minimum pipeline diameter, based on the pressure drop, which is calculated as an intermediate step. Furthermore, it must be noted that only whole inches of diameter are considered. The minimum required pipeline diameter is used to calculate the hydrogen transmission CAPEX.

Figure 3.4 presents the required pipeline diameter versus the input pressure for a pipeline length of 100 km, at a hydrogen mass flow of 19 tonnes per hour, assuming an offtake pressure of 10 bar, for a PEME based system.

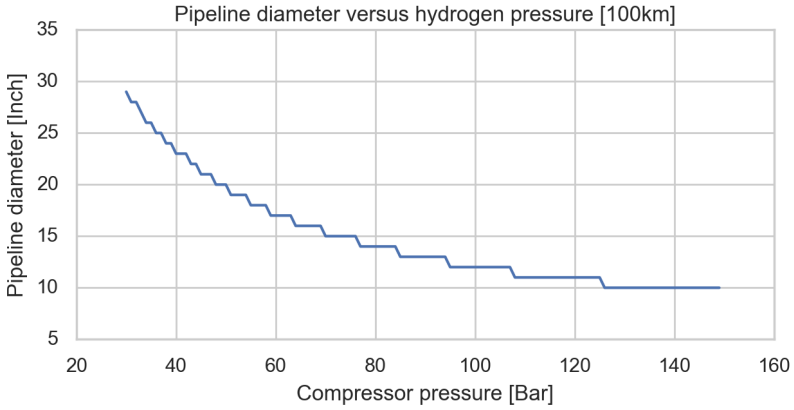

Figure 3.4: Pipeline diameter versus hydrogen pressure.

Figure 3.4 presents that an increase in pressure at the hydrogen transmission system inlet, leads to a decrease in minimum required pipeline diameter. This was described in the work of DNV [33]. The effect of the first compression steps is larger than that of the larger compression steps. Figure 3.5 presents the associated transmission CAPEX.

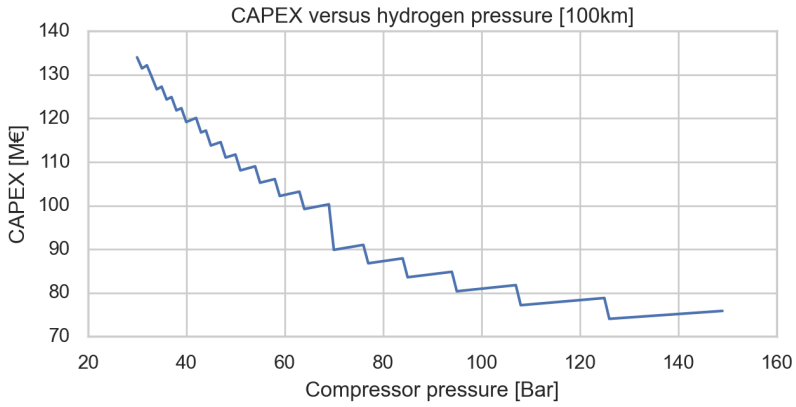

Figure 3.5: Transmission CAPEX for different output pressures.

With each decrease in pipeline diameter, the hydrogen transmission system CAPEX decreases as well. However, when increasing hydrogen pressure, but remaining at the same diameter, the pipeline CAPEX increases, as a more expensive material is required to be used to handle this increased pressure. A relatively larger jump in CAPEX is made around 70 bar of inlet pressure. Due to the decrease in pipeline diameter, a different less expensive, installation method could be used. The OPEX of the transmission system is determined according to Equation 3.59.

$$OP_{HTS} = C_{HTS} \cdot f_{OPEX,HTS} \tag{3.59}$$

The fixed input parameters of the transmission submodel are presented in Table 3.21.

Parameter	Symbol	Value	Unit	Source
OPEX factor	$f_{OPEX,HT}$	2.0	%	[76]

Table 3.21: Model constants of the transmission submodel

3.14. Transport, installation and commissioning modelling

Since the activities performed during the transport, installation, and commissioning of the COHP are interrelated, it was chosen to include them in a single submodel. Table 3.22 presents the input and output parameters of the transport, installation, and commissioning submodel.

Case parameter	Variable parameter	Fixed parameter	Output
Superstructure mass		Vessel day rates	TIC CAPEX
Substructure mass		Action time	Decommissioning costs
Transport time			

Table 3.22: Input and output overview of the transport, installation, and commissioning (TIC) submodel

The CAPEX expenditure of the transportation and installation of the platform is calculated through a commonly used method, using the day rates of the used vessels and the time certain activities require. The vessel choice and the actions to be taken depend on the mass of the topside and substructure. However, it is assumed that an increase in the mass of the topside and substructure, when staying within the lifting capacity of a given vessel, increases the transport, installation, and commissioning CAPEX negligibly [53]. Six different transportation and installation methods are proposed, depending

on the mass of the topside and substructure, presented in Table 3.23. In methods 1 and 4, a single-lift installation using the Sleipnir is performed. In methods 2 and 5 a single-lift installation using the Pioneering Spirit is performed, and in methods 3 and 6, a modular lift installation. This modular installation is required when the mass of the topside exceeds the lifting capacity of the proposed vessels.

Method	$m_{topside} < L_{SL}$	$L_{SL} < m_{topside} < L_{PS}$	$m_{topside} > L_{PS}$
$m_{substruc} < L_{vessel}$	1	2	3
$m_{substruc} > L_{vessel}$	4	5	6

Table 3.23: Methods of transport and installation.

The total transport, installation, and commissioning CAPEX, C_{TIC} consists of four different components and is calculated according to Equation 3.60.

$$C_{TIC} = C_{trans} + C_{instal} + C_{piling} + C_{comm} \tag{3.60}$$

In the Equation, C_{trans} represents the transportation CAPEX, C_{instal} presents the installation CAPEX, C_{piling} the piling CAPEX, and C_{comm} the commissioning CAPEX.

3.14.1. Transport modelling

The transport CAPEX is calculated according to Equation 3.61.

$$C_{trans} = DR_{vessel} \cdot (T_{mob} + (1 + n_{trips}) \cdot T_{loading} + (1 + 2n_{trips}) \cdot T_{dist} + T_{wait} + T_{demob}) \tag{3.61}$$

Here, T_{mob} and T_{demob} represent the mobilisation and demobilisation time, $T_{loading}$ represents the time required to load the topside section or substructure from the docks to the vessel, T_{dist} the time required to travel the distance between the harbour and the designated location, T_{wait} the time the vessel has to wait, and n_{trips} the number of trips the vessel needs to make to install all sections of the topside. If the topside is installed using a single lift installation, n is equal to 1. Otherwise, the amount of trips is calculated using Equation 3.62. It is assumed that after the final instalment procedure, the installation vessel is not required to sail back to the harbour but starts its demobilisation.

$$n_{trips} = \left\lceil \frac{M_{topside}}{L_{SL}} \right\rceil \tag{3.62}$$

The costs associated with the mobilisation and demobilisation of the used vessel is taken into account in the transport CAPEX.

3.14.2. Installation modelling

The CAPEX associated with installing all components of the COHP is divided into two parts, the installation of the piles and the substructure and the topside. For each method, the piles are assumed to be installed similarly, using a crane vessel. The pile installation CAPEX is calculated according to Equation 3.63.

$$C_{piling} = DR_{CV} \cdot (T_{mob} + T_{piling} + T_{demob}) \tag{3.63}$$

Here. DR_{CV} represents the day rate of the crane vessel, and T_{mob}, T_{piling} and T_{demob} the time required for mobilisation, piling and demobilisation. The installation of the topside and substructure is method-dependent and is calculated according to Equation 3.64.

$$C_{instal} = DR_{vessel} \cdot (T_{substruc} + n_{trips} \cdot T_{topside}) \tag{3.64}$$

Here, $T_{substruc}$ is the time required to install the substructure. This includes the horizontal levelling of the legs. The time required to install the topside is denoted by $T_{topside}$.

3.14.3. Commissioning modelling

Once all components of the COHP are installed at the designated location, the platform must be connected to the IAC to receive the incoming electricity and to the export pipeline to discharge the hydrogen produced. In addition to these connection activities, all equipment must be tested to verify their proper functioning. All these actions are considered as commissioning CAPEX. The commissioning CAPEX is determined according to Equation 3.65 [77].

$$C_{comm} = \begin{cases} f_{comm,modular} * C_{HPU}, & \text{if installation is modular} \\ f_{comm,singlelift} * C_{HPU}, & \text{if installation is single lift} \end{cases} \tag{3.65}$$

Here, C_{HPU} is the is the capital expenditure of the HPU and $f_{comm,x}$ is the commissioning factor. A distinction is made between commissioning a platform that is single-lift installed or modular installed. This is because, after a modular installation, the different modules will be connected offshore to complete the full commissioning. Using a single lift installation, most of the commissioning is performed onshore, which is significantly less cost-intensive [53]. The transport, installation, and commissioning CAPEX per method is shown in Figure 3.6.

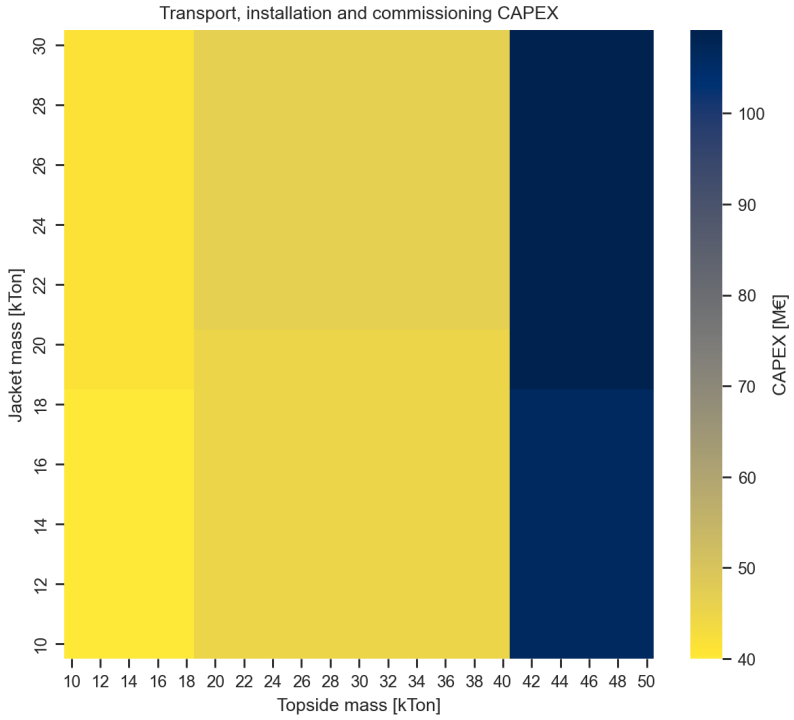

Figure 3.6: Transport and installation CAPEX for different topside and substructure masses.

3.14.4. Decommissioning

The costs for decommissioning are included to determine the lifetime cost. The decommissioning costs are presented in Equation 3.66.

$$C_{decom} = C_{TIC} \cdot f_{decom} \tag{3.66}$$

3.14.5. Transport, installation and commissioning model constants

The model constants are presented in Table 3.24

Parameter	Symbol	Value	Unit	Source
Mobilisation	T_{mob}	5.0	Days	Estimate
Demobilisation	T_{demob}	5.0	Days	Estimate
Pile installation	T_{piling}	10.0	Days	Estimate
Substructure installation	$T_{substruc}$	2.0	Days	Estimate
Loading	$T_{loading}$	1.0	Days	Estimate
Installing topside(section)	$T_{topside}$	1.0	Days	Estimate
Pioneering Spirit day rate	DR_{PS}	1.0	M€/day	Estimate
Sleipnir day rate	DR_{SN}	0.8	M€/day	Estimate
Crane vessel day rate	DR_{CV}	0.4	M€/day	Estimate
Tug vessel day rate	DR_{TB}	0.03	M€/day	Estimate
Commissioning single lift	$f_{comm,singlelift}$	3.0	%	[77]
Commissioning modular	$f_{comm,modular}$	18.0	%	[77]
Decommissioning factor	f_{decom}	50.0	%	Estimate

Table 3.24: Model constants for the transport, installation, and commissioning CAPEX submodel.

3.15. Other CAPEX modelling

Table 3.25 presents the input and output parameters for the soft CAPEX submodel.

Case parameter	Variable parameter	Fixed parameter	Output
	Material CAPEX	EPCm factor	EPCm CAPEX
		Owners costs factor	Owner CAPEX
		Contingency factor	Contingency CAPEX

Table 3.25: Model constants of the other soft CAPEX submodel

The soft CAPEX is calculated according to Equations 3.67, 3.68, and 3.69. The equations to determine the soft CAPEX are derived from the work of ISPT [35].

$$C_{EPCm} = C_{material} \cdot f_{EPCM} \tag{3.67}$$

$$C_{owner} = C_{material} \cdot f_{owner} \tag{3.68}$$

$$C_{cont} = (C_{material} + C_{EPCm} + C_{owner}) \cdot f_{cont} \tag{3.69}$$

Here, $C_{material}$ is the CAPEX for all physical components of the COHP. Table 3.26 presents the model constants for the soft CAPEX submodel. The costs factors of the EPCm and Owner costs are similar for the PEME- and AE-based systems. The contingency factor is higher for the PEME-based system, due to the lower technology readiness level. The model constants for the soft CAPEX submodel are presented in Table 3.26.

Parameter	Symbol	PEME value	AE value	Unit	Source
EPCm factor	f_{EPCM}	23.0	23.0	%	[35]
Owners costs factor	f_{owner}	16.0	16.0	%	[35]
Contingency factor	f_{cont}	35.0	25.0	%	[35]

Table 3.26: Model constants of the soft CAPEX submodel.

4

Case study, results and discussion

In the following chapter, the results of deploying the established model for a case study, are presented. First, section 4.1 provides information about the intended location and the resulting case-specific input parameters. Then, in section 4.2, the results of the case study over a fixed range of installed HPU capacities for both technologies are presented. Here, a preliminary optimal installed HPU capacity and associated LCOH are presented for two different optimisation objectives. The preliminary optimal installed HPU capacity will then be used to find the optimal compressor output pressure in Section 4.3, together with a final optimal installed HPU capacity. Then, Section 4.4 further analyses the system at the found optimal HPU capacity and compressor output pressure. Here, the system's performance over the project's lifetime is discussed. Also, a breakdown of the different cost factors is presented. Subsequently, Section 4.5 and Section 4.6 present the sensitivity and uncertainty analysis, respectively. Finally, Section 4.7 presents the discussion, and Section 4.8, the summary of Part I.

4.1. Background case study

In consultation with Vattenfall, it was decided to conduct a case study for a COHP project to be installed in the Europe, relatively close to the coast, as shown in Figure 4.1. This selection may be in contradiction with previously made statements regarding the ideal placement of hydrogen-producing offshore wind farms, due to the relatively short distance to the coast. It was previously explained that hydrogen-producing wind farms are advantageous over electricity-producing wind farms when located far offshore, because of the favourable transportation costs of hydrogen compared to electricity. Therefore, the proposed site could have served well as an electricity-producing wind farm.

Figure 4.1: Intended location.

4.1.1. Maritime condition

The maritime conditions affect the substructure and the time required to transport the platform from the port to the designated location. Table 4.1 presents an overview of the case parameters related to the present maritime conditions and transportation time.

A mean sea level of 35.0 meters is assumed which is representative of the average depths in the area of the intended location. The tide, storm

surge, wave crest height, and expected sea level rise at this mean sea level are provided by a Metocean analyst [78].

The time required to sail from the docks to the designated location is set to 1.0 days. This assumption is considered reasonable given the presence of multiple ports used for offshore wind farm installation and commissioning. These ports provide the facilities required during the installation and commissioning phase of an offshore wind farm.

Case parameter	Symbol	Value	Unit	Source
Mean sea level	MSL	35.00	m	Estimate
Tide height	H_T	0.42	m	[78]
Storm surge height	H_{SS}	1.50	m	[78]
Wave crest height	H_{WC}	6.50	m	[78]
Sea level rise	H_{SLR}	0.30	m	[78]
Transport time	T_{dist}	1.0	Day	Estimate

Table 4.1: Maritime conditions at the designated location.

4.1.2. Wind conditions and wind farm power curve

Figure 4.2 presents a representation of an offshore wind farm power curve and the wind speed distribution at the designated location. The exact offshore wind farm used in this work is not presented due to confidentiality reasons. An installed capacity of the wind farm of 1.0 GW was selected. This installed capacity does not change during the evaluation of the different cases. The power curve presented in the figure represents the power output of the wind farm per wind speed at the start of the farm's lifetime, measured before the inter-array cable losses.

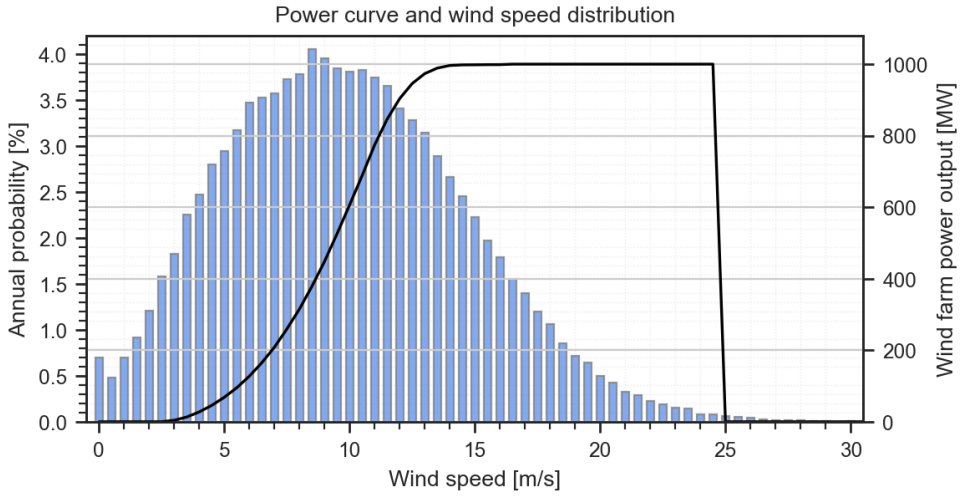

Figure 4.2: Representation of a wind farm power curve and wind speed distribution, provided by Vattenfall.

The exact offshore wind farm power curve used in this work is tailor-made to the intended wind climate and installed capacity. Furthermore, it is assumed that the wind speed distribution is constant for each year of the project's lifetime.

Figure 4.2 shows that a certain fraction of the time during the year, the wind speeds are not enough high for the offshore wind farm to produce power. As result, the offshore wind farm is not operational every hour of the year. A method to show the duration of time the offshore wind farm is operating at a certain load is shown in Figure 4.3, representing the load duration curve. The load duration curve is

a graphical representation of the relationship between the proportion of a year that a certain load, or higher, is experienced. A load equal to 1 implies operation at rated power.

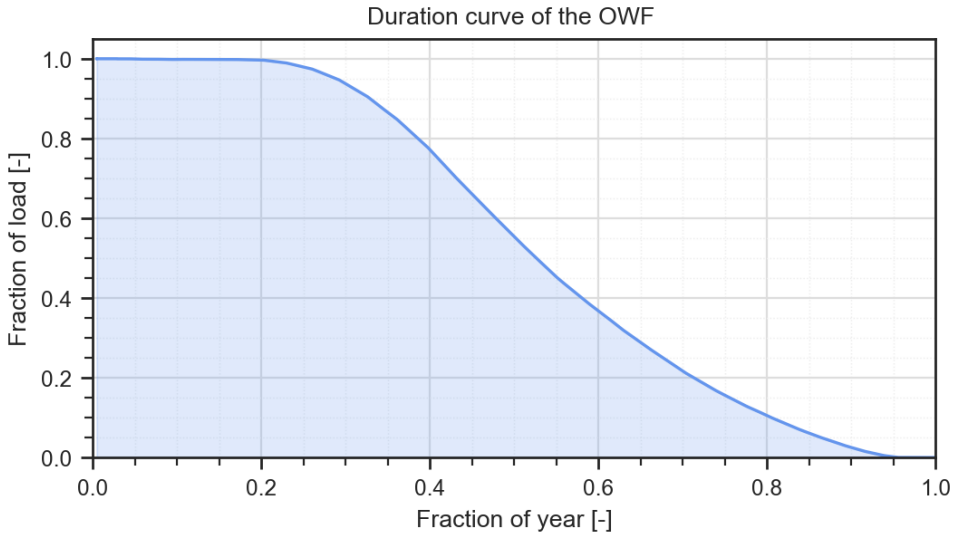

Figure 4.3: Load duration curve of the offshore wind farm.

From the load duration curve of the offshore wind farm it becomes evident that the offshore wind farm is only operating around 20% of the year at rated capacity and that the offshore wind farm is not producing any power around 5% of the year.

4.1.3. Other case parameters

Some of the input parameters are difficult to categorise into one of the previously mentioned categories and are therefore treated together here. The lifetime of the project, $Lt_{project}$ is set at 35.0 years. It is assumed that the lifetime of the offshore wind farm is equal to that of the COHP. Although current offshore wind farms do not achieve such lifetimes, it is expected to be possible in the future due to the use of more durable and efficient turbines, as well as improved maintenance practices [79].

The assumed distance to the shore, $L_{pipeline}$ is 70.0 km and a moderate offtake pressure of 50.0 bar is assumed. Furthermore, a COHP availability of 96.0% is taken and is assumed to be constant throughout the lifetime of the project [35].

The WACC of the project is a crucial component for the LCOH and is dependent, among other things, on the risk of the investment. In Europe, a WACC between 4.0% and 7.0% is typical for offshore wind projects [80]. However, a higher WACC of 10.0% is currently recommended because the project's risks are larger due to the additional hydrogen generation and the novelty of the concept [13]. Over time, it is anticipated that the hazards connected with this undertaking would lessen. Therefore, a WACC factor of 7.0% is assumed.

4.2. Preliminary sizing results

The results of implementing the case-specific parameters in the built model, as presented in Chapter 3, for a range of installed HPU capacities will be discussed in the following section. The final objective of this section is to determine the preliminary installed HPU capacity that provides either the lowest LCOH or the highest NPV. But first, all aspects contributing to the LCOH are presented.

The results are divided into the different relations as illustrated in Figure 3.1 of the techno-economic model overview. The results are presented for both PEME- and AE-based technologies over the installed HPU capacity range of 600 MW to 1000 MW. The first section focuses on the hydrogen production of both technologies, followed by the CAPEX and OPEX analysis. Additionally, the topside and substructure mass of the two technologies is presented. Finally, by integrating all the relations, the LCOH curves, and the NPV curves are presented. As one of the primary objectives of this study is to

compare the differences between the PEME- and AE-based systems, the results for both technologies will be presented side by side.

At this stage in the optimisation process for determining the optimal installed HPU capacity, a decision must be made regarding the required hydrogen compressor output pressure. Therefore, an educated guess is made, resulting in a chosen compressor output pressure of 60 bar. A hydrogen pressure level of 60 bar is sufficient to compensate for the pressure drop and to achieve a 50 bar pressure level upon reaching the shore, without necessitating excessive utilisation of compressor power. In Section 4.3, the exact hydrogen compressor outlet pressure is determined.

4.2.1. Optimum hydrogen production

As the COHP operates in island mode with the offshore wind farm, it relies on the latter for its power supply. This reliance is increased by the fact that the offshore wind farm runs only partially during the year, restricting the COHP's operating fraction of the year accordingly. Figure 4.4 presents the load duration curve of the COHP for different installed HPU capacities. This load duration curve is valid for both technologies since the whole HPU is considered.

The area underneath the graph represents the full load hours the HPU operates on an annual base. Therefore, from the HPU load duration curves, it is visible that decreasing the installed HPU capacity results in a larger number of full load hours and a larger fraction of the HPU is operating at rated capacity. This is because the offshore wind farm capacity is kept constant at 1.0 GW and, as seen in Figure 4.3, the offshore wind farm operates for a smaller fraction of the year at an output power of for example 900 MW than at 600 MW. The curve drops for a higher installed HPU capacity due to the normalisation of the rated HPU capacity.

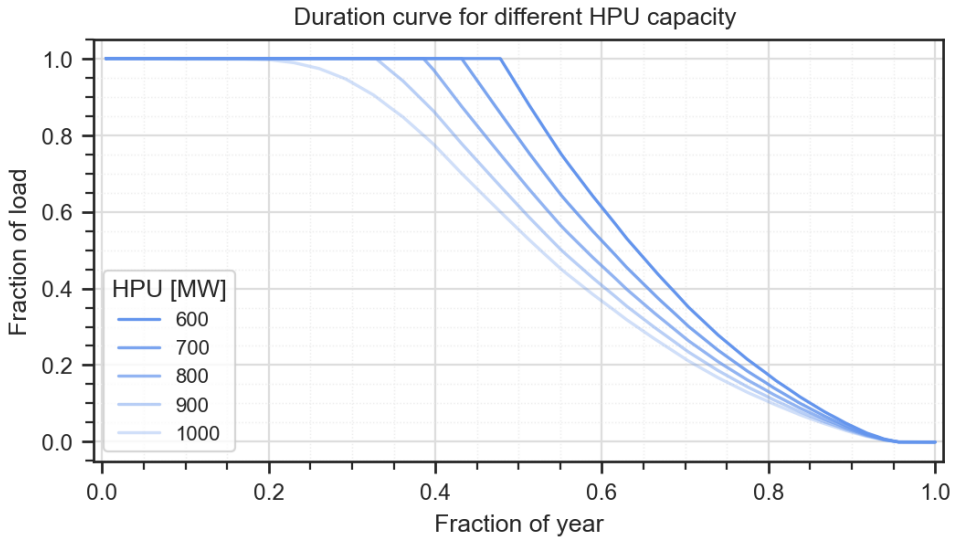

Figure 4.4: Annual load duration curves of the COHP for different installed HPU capacities.

The effect of this increased load factor on hydrogen production per installed HPU capacity is shown in Figure 4.5. Here, the annual hydrogen production per installed HPU capacity for both the first and final year of operation for both technologies is shown. The annual hydrogen production is determined according to the hydrogen production model, as presented in Section 3.3.

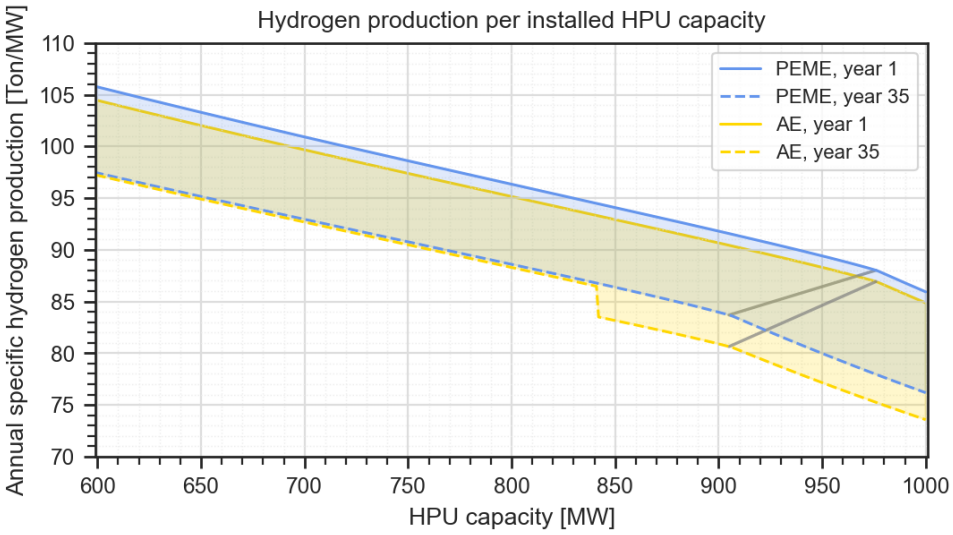

Figure 4.5: Annual hydrogen production per installed HPU capacity for a PEME- and AE-based system

Figure 4.5 demonstrates a decline in marginal hydrogen production with increasing HPU capacity. The slope of this decline steepens beyond a certain capacity threshold. In the initial year of operation, this is 975 MW. This is the result of having a larger HPU capacity than the maximum power delivered to the COHP. Due to availability and inter-array cable losses, there will not be a maximum power of 1.0 GW delivered at the COHP. This threshold shifts towards a lower value over time as the performance of the offshore wind farm, and therefore the maximum delivered power to the COHP, decreases, as seen in Section 3.4. The shifting maximum delivered power is depicted by the grey line. The final year maximum power delivered to the COHP is 907 MW.

The undersizing of the HPU capacity in relation to the offshore wind farm capacity results in a surplus of energy generated when the wind farm operates at its maximum capacity, as the COHP operates in island mode. This surplus energy increases as the ratio of HPU to offshore wind farm capacity decreases, leading to a reduction in the effective utilisation of generated electricity.

Moreover, the higher hydrogen production is associated with increased operational hours per year and therefore faster degradation of the stacks. Since it is assumed that the stacks are operational for a certain maximum number of hours, the end of life of the stacks is reached earlier during the project's lifetime. As a result of this increased use, the stacks need to be replaced an extra time. This results in an additional required stack replacement for the AE-based system at an installed HPU capacity of lower than 840 MW. The presence of the relatively new stacks in the final year, as a result of these extra replacements, contributes to higher hydrogen production in that year compared to a scenario with a higher installed HPU capacity.

Besides, as a result of the difference in the degradation rate of the two technologies, the difference in annual hydrogen production between the PEME- and AE-based systems decreases when comparing the first and final year of operation for installed HPU capacities of lower than 840 MW. These values can be compared since at these capacities, the number of stack replacements is equal for both technologies.

4.2.2. Optimum cost

The numerator of the LCOH equation is determined by the costs incurred during the initial investments and the lifetime of the project. Figure 4.6 presents the total COHP CAPEX and specific CAPEX for a PEME- and AE-based system. The total COHP CAPEX is obtained by summation of all contributors to the total CAPEX of the COHP. The specific COHP CAPEX is the total COHP CAPEX divided by the installed HPU capacity.

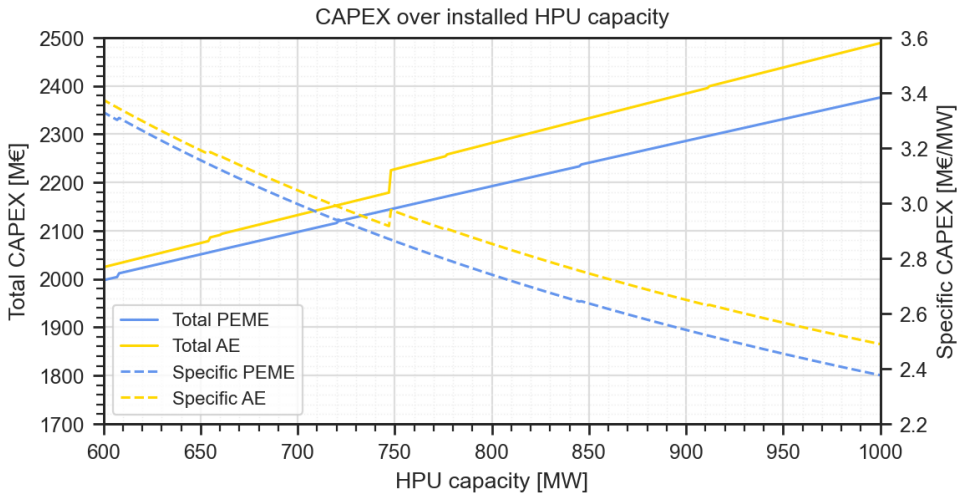

Figure 4.6: Total and specific CAPEX for a PEME- and AE-based system over installed HPU capacities for a 60 bar compressor output pressure.

Figure 4.6 demonstrates that the total COHP CAPEX increases as the installed capacity decreases. However, the specific COHP CAPEX decreases with installed HPU capacity. Both curves show a non-linear trend. For the total CAPEX curve, this is attributed to the economies of unit scale. For the specific CAPEX curves, this is attributed, besides the economies of unit scale, also to the fact that the offshore wind farm CAPEX is unaffected by the installed HPU capacity.

Some of the contributors to the total COHP CAPEX do not exhibit economies of unit scale. The installation CAPEX is fixed when staying within the limits of an installation vessel. The transmission system is constant when staying within the limits of a certain diameter. The other components of the HPU exhibit economies of unit scale at lower or higher rates. The economies of scale are not well visible in the higher range. This is mainly because the highest contributors to the total COHP CAPEX, the electrical equipment and stacks, have a scaling factor relatively close to 1, implying low economies of unit scale. From Figure 4.6, it can be concluded that the CAPEX of the AE-based system is overall higher than the CAPEX of the PEME-based system. Readers interested in the CAPEX curve ranging from 0 to 1000 MW, are referred to Figure A.1 in the appendix.

For the PEME-based CAPEX curves, several jumps are observed at installed HPU capacities of 608 MW, 721 MW, and 846 MW. As a result of increasing installed capacity and therefore increase of produced hydrogen mass flow at rated capacity, a larger diameter of the hydrogen transmission system is required. This larger diameter results in higher transmission CAPEX. Furthermore, throughout the observed range, there is no need to alter the transportation and installation method, and the same number of stack replacements is necessary. Any deviations in the installation method or a difference in the number of stack replacements would have led to a significant jump in the LCOH curve.

For the AE-based CAPEX curve, more jumps are observed. First, the smaller upwards jumps are addressed. It must be noted that these jumps are small and therefore poorly visible in the figure. These are the result of the same necessary increase in pipeline diameter and occur at installed capacities of 654 MW, 778 MW, and 910 MW. The occurrences of these jumps are at a higher installed HPU capacity compared to the PEME-based system. This is because the stack capacity of a certain HPU capacity in the AE-based system corresponds to a lower stack capacity than in the PEME-based system. This is the result of the higher power requirements of the other equipment besides the stacks in the HPU. Larger power consumption of this other equipment results in a lower possible installed stack consumption. A significant jump is observed at 749 MW. This jump is the result of the increasing mass of the topside of the AE-based system. This increase surpasses the limit of the lifting capacities of the Pioneering Spirit and thereby demands a modular installation method, as discussed in Section 3.14. This results in a significant increase in CAPEX.

Figure 4.7 presents the total offshore wind farm and COHP OPEX and specific OPEX over the range of installed capacities. The total COHP OPEX is obtained by summation of all contributors to the total

OPEX of the COHP. The specific COHP OPEX is the total COHP OPEX divided by the installed HPU capacity.

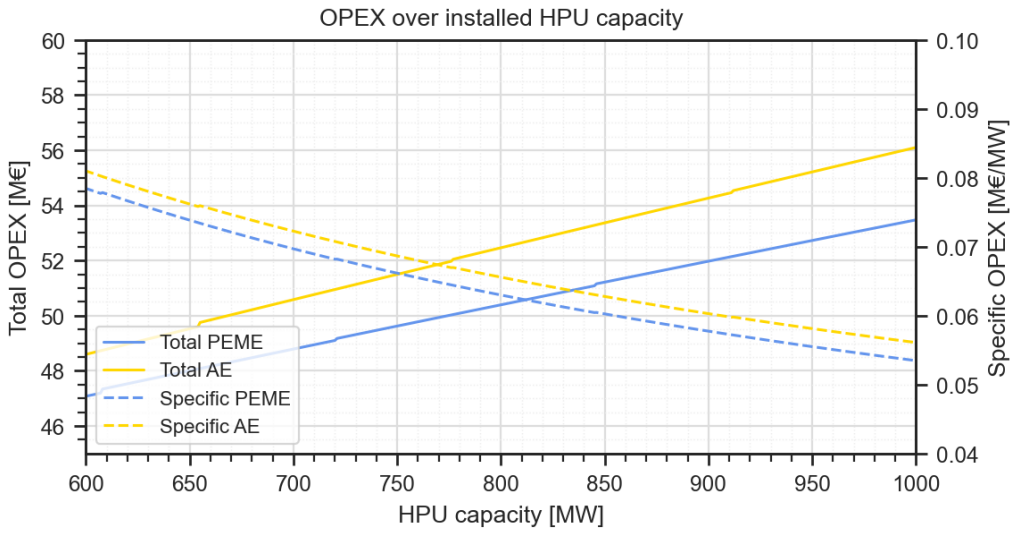

Figure 4.7: Total and specific COHP OPEX for a PEME- and AE-based system over installed HPU capacities.

Similarly to the CAPEX and specific CAPEX curves, the total OPEX and specific OPEX curves show an upward and downward trend, respectively. Both trends show small non-linear progress since the OPEX is directly linked to CAPEX. Since only the physical components of the COHP contribute to the OPEX, the increase in required vessel size does not result in additional OPEX costs. The OPEX of the AE-based system is higher over the entire presented range.

4.2.3. Optimum mass

The significant difference between the two technologies and a contributor to the total CAPEX is the mass of the COHP. Figure 4.8 presents the mass of the topside and substructure for the two technologies over the range of considered installed HPU capacities.

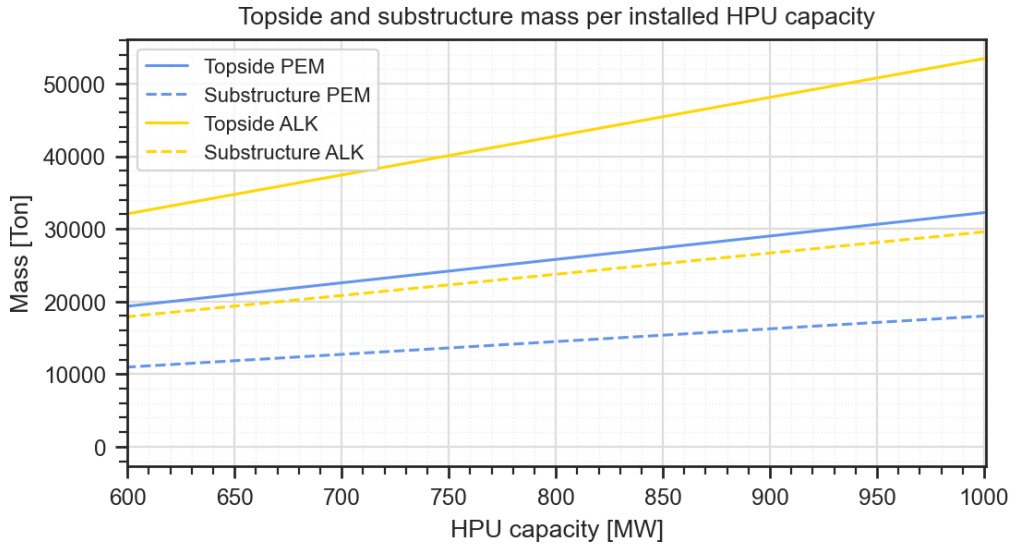

Figure 4.8: Mass of the topside and substructure for the PEME- and AE-based system.

With increasing HPU capacity, the mass of the topside and substructure increases linearly. From Figure 4.8 it is evident that there is a significant difference in the mass of the PEME-based and AE-based topside and substructure. For both the topside and substructure, the mass of the AE-based system is higher. This is due to the higher mass of the stacks, water treatment equipment, gas conditioning equipment, and compressors.

Furthermore, it is important to highlight that masses associated with the maximum installed HPU capacities are relatively high compared to the structures that have been currently installed in offshore environments. This could pose significant challenges in terms of transportation and installation.

4.2.4. Optimum levelised cost of hydrogen

Combining the hydrogen production, CAPEX, and OPEX as presented previously, creates the LCOH curve, visualising the LCOH per installed HPU capacity, as calculated according to Equation 3.1. Figure 4.9 presents the LCOH-curve for both technologies given the case-specific input parameters presented previously. Furthermore, the results of assuming a $\pm$ 10% higher or lower CAPEX are shown in yellow and blue areas.

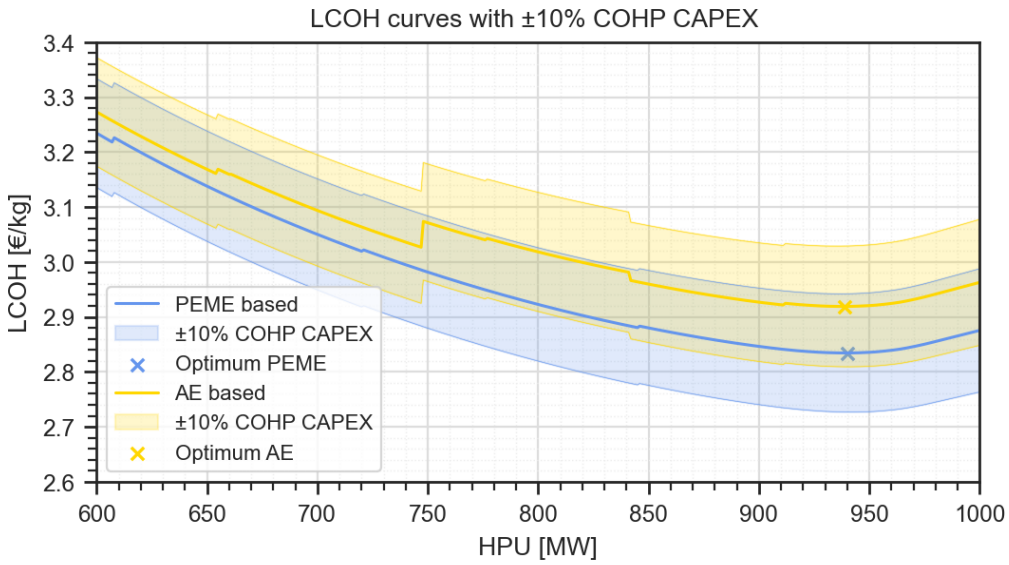

Figure 4.9: LCOH curves with 10 percent CAPEX difference.

Over the course of the LCOH curve in Figure 4.9, it can be seen that an optimum develops, indicated by the cross. Maximising the installed HPU capacity does not result in the optimal capacity when considering the lowest LCOH. The optimal HPU capacity is a balance between various factors that influence both hydrogen production and the associated costs. The optimal HPU capacity is the capacity where the balance between the total hydrogen production and associated costs results in the cheapest production of one kilogram of hydrogen. In general, higher overall hydrogen production and lower overall costs benefit the LCOH. How the hydrogen and costs curves influence the found optimal HPU capacity is as follows.

Regarding hydrogen production, as HPU capacity increases, the total hydrogen production increases, driving the optimal HPU capacity upward. However, the specific hydrogen yield per unit of HPU capacity decreases with an increase in HPU capacity, pulling the optimal HPU capacity downward (Figure 4.5). Additionally, the stack degrades with operational hours, and increasing installed capacity results in a decrease in FLH production and therefore total degradation, which drives the optimal HPU capacity upward (Section 3.5). Furthermore, the decrease in the nominal delivered power by the offshore wind farm over time, as a result of its decreasing performance, drives the optimal HPU capacity downward.

In terms of costs, the total COHP CAPEX of the system increases with an increase in HPU capacity, driving the optimal HPU capacity downward. However, the fixed offshore wind farm costs and economies of scale result in a decrease in specific CAPEX per unit of HPU capacity, which drives

the optimal HPU capacity upward (Figure 4.6). The same holds for the OPEX incurred during the project's lifetime, with the total OPEX increasing with HPU capacity. The specific OPEX, linked directly to CAPEX, decreases with HPU capacity, driving the optimal HPU capacity upward (Figure 4.7). Table 4.2 presents the lowest LCOH and associated HPU capacity and stack capacity

Overall, a small benefit in favour of the PEME-based system in terms of LCOH is observed over the entire range of considered HPU capacities. Table 4.2 presents the LCOH at the optimal installed hydrogen production unit capacity and associated stack capacity. Readers interested in the LCOH-curve per technology are directed to Figure A.2 and Figure A.3 in the appendix.

Technology	LCOH [€/kg]	HPU [MW]	Stack [MW]
PEME	2.84	940	899
AE	2.93	938	886

Table 4.2: Values at minimum LCOH for both systems.

4.2.5. optimum NPV

A different method to evaluate the project but also to find the optimal installed HPU capacity is by looking at the NPV of the project. To determine the NPV of a project, the selling price of the produced good is necessary. Currently, the selling price of renewable-produced hydrogen for the year 2030 is still very uncertain. Therefore, a range of selling prices between 2.5 €/kg and 3.5 €/kg are evaluated. The results of this method are presented in Figure 4.10 and Figure 4.11 for the PEME-based system and the AE-based system, respectively. The NPV is calculated according to Equation 3.2. Furthermore, it is assumed that the selling price of hydrogen remains constant during the years of operation. The red line presents an NPV equal to zero.

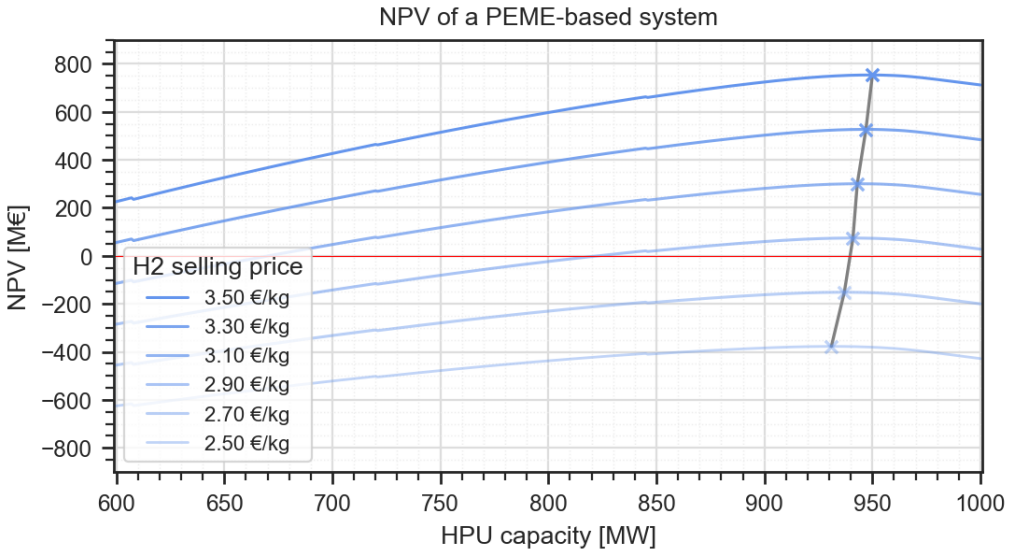

Figure 4.10: NPV of a PEME-based system for different assumed hydrogen selling prices.

Similar to the LCOH curves, an optimum installed HPU capacity emerges along the NPV curve. Furthermore, it can be seen that the expected hydrogen selling price influences the optimally installed HPU capacity. The highest NPV is found at the installed capacity where the product of the profit per produced unit of hydrogen and the total amount of produced hydrogen is the highest. Therefore, a hydrogen selling price equal to that of the hydrogen production price would result in an NPV of zero and an optimal installed capacity equal to that found when the objective is to find the capacity associated with the lowest LCOH. A hydrogen selling price larger than the hydrogen production costs results in a

higher optimal installed HPU capacity than when it is optimised for the lowest LCOH. Given a hydrogen selling price higher than the hydrogen production price results in a reward for increasing hydrogen production by installing a larger HPU capacity. Noteworthy is that the turnover does not scale linearly with increased HPU capacity since the marginal hydrogen production decreases with installed HPU capacity is decreasing. A hydrogen selling price below the hydrogen production price seems to influence the optimal installed HPU capacity more than a hydrogen selling price above the hydrogen production costs, depicted by the grey line. Optimising for maximum NPV resulted in an installed HPU capacity of 950 MW for the PEME-based system and a capacity of 948 MW for the AE-based system, assuming a hydrogen selling price of 3.50 €/kg. For a hydrogen selling price of 2.50 €/kg, the optimal installed HPU capacities were found to be 931 MW and 911 MW for a PEME- and AE-based system, respectively.

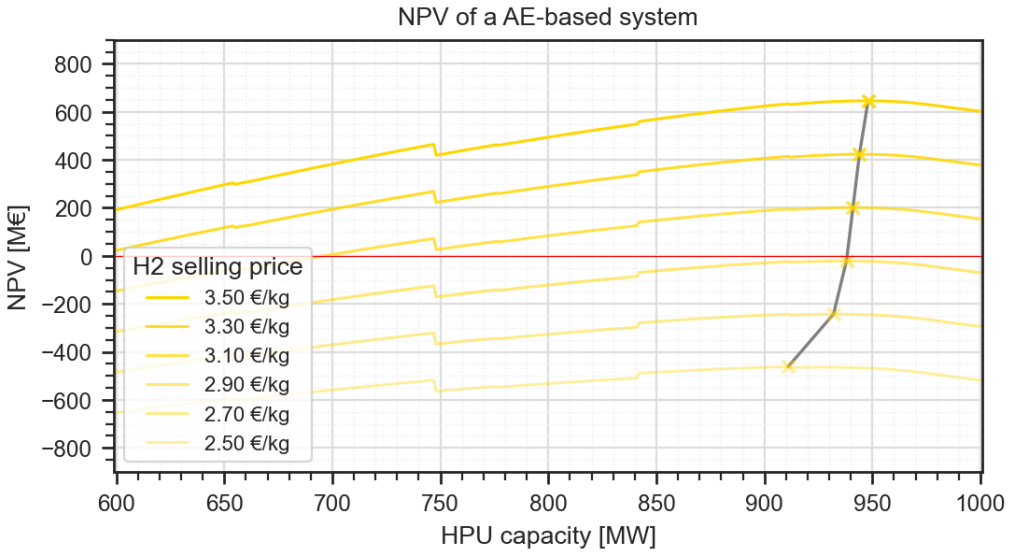

Figure 4.11: NPV of an AE-based system for different assumed hydrogen selling prices.

As a result of the higher LCOH for the AE-based system, a higher hydrogen selling price is required to obtain a positive NPV. Therefore also more of the considered hydrogen selling prices result in a negative NPV. A similar phenomenon regarding the sizing of the HPU capacity in reference to the hydrogen selling price is observed. Here, the effect of a hydrogen selling price lower than the hydrogen production price is more significant, depicted by the grey line.

4.3. Optimal compressor output pressure

In this section, the optimal compressor output pressure is derived. It was observed in Section 4.2 that the optimal installed capacity of the HPU is dependent on the uncertain hydrogen selling price when seeking to maximise the NPV. Therefore, it has been decided to exclusively explore the installed capacities that lead to the lowest LCOH. In Section 4.2, the results indicate that the most suitable HPU capacity would be situated between 0.9 and 1.0 GW for both the PEME- and AE-based systems, under the assumption of an unoptimised compressor pressure of 60 bar.

An increase in compressor outlet pressure corresponds to an increase in the pressure of the hydrogen in the pipeline, as presented in Section 3.13, leading to a potential reduction in pipeline diameter and cost of the hydrogen transmission system. However, increasing pressure in the compressors requires additional power consumption, decreasing total hydrogen production and increasing compressor costs, presenting a trade-off scenario. As such, further optimisation will be performed within the 900 MW to 1.0 GW range to determine the optimal compressor output pressure. Figure 4.12 presents the LCOH for the PEME-based system over a range of HPU capacities and compressor output pressures.

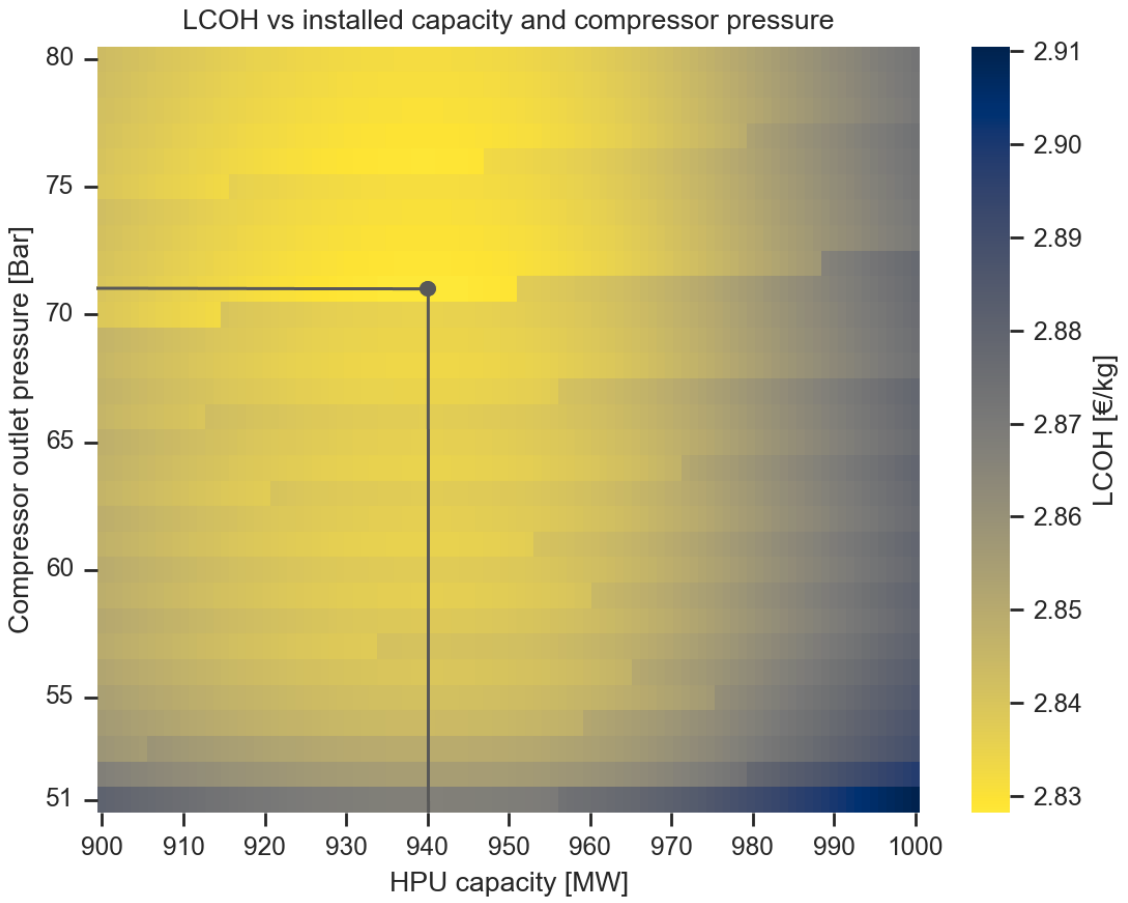

Figure 4.12: LOCH for a PEME-based system versus installed HPU capacity and compressor output pressure.

The jumps in LCOH, when remaining in a certain compressor output pressure are the result of the requirements of a larger pipeline diameter, as seen earlier in Figure A.2. The jumps in LCOH, when remaining in a certain HPU capacity, are the result of the possible use of a smaller pipeline diameter due to the compacter hydrogen mass flow due to the larger pressure of the hydrogen entering the pipeline. A significant lowering of the LCOH is observed around after a certain increment of the pressure. For an installed HPU capacity of 900 MW this is at 69 bar and at 1.000 MW this is at 72 bar. This is because this facilitates the possibility to use a pipeline diameter of smaller than 16 inches, resulting in a cheaper pipeline installation method, as described in Figure 3.5.

As illustrated in Figure 4.12, the results indicate that the optimal compressor output pressure is 71 bar, which is not in accordance with the previously assumed value of 60 bar. The HPU capacity remains at 940 MW, which implies that the installed stack capacity decreases since a larger part of the total available power must be directed to the compressors. For this new combination of optimal installed HPU capacity and compressor output pressure, a total stack capacity of 896 MW is to be installed. This is 3 MW less than in the unoptimised configuration. The resulting LCOH is 2.83 €/kg which is 0.01 €/kg less than in the unoptimised configuration. Figure 4.13 presents the range of LCOH versus installed HPU capacity and different compressor output pressures for the AE-based system.

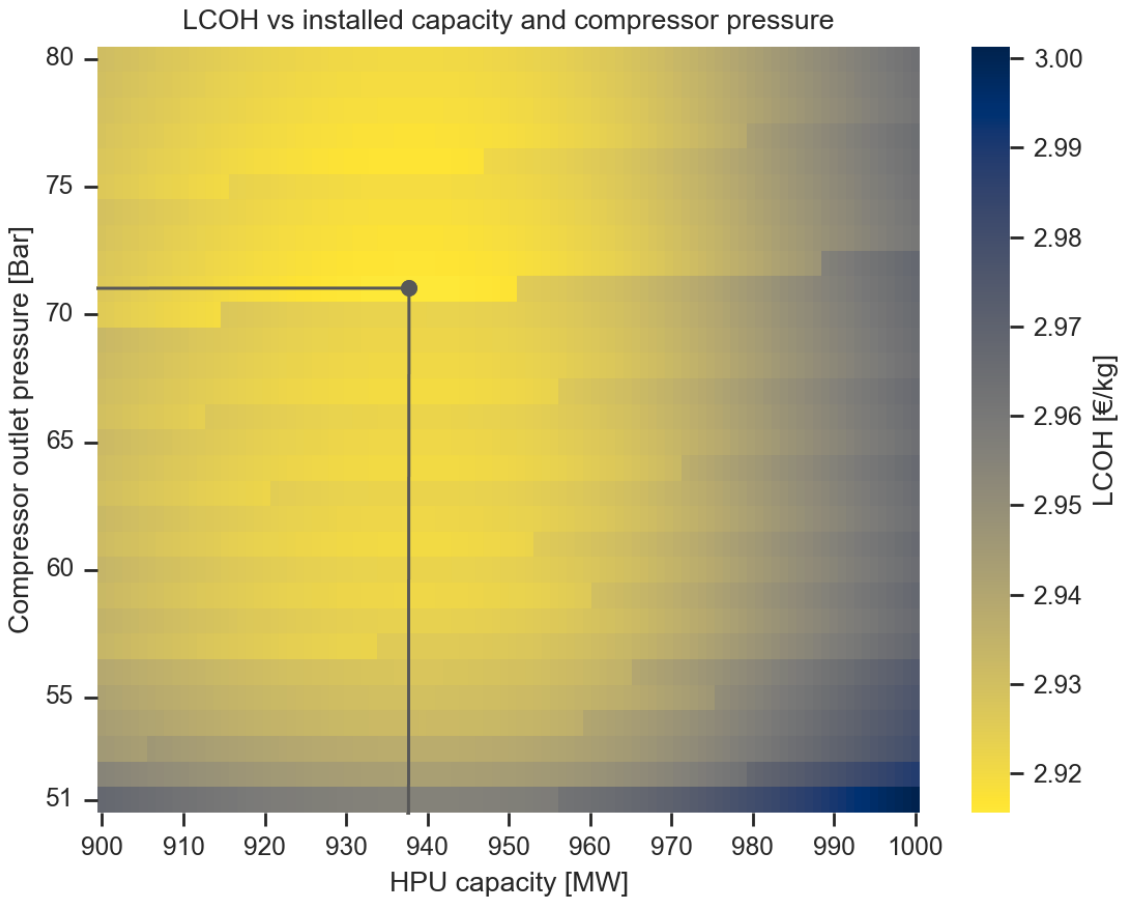

Figure 4.13: LOCH for a PEME-based system versus installed HPU capacity and compressor output pressure.

Figure 4.13 highly resemblances to the PEME-based variant. The jumps in LCOH are again the result of the different required pipeline diameters. For the AE-based system, the optimal installed HPU capacity is 938 MW, 1 MW less than the HPU capacity found in Section 4.2. The optimal compressor output pressure is found to be 71 bar, resulting in an installed stack capacity of 884 MW, which is a decrease of 2 MW. This setup realises an LCOH of 2.92 €/kg, which is 0.01 €/kg less then at a pressure of 60 bar. At this pressure, equal to the PEME-based system, a pipeline diameter of 16 inches could be used therefore decreasing the pipeline installation costs.

4.4. Analysis at optimal installed capacity

The optimal HPU capacity and compressor output pressure, as found in Section 4.3, will be further analysed in this section. For this specific installed capacity, the hydrogen production throughout the project, and a breakdown of the CAPEX and OPEX per contributor are presented. Finally, a breakdown of the LCOH for both technologies is provided.

4.4.1. Hydrogen production

The annual hydrogen production is affected by the duration the COHP and offshore wind farm have been in operation, as shown in Figure 4.14. Here, the annual hydrogen production over the lifetime of the project, installing the technology-specific optimal HPU capacity, is presented for both systems.

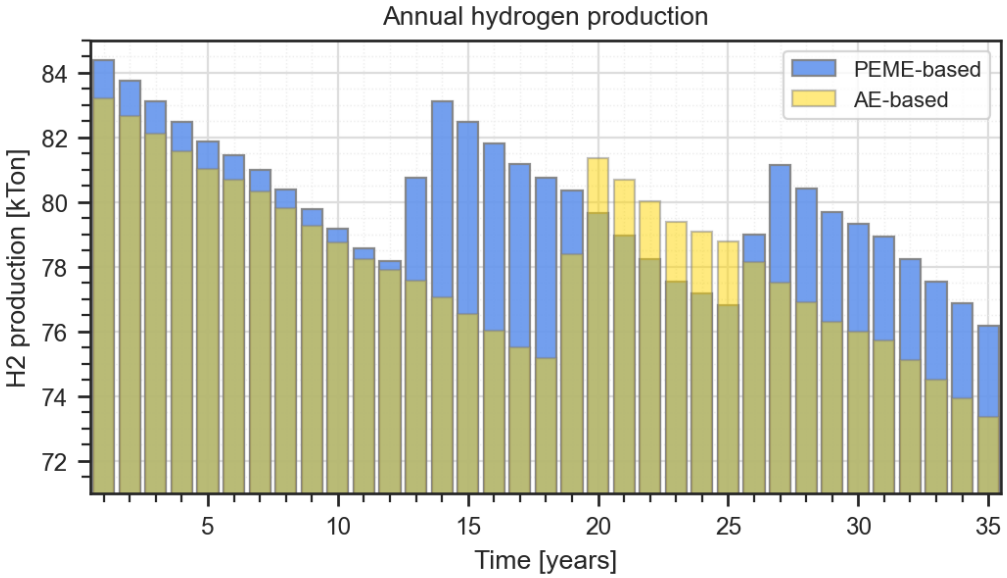

Figure 4.14: Annual hydrogen production of both technologies. The minimum amount of stack replacements.

The total annual hydrogen production is affected by the degradation of the stacks, and the decline in offshore wind farm performance and availability. A large jump in annual hydrogen production is made due to the replacement of the stacks. Due to the decline in wind farm performance, initial annual production quantities are not reached after stack replacements. The large maintenance campaign, every 6 years, shows relatively little effect on the produced amount of hydrogen.

Furthermore, a difference in hydrogen production between the two technologies is demonstrated as the result of the difference in system efficiency. Increasing the pressure to 71 bar in the compressors to prepare the hydrogen for transmission demands significantly more power in the AE system than in the PEME system, which negatively affects the amount of hydrogen that is produced. In the initial year of operation, for the given set-up, a difference of 1.3% is observed. However, due to the lower degradation of the AE stacks, this difference in annual hydrogen production decreases up until the first round of replacing the stacks.

In Figure 4.14 the minimum amount of replacements is shown. Due to the difference in the lifetime of the stacks, the PEME-based system requires two replacements of stacks, and the AE-based system only once. Replacing the stacks has a positive impact on the annually produced amount of hydrogen, but is also a costly procedure. For both the PEME-based and AE-based system, it was found that an additional stack replacement would result in a higher LCOH compared to the minimum number of stack replacements. An additional stack replacement results in a LCOH of 2.86 €/kg and 2.94 €/kg for the PEME- and AE-based system.

4.4.2. Costs

After discussing the denominator side of the LCOH equation, it is time to dive deeper into the costs of the different project aspects, as presented in Figure 4.15.

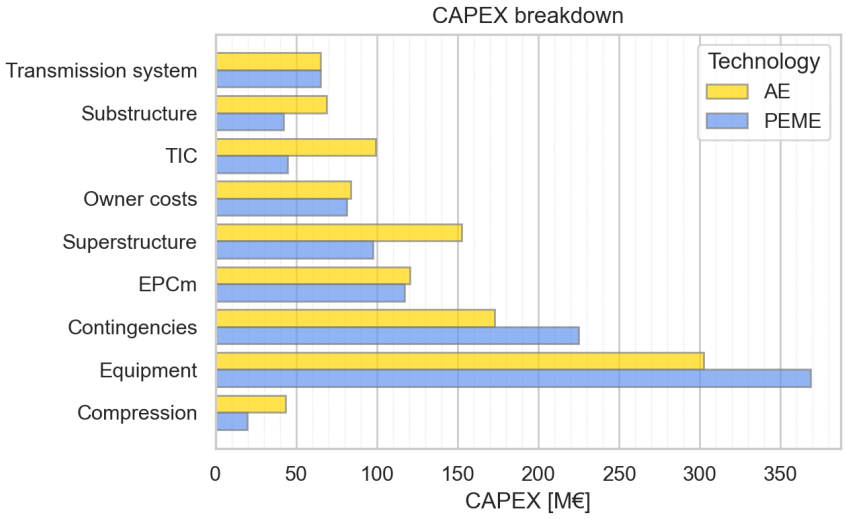

Figure 4.15: CAPEX of all COHP project aspects of both the PEME- and AE-based system at optimal installed HPU capacity.

In this figure, the CAPEX of the different components of the COHP at their optimal installed capacity are shown. In the figure, the electrical equipment, stacks, water treatment equipment, and gas conditioning equipment are grouped in the category Equipment. At the optimal installed HPU capacities, the PEME-based COHP system has a total CAPEX of 1061.6 M€, and a specific CAPEX of 1129.4 €/kW. The AE-based COHP has a total CAPEX of 1109.3 M€, and a specific CAPEX of 1182.6 €/kW. The prevailing literature suggests that PEME-based systems are more costly than AE-based systems. However, as depicted in Figure 4.15, this generalisation is not supported by the findings. The costs associated with procurement of the equipment and contingencies are indeed lower for the AE-based system due to the use of widely available materials and the maturity of the technology. However, when considering the project as a whole, the PEME system proves to be more economical in several areas, particularly those in which the system weight is a significant factor, such as the superstructure, substructure, transportation, installation, and commissioning. The lighter mass of the PEME-based system confers a cost advantage in these areas. Additionally, the PEME-based system exhibits a lower cost for compressors, due to the requirement for a less powerful compressor as a result of the higher stack hydrogen output pressure. This difference is reflected in both direct compressor costs and indirect costs associated with the extra weight of the compressors.

Figure 4.16 presents an overview of the annual OPEX for the first year. In the figure, the superstructure, substructure, and foundation are grouped in the Structural category.

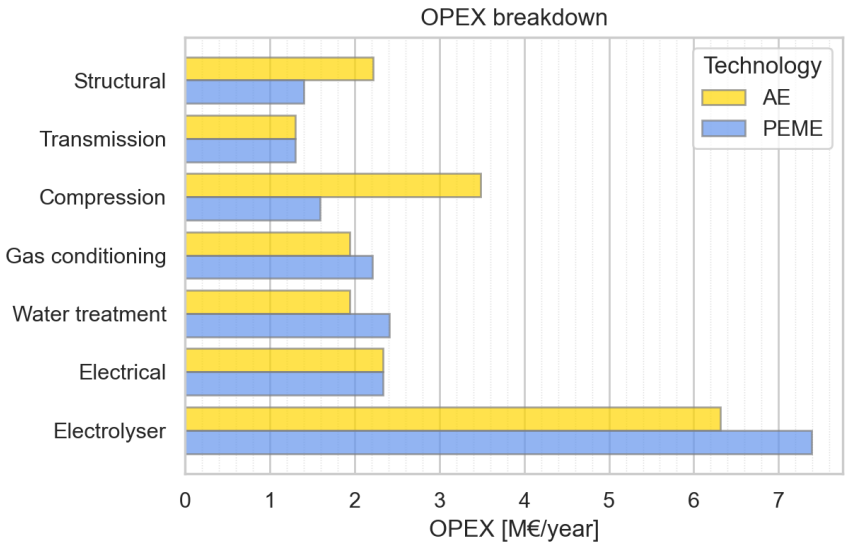

Figure 4.16: Breakdown of the OPEX

The difference in the annual OPEX shows large similarities with the CAPEX for most of the categories. This is because for the structural, transmission, compression, gas conditioning, water treatment, and electrical equipment an equal OPEX factor for both technologies is assumed. Only for the stacks, a different OPEX factor was assumed. A higher OPEX factor is assumed for the stack of the AE-based system than for the stacks of the PEME-based system. However, since the OPEX is directly linked to the CAPEX, and the CAPEX of the PEME-based stacks is significantly higher, the total PEME-based stack's annual OPEX turns out higher.

The annual OPEX for both technologies shows large similarities. One main difference is observed regarding the OPEX of the compressors. As known, hydrogen compressors are maintenance intensive [Section 3.9]. The compression requirements of the AE-based system are larger than in the PEME-based system, resulting in higher annual OPEX requirements.

The summation of the undiscounted COHP OPEX costs of the PEME-based system totals 18.63 M€. This comes down to of 1.7 % of the COHP CAPEX. The undiscounted COHP OPEX for the AE-based system amounts to 19.52 M€, representing 1.8 % of its CAPEX.

4.5. Sensitivity analysis

A sensitivity analysis was conducted to determine the key factors affecting the LCOH and optimal HPU capacity. The model utilises numerous input parameters, some of which, such as cost, were further subdivided. However, evaluating each sub-component's sensitivity individually offered limited insight due to the small contribution to the total. Thus, the analysis focused on major categories only. The categories are presented in Table 4.3

Category	Attributes
OWF CAPEX	CAPEX of the OWF
WACC	WACC
COHP CAPEX	CAPEX of the electrical equipment, stacks, water treatment equipment, gas conditioning equipment, compressors, superstructure, substructure, foundation, transmission system, transport, installation, commissioning, decommissioning.
Stack efficiency	Efficiency of the stacks
OWF OPEX	OPEX of the OWF
COHP OPEX	OPEX of the electrical equipment, stacks, water treatment equipment, gas conditioning equipment, compressors, superstructure, substructure, foundation, transmission system
Mass	Specific mass of the stacks, electrical equipment, primary steel, secondary steel
Inavailability	Initial OWF inavailability, annual OWF inavailability loss, COHP inavailability
Degradation	Degradation of the OWF power conversion and stacks
Consumption/losses	Inter-array cable losses and electrical equipment losses, water treatment equipment consumption, gas conditioning consumption, compressor efficiency

Table 4.3: Explanation of the different categories.

Each category underwent a sensitivity analysis with $\pm$ 10% and $\pm$ 20% variations. It was chosen to use the inefficiency and inavailability instead of the availability and efficiency since increasing the availability and efficiency by 20% would result in unrealistic values.

The sensitivity analysis of the obtained LCOH is first presented for both PEME- and AE-based systems. Then, the sensitivity analysis of both systems regarding optimal HPU sizing is presented. For ease of comparison, the sequence of categories in the figure, showing the change in LCOH, is based on the rate of change of the LCOH in the PEME-based system, starting with the greatest change. This is done to facilitate comparison with the AE-based system. The presentation of results from the sensitivity analysis on optimal sizing follows this same sequence.

4.5.1. Sensitivity of obtained LCOH PEME-based system

Figure 4.17 presented the obtained results of the aforementioned sensitivity analysis method. The results shown are the lowest LCOH obtained for these input parameters. The baseline LCOH for the PEME-based system is 2.83 €/kg.

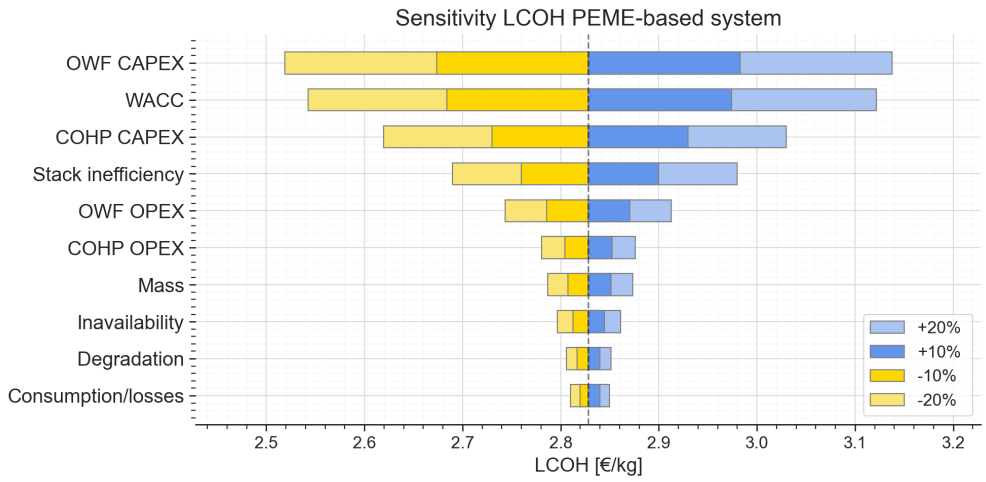

Figure 4.17: Tornado LCOH sensitivity chart of the main categories of a PEME-based system.

The results of the sensitivity analysis present that a difference of some input parameters have a significantly greater difference in the results obtained than others. A difference in the CAPEX categories results in a large difference in the results obtained. Thereby, the difference between results due to variation of the offshore wind farm and the COHP CAPEX is also approximately proportional to their initial costs. The same phenomenon applies to the sensitivity of the OPEX categories, however, they have significantly smaller results. Moreover, it should be noted that variance in the WACC used employed can lead to significant disparities in the outcome obtained, comparable to the outcome obtained by variations of the OWF CAPEX.

Furthermore, attention should be paid to the amount of impact that the stack's efficiency has on the obtained LCOH. This initial stack inefficiency amounts to 20%. Thus, a maximum change of 20% results in a stack efficiency of either 84% or 76%, both still high efficiencies, yet the change has a significant effect on the LCOH.

Noteworthy are the results obtained for change in degradation, inavailability, consumption, and losses. The reason for their relatively small influence is the fact that these input parameters are relatively small and thus a difference in these input parameters has little effect.

4.5.2. Sensitivity of obtained LCOH system AE-based system

Figure 4.18 presents the results of the sensitivity analysis performed on the LCOH for the AE-based system. The baseline LCOH for the AE-based system is 2.92 €/kg.

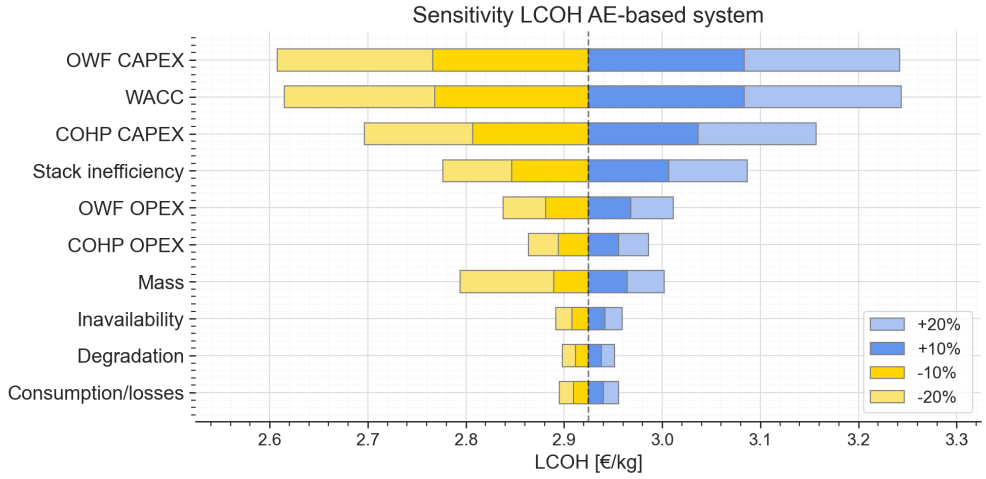

Figure 4.18: Tornado LCOH sensitivity chart of the main categories of an AE-based system.

The sensitivity analysis of the LCOH for the AE-based system is largely similar to that of the PEME-based system, with two key differences in the Mass and Consumption/losses categories. A variation in the mass has a much larger impact, especially at a 20% decrease. First, it must be realised that the decrease in mass is passed on. The foundation mass results from the substructure mass, the substructure mass results from the topside mass, and the topside mass results from the equipment mass. For example, a decrease in specific mass first has the effect of decreasing the total mass of the HPU equipment, so the total mass of steel needed for the superstructure decreases. However, it is also assumed that the specific mass of the substructure steel is decreased, resulting in even a lower total mass. This phenomenon affects all mass-related costs. When a 20% decrease in mass is considered, it is realised that the AE-based COHP can be installed by single lift method, instead of the modular installation as in the baseline. This has a significant impact on the obtained LCOH. The other difference was observed in the Consumption/Loss category. A variation in the Consumption/losses category result in a larger difference than was observed for the PEME-based system. This is mainly because pressurising the hydrogen to 71 bar requires more power compared to the PEME-based system leading to a larger effect of variation in this power.

4.5.3. Sensitivity of obtained sizing PEME-based system

Figure 4.19 presents the results of the sensitivity analysis performed on the sizing of the HPU installed capacity for the PEME-based system. The baseline HPU sizing for the PEME-based system is 940 MW.

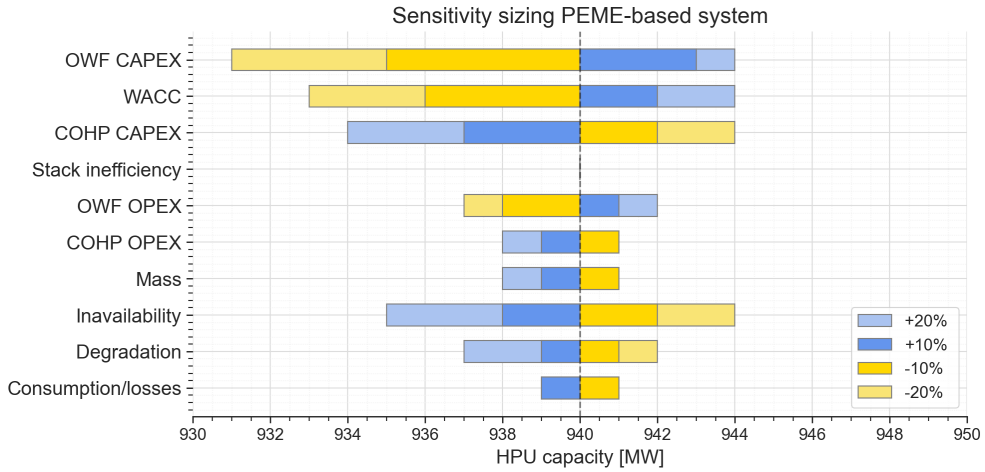

Figure 4.19: Tornado sizing sensitivity chart of the main categories of a PEME-based system.

The categories are shown in the same order as those of the sensitivity analysis of the LCOH and scaling occurs solely based on whole megawatt increments of installed HPU capacity, leading to rounding in the model. It can be seen that the magnitude of the effect of the variations on the optimal installed capacity are distributed differently, compared to the sensitivity analysis of the LCOH. Furthermore, it is observed that the results are less symmetrical. In instances where the difference between a 10% and 20% change may not be significant enough to result in a change in installed optimal capacity, only the 10% change is displayed.

Variations in the costs incurred for the offshore wind farm and the COHP have an opposite effect on the optimally installed HPU capacity. Higher costs for the COHP result in a lower optimal installed HPU capacity while higher costs for the offshore wind farm result in a higher optimal installed HPU capacity. When the costs of the OWF becomes higher, the power consumed by the HPU becomes relatively more expensive and curtailment therefore less beneficial. When the costs associated with the COHP become higher, it implies that the COHP is too expensive for the amount of time the capacity is not used, hence optimal installed capacity goes down.

As was also seen with the LCOH, the optimal installed HPU capacity is relatively sensitive to variation in the WACC. This is noteworthy because changes in the WACC affect both the cost of the COHP and the offshore wind farm. However, given the initial ratio of the offshore wind farm and COHP costs,

variations in the WACC result in proportional changes in the optimal HPU capacity, similar to the impact of variations in the offshore wind farm CAPEX.

The sensitivity analysis results reveal that changes in stack efficiency do not alter the optimal installed capacity of the HPU. This is because variations in stack efficiency result in a shift of the entire LCOH curve, but do not affect the shape of the curve's convexity. In terms of consumption and losses, again a small difference is observed. The difference due to the 10% change is so small that it is not enough to jump to the next megawatt.

Furthermore, it can be noted that for the PEME-based system, the change in optimal installed HPU capacity tends to be more in the lower direction. A change of input of a category, pulls the optimal HPU power to be installed further down than up. All capacities found due to changes in the input parameters of the categories give an individual difference of up to 10 MW, which is 1% of the maximum installed capacity. This suggests that the sizing is relatively insensitive.

4.5.4. Sensitivity of obtained sizing AE-based system

Figure 4.20 presents the results of the sensitivity analysis performed on the sizing of the HPU installed capacity for the AE-based system. The baseline HPU sizing for the AE-based system is 938 MW.

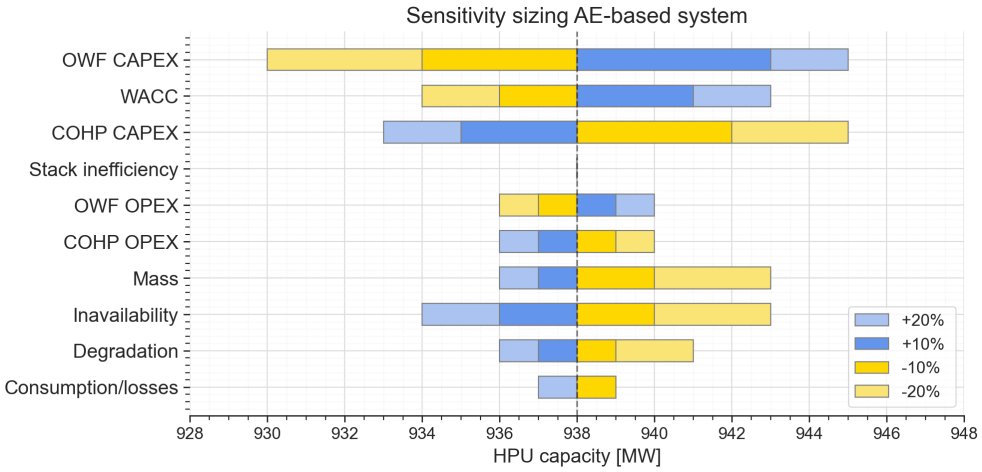

Figure 4.20: Tornado sizing sensitivity chart of the main categories of an AE-based system.

Similar to the PEME-based system, the offshore wind farm, and COHP CAPEX variations cause a significant change in optimal installed HPU capacity. Again, the WACC factor variations have a significant effect on the newly found optimal installed HPU capacity. A comparison of the sizing sensitivity between the AE-based and PEME-based systems reveals differences in the mass category. As previously noted, a decrease in mass has a considerable impact on the overall platform CAPEX, leading to a correspondingly large change in the optimal installed HPU capacity.

4.6. Uncertainty analysis

To account for the uncertainty of the input parameters, a Monte Carlo Method analysis was employed, similar to the work of Jang [81], on all individual input parameters of the model. As the probability distributions for the input parameters were not available, an assumption of a uniform distribution was made, with random values ranging from $\pm$ 10% of the reference value. The method used to generate the new input values is presented in Equation 4.1.

$$Y_{new} = Y_{ref} \cdot (1 + Var \cdot rand.uniform[-1, 1]) \tag{4.1}$$

Here, Y_{ref} and Y_{new}, represent the reference and new input values, respectively, while Var is the maximum percentage change. All input variables not explicitly defined by the project scope are randomised according to the method. An overview of all parameters affected by the variation can be found in Appendix A.2. The results of this analysis are presented in Figure 4.21.

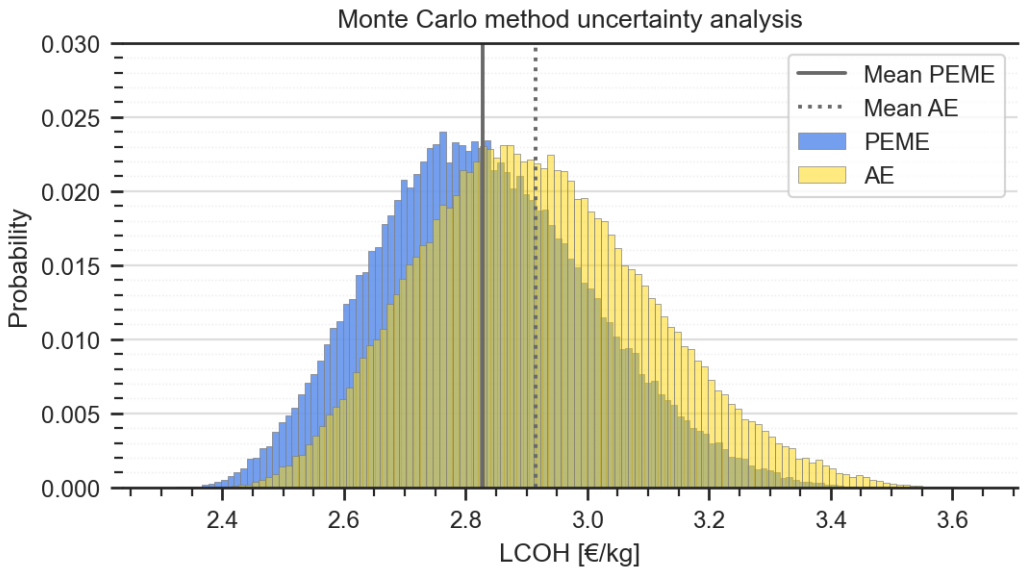

Figure 4.21: PEME- and AE- based system Monte Carlo Method simulation. Based on an input variance of $\pm 10\%$. 100.000 simulations for both technologies.

Certain positive skewness is observed as the mean is observed on the right side of the mode of the distribution. The reason behind this skewness is due to the deviation in both costs and hydrogen production-related input parameters. Costs only appear in the nominator of the LCOH equation, while the amount of hydrogen production only appears in the denominator of the LCOH equation 3.1. Deviation of only costs would have resulted in a symmetrical Gaussian distribution. Since the amount of hydrogen is also affected, a certain skewness is observed.

Furthermore, it must be noted that, although the mean LCOH for the PEME- and AE-based system differentiates, there is a large overlapping area when the uncertainty is included. This was already observed in the sensitivity analysis, where for instance a difference in stack efficiency could be a decisive factor for the AE-based system to realise a lower LCOH, as was seen in Figure 4.18.

It must be noted that some of the variations of input parameters would be influential on both systems, for instance, a lowering costs of steel or costs of the offshore wind farm. Nevertheless, a significant number of input parameters do not influence both systems, hence the overlap is seems justified.

4.7. Discussion Part I

A model was built to gain inside into the principles of centralised offshore hydrogen production from a techno-economic point of view, as presented in Section 3. Due to the novelty of such concepts, and therefore the absence of concrete data, assumptions had to be made which causes the obtained results to deviate from how such a project might perform once build. These deviations are discussed in the following section, to understand what the weaknesses of the model are and where, if all resources would be available, improvements to the model could be made.

4.7.1. Optimal HPU capacity

The model assumes that all possible installed HPU and stack capacities are possible. However, in an actual design, the sizing will also depend on the capacity of individual components. At the time of carrying out this research, the sizes of these individual components were not known and therefore not applied. Future design of such COHP must take into account the capacity of individual components and size accordingly. Incorporating the sizes of the individual components implies that not every HPU and stack capacity is possible. The result then obtained will probably be that the optimal sizing is related to the individual capacity of the most expensive component and that this capacity is maximally utilised.

4.7.2. Statistical model
The model works on Statistical wind speed data and therefore the effects of power input fluctuations are not taken into account. The fluctuations could cause a lower use of the available electricity. Utilising time series data in the model would allow for the inclusion of the impact of fluctuations. These fluctuations are addressed in Part II. Furthermore, the yearly average wind conditions are used. This doesn't provide insight into the difference in performance per month. Having insight into the differences in hydrogen production per month would realise the possibility gain insight into the optimal scheduling of maintenance procedures to optimise the technical availability.

4.7.3. Mass data
The masses used for the components, resulting in costs for the superstructure, substructure, and foundation, are obtained from literature. Such HPU equipment was not installed offshore at the time of writing, but onshore. For an onshore installation, the weight of components is a much less relevant aspect. This resulted in very limited available data regarding the mass of the components, which ultimately had a reasonable influence on the final results since the larger assumed AE-based COHP resulted in a more expensive commissioning method.

4.7.4. Transport and installation
It is anticipated that for transport and installation purposes, the use of the largest and second-largest installation vessels, namely the Pioneering Spirit and the Thialf, will be employed, as presented in Section 3.14. However, given the anticipated rise in the decommissioning of oil and gas offshore structures and the installation of renewable energy generation structures, the availability of these two installation vessels is uncertain [42]. As such, alternative installation methods, such as float-over, should also be considered. A float-over installation method could be a cost-competitive variant. Its availability is in general higher but the workable weather window is smaller [42].

4.7.5. Assumed lifetime
Several remarks can be made to the model regarding the life span considered. A lifetime of 35 years for the entire project has been assumed. For turbines, such a lifetime has not yet been achieved simply because the turbines as they are known today were first installed not that long ago. Therefore, they have not yet had the opportunity to achieve such a lifetime. A longer project life means that there is a longer period in which the investments made can be recouped. Here, however, the profits must continue to outweigh the costs incurred. In addition, such a project does occupy a certain location which could perhaps be better used for a newer project should the performance of this project decline significantly. Research should continue to show whether it is both technically and economically feasible to operate the turbines for this lifetime.

The model accounts for the lifetime of the stacks and the associated replacement costs. However, it is likely that other components within the COHP also have shorter lifetimes than the proposed project lifetime and will require replacement. For example, compressors are wear-sensitive components. To ensure the completeness and accuracy of the model, it is necessary to include the lifetimes and replacement costs of all components within the COHP in the calculations.

4.7.6. Assumed dynamic response
PEME-based systems are known for their fast dynamic response. However, current AE-based systems are less able to withstand sudden variations in power input. In the model, however, it was assumed that both technologies can handle these fluctuations adequately, so there is no need to differentiate the efficiency of hydrogen production. Whether this assumption is valid is addressed in Part II.

4.8. Summary Part I
For readers who have just read this chapter, this summary is superfluous. In the previous chapter, a case study was conducted. By using this data and the model as described in Chapter 3, an optimal HPU capacity with matching compressor output pressure and matching LCOH were found for this location. This was done to gain more insight into which stack technology resulted in the lowest LCOH or highest NPV.

First, a preliminary sizing was performed to find out in which range the optimal HPU capacity would

lie. For this, a compressor output pressure of 60 bar was assumed, as described in Section 4.2. Over a range of 600 MW to 1.0 GW installed HPU capacity trend lines were presented. These trend lines were constructed using the same principal relations as the model in Section 3.1. These are the total amount of hydrogen to be generated, the initial and ongoing costs, and the masses of the two technologies. Once these trend lines were established, the LCOH- and NPV curves were drawn up. For both the LCOH and NPV curves, an optimum HPU capacity was found. Furthermore, both lines presented a small preference for the PEME-based system. A preliminary optimal HPU capacity of 940 MW, resulting in an LCOH of 2.84 €/kg was found for the PEME-based system. For the AE-based system, the lowest LCOH of 2.93 €/kg was found at an installed HPU capacity of 939 MW. The optimal installed HPU capacity, when optimising for the highest NPV, showed dependence on the hydrogen selling price. A hydrogen selling price above the lowest LCOH resulted in an increase in optimal installed HPU capacity.

After the range over which the optimal HPU capacity was approximately in view, a subsequent optimisation was carried out, in Section 4.3. This was performed to find the optimal compressor output pressure. The higher hydrogen pressure is associated with lower pipeline costs, however, it is also associated with higher compressor costs and power consumption. This optimisation showed that for both systems the optimal pressure is 71 bar as this facilitates the use of a pipeline diameter smaller than 16 inches. The optimal HPU capacity remained at 940 MW for the PEME-based system and decreased to 938 MW for the AE-based system. The resulting LCOH are 2.82 €/kg and 2.92 €/kg for the PEME- and AE-based system, respectively.

This combination of compressor pressure and HPU capacity was then further analysed in Section 4.4, where the effect of time on the performance of the COHP was considered to analyse the effect of the degradation of the stacks and wind farm on the annual amount of hydrogen to be generated. Furthermore, the CAPEX and OPEX components were broken down into all their contributors, and the total LCOH was broken down into the CAPEX and OPEX of the offshore wind farm and COHP.

Finally, a sensitivity and uncertainty analysis was performed. The sensitivity analysis showed that the offshore wind farm and COHP CAPEX, and the WACC were most influential on the obtained LCOH. The optimal sizing however was relatively insensitive to the variations of 10 and 20 percent with respect to the base value. All newly obtained optimal installed HPU capacities showed a maximum deviation of 1% of the base value.

Note to reader: This was the final section of Part I. Hereafter, Part II commences.

Part II

Dynamic analysis

5

Power fluctuations theoretical background

After discussing both hydrogen production and the affiliated costs in Part I, with this chapter, Part II starts. In this part, the focus is shifted towards hydrogen production solely. In the following chapter, the effect of power fluctuations on hydrogen production and the model used to assess these effects, are presented.

First, the implications of a fluctuating power source on stacks and hydrogen production are presented in Section 5.1. Then, the power output fluctuations of an individual wind turbine and an offshore wind farm are addressed in Section 5.2 and 5.3, respectively. The time-series based model, used to determine hydrogen production from a fluctuating power source, is presented in Section 5.4. The adaptions made to this existing model to make it suitable for centralised hydrogen production are presented in Section 5.5. Finally, the applied control strategy is presented in Section 5.6.

5.1. Power fluctuations and hydrogen production

The practice of connecting stacks to wind power differs significantly from the traditional industrial water electrolysis systems that are powered by the grid. Conventional grid-connected stacks can rely on a constant power supply, whereas the power supply for a stack in an offshore wind-hydrogen system is significantly less stable. This intermittent power supply to the hydrogen producing system has several negative consequences.

The changing power input leads to changes in temperature, gas pressure, gas purity, and hydrogen massflow. These fluctuating operations can have negative influence on the lifetime of the system components [82]. Besides, the equipment requires energy to start-up and shut-down, procedures necessary when the delivered power increases or decreases and surpasses the capacity of the operational electrolysers. These processes do not contribute to hydrogen production and thus adversely affect the overall production efficiency [82]. Finally, frequent complete interruption of the power supplied to the electrolysers increases the degradation of the stacks. The degradation of the stacks affects the system's performance and therefore the production of hydrogen [59].

The above findings argue why an electrolyser system thrives on a more constant power supply as it both positively affects the performance degradation of the stacks and system components, and contributes to a more efficient use of the available energy.

5.2. Fluctuations of wind turbines output power

The variability of power output of wind turbines is directly related to the variability of the incoming wind speed. The variability of wind speed can be divided in two components. The first is a deterministic component caused by the daily or seasonal patterns of wind speed, while the second is a stochastic component caused by various random events. This deterministic, mesoscale component is observed at the left side of the spectral gap as seen in Figure 5.1. The stochastic, microscale component of wind speed variations is observed at the right side of the spectral gap and fluctuates at a rate ranging

from 0.1 seconds to minutes. Wind turbine power output fluctuations, are somewhat minimised by rotor inertia, although the fluctuation period would still be in the order of seconds [83]. Since the long-duration fluctuations are deterministic, the means to attenuate them are limited. In addition, given the low frequency at which these fluctuations occur, they contribute less to the aforementioned problems resulting from coupling electrolyser stacks to a wind energy power source. However, there is reason to assume that short-term fluctuations can be attenuated. In addition, because these fluctuations occur with high frequency, damping these fluctuations would have significant positive effects on the wind-hydrogen system. Therefore, for this study, there is only interest in the short-term power fluctuations of the wind turbine power output. Thus, when fluctuations are mentioned, reference is made to the stochastic short-term fluctuations.

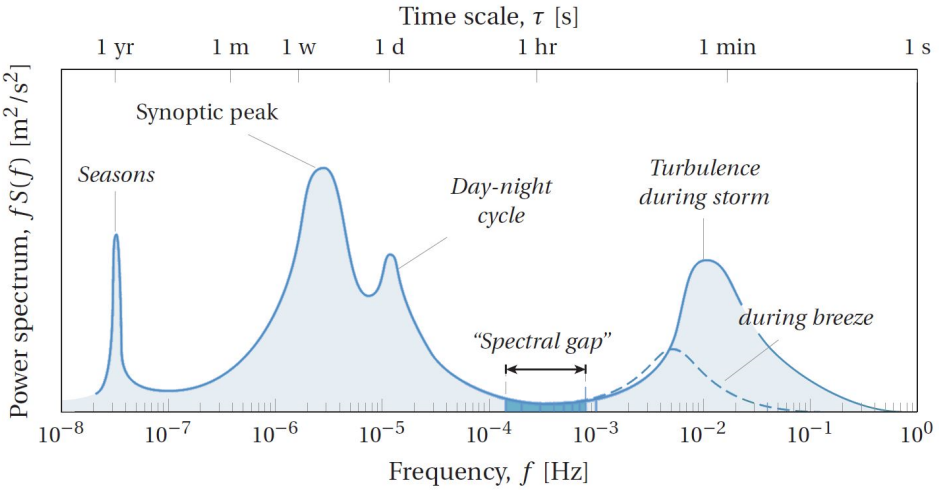

Figure 5.1: Van der Hoven Spectrum (1957) as drawn by Alan Davenport. Taken and adapted from [84].

These fluctuations in the power output are due to both natural and mechanical aspects. The first and foremost reason behind power fluctuations is the variability in wind speed and turbulence as received by the wind turbine. Wind speed variations occurring below cut-in wind speed and above rated wind speed generally do not influence the power output of the wind turbine. However, wind speed changes in the partial load region are amplified by the steepness of the wind turbine's power curve. Hence, wind speed changes near rated wind speed cause large power fluctuations [85]. Other natural effects resulting in power output fluctuations are rapid changes in wind direction and wind shear.

5.3. Power fluctuations in large offshore wind farms

The power source of the COHP is the entire offshore wind farm, consisting out of multiple wind turbines. The spatial arrangement of these wind turbines, characterised by a high density of wind turbines that spread over a large area, influences the wind speeds and power output within the offshore wind farm.

In an offshore wind farm, the presence of upstream wind turbines generates wake effects that have an impact on the performance of downstream wind turbines. The high wind turbine density in an offshore wind farm leads to an incomplete recovery of airflow before it reaches the next wind turbine, resulting in a decrease in wind speed and an increase in turbulence experienced by the downstream wind turbine. This amplified turbulence subsequently enhances the short-term variations of the individual wind turbine's power output. Two other effects of the high concentration of wind turbine are wake meandering and wind shifts [86]. Wake meandering is the oscillation of the whole wind turbine wake [87] at low frequencies. As a consequence, downstream wind turbines may intermittently experience increased turbulence due to being within the wake of an upstream wind turbine or beyond its reach. Wind shifts could cause temporary yaw misalignment, decreasing the observed relative wind speed and therefore decrease the power output of the wind turbine. Figure 5.2 presents the power output of a wind turbine versus incoming wind speed and shows the variability in power output, even at equal wind speeds.

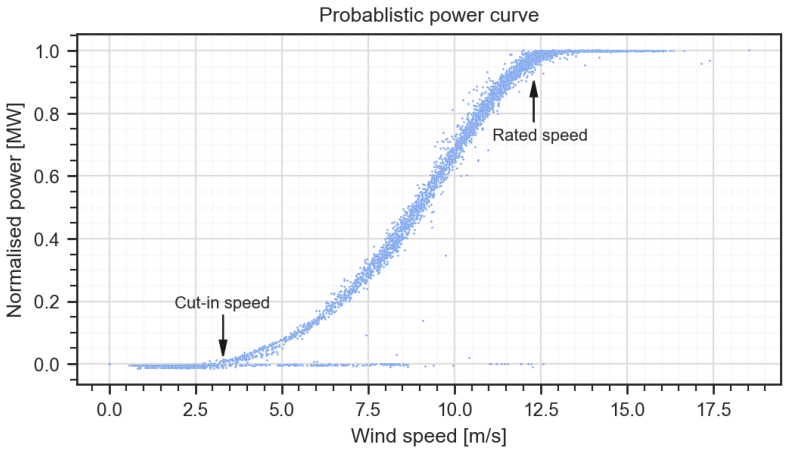

Figure 5.2: Normalised wind turbine power output versus wind speed. Made with historical data provided by Vattenfall.

It is expected that as technology continues to advance and economies of scale are realised, the power rating of offshore wind farms will increase. This increase in power rating will likely result in an expansion of the physical footprint of the offshore wind farm, either through the installation of more wind turbines or through the use of larger wind turbines that require larger distances between them [88]. This increase in surface area, decreases the coherence of wind speeds observed at a specific time. The level of correlation is dependent on the distance between two points and decreases as the distance between measured points increases [89]. This spatial distribution of wind turbines results in an instantaneous power output that differs from one wind turbine to another, both because of the difference in wind speed due to turbulence, but also because it takes some time, for example, for a wind gust to reach the next wind turbine.

In the centralised configuration, the power output of all wind turbines is collected at a central platform through the aggregation of the individual wind turbine outputs. Although the power fluctuations of an wind turbine are enhanced because of its situation in the offshore wind farm, the aggregation of the multiple stochastic fluctuations leads to a dampening of total fluctuation, resulting in significantly more stable power output. Figure 5.3 presents the time series power output of an individual wind turbine versus that of an offshore wind farm.

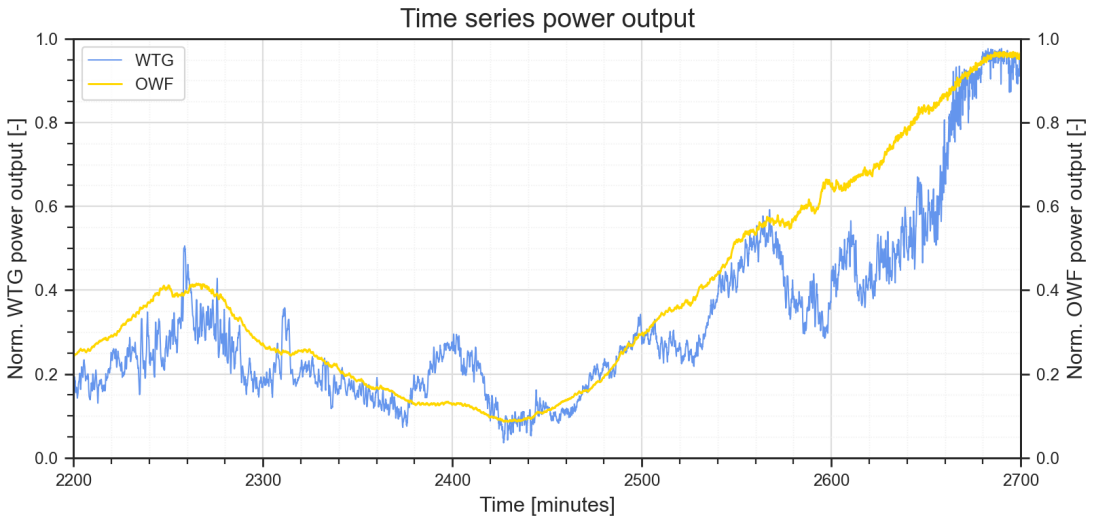

Figure 5.3: Time series power output of an individual wind turbine versus offshore wind farm.

This damping effect was observed, for example, around minutes 2260 and 2320. These short-term peaks in power output have a duration of no longer than 10 minutes. Additionally, medium-term temporary increases in power output have also been observed to be mitigated, with examples observed around minutes 2400 and 2560. These increases in power production are up to one hour. A final observation has been made regarding situations caused by an overall increase in power production due to wind rise. After minute 2440, an overall increase in wind speed was experienced, leading to an increase in power output from near cut-in levels to rated capacity for both the wind turbine and the offshore wind farm. However, during this overall increase, significant temporal reductions in the power output of the wind turbine are also observed. To compensate for these intermediate decreases, the incremental rate of change of the power output was observed to be larger, as seen between minutes 2600 and 2680. Since the increasing wind speed is experienced in phases across the offshore wind farm, the offshore wind farm power output increase is more gradual.

The phenomenon of a more consistent power output resulting from the spatial distribution of wind turbines in an offshore wind farm has been previously documented in the literature [15][83][90][91][92]. It has been established that the spatial and temporal distribution of wind turbines within an offshore wind farm has a significant smoothing effect on the power output for fluctuations in periods shorter than 10 minutes. However, the effectiveness of this smoothing effect diminishes for periods longer than 10 minutes.

5.4. Time-series model description

The following section will describe the model used for the examination of the effects of the power profile in the centralised configuration. To understand how short-term power input fluctuations affect hydrogen generation, a time-series model must be used. For this study to produce appropriate findings, the model must be able to handle high-frequency data.

Such a model was built by Helgason [93]. The model was initially developed to gain an understanding of the effects of different operational strategies for decentralised stand-alone hydrogen-only wind turbines and their response to short-term power fluctuations. For this model, modular containerised electrolysers were directly connected to the power output of a wind turbine. Anticipating the increasing size of wind turbines and the limited size of electrolysers, multiple electrolysers were connected to a single wind turbine. Therefore, a control strategy had to be adopted to operate the electrolysers most advantageously. Two main topics of interest in this study were the influence of the control strategy on overall hydrogen production and the frequency of electrolyser turn-ons and turn-offs. It was performed to better understand how power should be allocated among various electrolysers and when to turn an extra electrolyser on. Also, whether to turn an operating electrolyser to idle, and subsequently off, once the incoming power is not sufficient to operate the electrolysers appropriately or effectively. Only those aspects of Helgason's model that are pertinent to this study will be discussed. Reference is made to Helgason's report to get a complete explanation of the model [93].

5.4.1. Electrolyser operation state

There are three possible states for an electrolysers. First, the status can be offline. When an electrolyser is offline, there will be no energy delivered to the electrolyser. Therefore, it does not consume energy nor does it produce hydrogen. The next operational state is online. An online electrolyser consumes energy and produces hydrogen. To arrive in an online state, an offline electrolyser needs to be warmed up. The final considered operational mode is being in idle mode. An electrolyser in idle mode, also referred to as hot standby, can transition to an online state within 10 seconds. While an electrolyser in idle mode does not produce hydrogen, it does consume energy.

The operational state of an electrolyser is determined through rule-based advisory control, which utilises predetermined thresholds as decision-making criteria. Several thresholds are applied in the advisory control, as presented in the following summation.

- *Turn-on threshold*: If the operational point of the online electrolysers surpasses the turn-on threshold, an additional electrolyser will be turned from its offline status to online. This turn-on threshold is set between 60% and 100% of the operational range of the electrolysers.
- *Turn-to-idle threshold*: If the operational point of the online electrolysers will drop below the turn-to-idle threshold, one of the online electrolysers will be set to idle. This is done to distribute the consumption of power over the operational electrolysers more efficiently. If there is already one

electrolyser in an idling state, this electrolyser will be turned offline and an online electrolyser will be set to idling mode. The turn-to-idle threshold is set between 10% and 20% of the operational range of the electrolyser

- *Turn-on-from-idle threshold*: If one of the electrolysers is in idling mode, and the operational point of the online electrolyser surpasses turn-on-from-idle threshold, the idling electrolyser will be turned online again. Similar to the work of Helgason, this threshold is 50% as this is a good trade-off between extra hydrogen production and decreasing the number of switches of the operational status of the electrolysers.
- *Turn-off threshold*: The turn-off threshold is only used when a single electrolyser is operational. When the operational point is below this threshold, the only operating electrolyser is set to offline.

5.4.2. Model assumptions

The model's operation rests on choices and assumptions since not all information was available. The most important and relevant ones are displayed in the following summation.

- *Rigidity*: The control strategy utilised by the model is based on predetermined rules. These rules will be followed in all situations, regardless of whether an alternative strategy may have been more beneficial.
- *Parallelism*: When multiple electrolysers are online, the power is divided equally across the electrolysers. As result, all operational electrolysers operate at the same operating point.
- *Quick-start*: An electrolyser in idle mode can be turned on in 10 seconds by supplying power to the electrolyser and initiating hydrogen production.
- *Activation*: To turn a certain electrolyser on, time and energy are required. During this start-up period, the electrolyser that is turning on does not contribute to the production of hydrogen but does consume energy.
- *Redistribution*: The power distribution must be reallocated when one of the electrolysers is turned on or off, based on the new number of operational electrolysers.
- *Rotational*: The electrolyser that has been in operation for the longest duration will be deactivated, once the threshold is passed to turn one of the operational electrolysers to offline. Conversely, when an electrolyser is to be turned on, the electrolyser that has been in offline status for the longest period will be turned on first.
- *Prioritisation*: When a control strategy decides to operate an additional electrolyser, an idling electrolyser will be activated before an offline electrolyser.
- *Overloading*: Stacks are able to operate above their rated capacity for a certain amount of time.

By implementing the model, insight is gained in the overall hydrogen production, number of switches between the operational states, total turn-offs, idle time and dumped power.

5.5. Model modification for centralised production

Several modifications of, and additions to, the model need to be made to use it for centralised hydrogen production. These modifications are needed because of the differences in characteristics between centralised and decentralised hydrogen production. The key difference is the use of modular electrolysers in the decentralised configuration versus the integrated electrolysers in the centralised configuration. This results in a difference in efficiency [5.5.1] and startup time [5.5.2]. Furthermore, in the centralised configuration, the power produced by the wind turbine has to be transported to the COHP before it is used for hydrogen production [5.5.3].

5.5.1. Efficiency curve

To compare the hydrogen production rate of the two configurations, a configuration-specific load-dependent efficiency curve is required. The efficiency curve is constructed using the average specific energy demand. Literature reports a specific energy demand of 47.6 kWh_{AC}/kg_{H2} for a 5 MW PEM electrolyser and a specific energy demand of 48.1 kWh_{AC}/kg_{H2} for a 100 MW PEME based system. While the water treatment equipment and gas conditioning equipment of the central configuration operate slightly more efficiently, larger losses in the electrical equipment are reported. This is due to the higher conversion

losses in the central configuration, as it is fed with medium voltage power, as opposed to the low voltage power supplied directly from the wind turbine in the decentralised configuration. It is chosen to compare the two configurations for a hydrogen output pressure of 30 bar, hence additional compression is not required.

Installation size	5 MW	100 MW	Unit
Electrical equipment	4.00	4.16	%
Water treatment equipment	0.76	0.75	%
Gas conditioning equipment	0.22	0.21	%
specific energy demand	47.6	48.1	kWh_{AC}/kg_{H2}

Table 5.1: Comparison of energy consumption for a small-scale and large-scale electrolysis system [68].

The specific energy demand values found are used to establish new efficiency curves. These new efficiency curves have the same shape as the efficiency curve of the electrolysers as found in literature for currently operational PEM electrolysers, as presented in Figure 2.4 [68]. However, to accommodate for future expected efficiencies and the difference in efficiency between the centralised and decentralised configuration, a scale factor is added. The resulting electrolyser efficiency curves are shown in Figure 5.4. The efficiency curves are scaled such that the average efficiency between 10% and 100% of the operational load is in accordance with the specific energy demand as stated in Table 5.1.

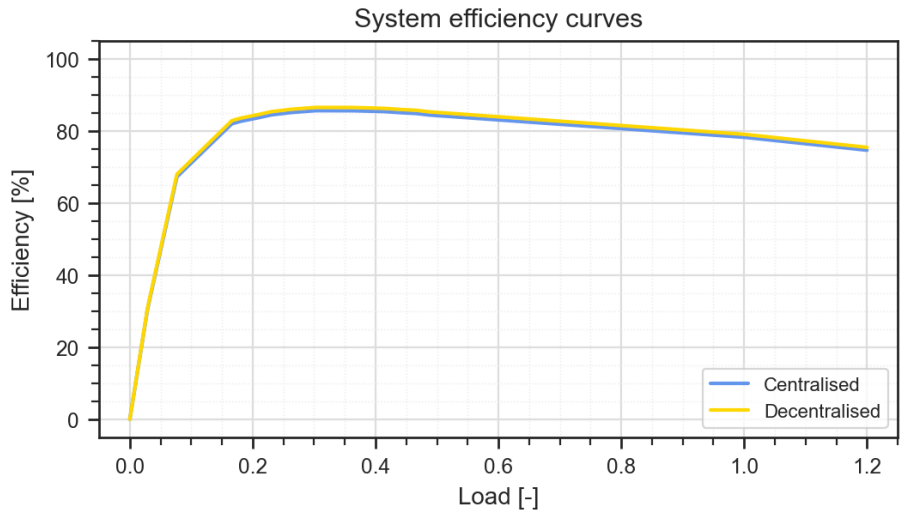

Figure 5.4: Efficiency curve of the centralised and decentralised configuration.

In the centralised configuration, it is assumed that all stacks in a single module will operate at the same operating point when online. This implies that all electrolysers operate at equal efficiency. Therefore, the efficiency curve as presented in Figure 5.4 is representative for an entire module.

5.5.2. Start up time and down time

The duration of the start-up time is a model input and is assumed to be different comparing the two configurations. For the decentralised configuration, a start-up period of 5 minutes is obtained from literature [13]. For the centralised integrated configuration, the start-up time is not known. However, the large size of the electrolysers modules and the large power rating of the individual components might argue that a longer start-up period is required. Therefore, a 10-minute start-up time for the decentralised configuration is assumed.

5.5.3. Inter-array cable losses

The transmission of power from the wind turbines to the COHP is accompanied by power losses due to resistance in the inter-array cables. The magnitude of these losses is determined by the current, voltage, resistivity, and length of the inter-array cable. The power delivered from a single inter-array cable string to the COHP, as well as the intermediate losses, are depicted in Figure 5.5. The losses in each section are dependent on the length of the section and the amount of power flowing through it. This power is influenced by the number of upstream wind turbines that have contributed power to the inter-array cable string, as well as the losses that have occurred in the preceding sections.

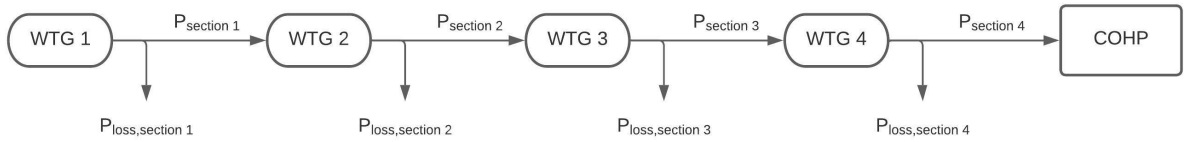

Figure 5.5: Power losses in inter-array cable sections. Distances between wind turbines and COHP are not proportional.

The power loss in each inter-array cable section, $P_{loss,sec}$, is calculated according to equation 5.1 [94].

$$P_{loss,sec} = 3 \cdot I_{sec}^2 \cdot R_{sec} \tag{5.1}$$

Here, I_{sec}, is the current through a specific inter-array cable section and R_{sec} is the resistance of that section. The resistance in each inter-array cable section is determined according to equation 5.2 [94].

$$R_{sec} = \rho \cdot L_{sec} \tag{5.2}$$

Here, ρ is the resistivity and L_{sec} the length of a specific inter-array cable section. The resistivity is dependent on the cable selected, which must be able to handle the highest power through the inter-array cable string. The distances between the different wind turbines and the COHP can be found in Table B.1 in the appendix. The current through each section is subsequently calculated according to equation 5.3 [94].

$$I_{sec} = \frac{P_{sec}}{\sqrt{3} \cdot U_{IAC}} \tag{5.3}$$

By maintaining the voltage in the inter-array cable grid, U_{IAC}, constant, the current in each section can be determined. The power in a section, P_{sec}, is equal to the power generated by the wind turbine and the power transmitted by the previous inter-array cable section combined.
The resistivity of the cable used depends on the required cable diameter to handle the maximum power through the cable. A constant cable diameter for all inter-array cable sections is assumed. This maximum power is determined according to equation 5.4.

$$P_{max} = \sqrt{3} \cdot I_{max} \cdot U_{IAC} \cdot cos(\theta) \tag{5.4}$$

Here, $cos(\theta)$ will be chosen as *X* [95]. To remain within margins, the maximum power through a cable section is determined by using the power rating of the wind turbine and the number of wind turbine on a single string. The lowered maximum power due to losses in the cable are here neglected.

5.6. Applied control strategy

To compare the two different configurations, equal control strategies will be adopted, referring to the turn-on threshold and the turn-to-idle threshold. The turn-on threshold relates to set value for turning on another electrolyser or module. A higher turn-on threshold implies that it demands more input energy before the next electrolyser is turned on. this on its term influences the number of operational mode switches. However, by setting the turn-on threshold higher, the electrolysers or modules will operate for a larger load in the less efficient region. Hence, this influences hydrogen production.

Two different turn-on and turn-to-idle thresholds will be tested, resulting in four different strategies. A turn-on threshold of 95% and 85 %, and turn-to-idle threshold of 15% and 10 % is adopted. It must be noted that this study is interested in comparing the two different configurations, not in finding the optimal control strategy, hence this approach deemed suitable. Multiple strategies are taken in order to make sure that the results obtained are not due to the chosen control strategy but because of difference in configuration characteristics.

6

Case study, Results and Discussion

In the following chapter, the model as presented in Chapter 5 is implemented on a chosen data set to perform a case study that will provide the results of Part II. First, the selection of the historical data set is presented. Section 6.1 addresses the chosen offshore wind farm and Section 6.2 the specific moment in time. Subsequently, Section 6.3 will outline the process for preparing the data set, as the original data set was not suitable for direct implementation.

The results of Part II are divided into two sections. First, an analysis of the obtained power output data set is performed to compare the power output of an individual wind turbine versus that of multiple wind turbines, and the entire offshore wind farm. This power output difference is presented in Section 6.4. Then, the time-series hydrogen production model and specific data set are used to gain insight into the effects of the different power input patterns on hydrogen production in Section 6.5. Finally, Section 6.6 and Section 6.7 present the discussion and summary of Part II, respectively.

6.1. Specific wind farm

The model is tested using historical data from an existing offshore wind farm that closely resembles the characteristics of a future GW-scale offshore wind farm. To ensure the highest level of relevance, the offshore wind farm was selected based on criteria such as wind turbine rating and the number of wind turbines. Despite the availability of data from multiple offshore wind farms within the company, data from GW-scale offshore wind farms was not available. Therefore, the offshore wind farm chosen for this study was the one with the highest possible wind turbine rating and the highest possible number of wind turbines.

These conditions were met in an offshore wind farm in Northern Europe. Due to seabed restrictions, the offshore wind farm features a gap in its layout. This gap increases the total surface area occupied by the offshore wind farm, thereby contributing to its resemblance to a future gigawatt-size offshore wind farm. On the other hand, the central gap also enables the wake to recover more, which resembles a future offshore wind farm less.

Since the original inter-array cable lay-out did not meet the requirements for centralised offshore hydrogen production, a new inter-array cable layout is proposed. The number of wind turbine per string is maintained at four. The wind turbines in the left section of the offshore wind farm are connected in the same configuration as the original offshore wind farm. However, the right section of the offshore wind farm has been given a new layout due to the absence of data of some of the wind turbine and the placement of the central platform. Connecting the original strings to the central platform would result in inter-array cables crossing each other, thus necessitating a new proposed string configuration. It should be noted that no further efforts were made to optimise the cable layout, as this is beyond the scope of this work. Additionally, it would have been impractical to optimise the layout of inter-array cable as the original wind turbine placement must be preserved, and optimising the combined wind turbine and inter-array cable layout is a simultaneous task rather than a sequential task. It is important to recognise that even though data of some wind turbine may not be available, their presence in the actual offshore wind farm still impacts the wakes observed by the wind turbine for which data is available.

According to the same analogy as in Section 2.1.2, the voltage in the proposed inter-array cable

is set at 66 kV, even though the voltage in the original offshore wind farm is 33 kV. It is assumed that difference in losses between stepping up the voltage to 33 kV and 66 kV are negligible [95]. Using Equation 5.4, it is found that a minimum diameter of 150 mm is required. Selecting the minimum necessary diameter is a common practise based on economic considerations since lowering the losses by using a larger diameter does not outweigh the additional costs.

6.2. Specific data set

When selecting a time-series data set, it is essential to ensure that the data set used captures a variety of wind turbine operations. This includes conditions where operation is in lower partial load, around the steep part of the power curve, and at nominal capacity. Additionally, wind phenomena such as wind rise, wind fall, wind gusts, and wind lulls should also be present in the data set to obtain a comprehensive understanding of the offshore wind farm's performance. Furthermore, it is important to have data with a sample rate in the order of seconds and a large enough total sampling time. A data set containing all the described wind phenomena, with a sampling rate of around 5 seconds over a 72-hour period, was found. This data set covers the 14th to 16th of October of the year 2022. Figure 6.1 presents the data set obtained of four wind turbines of the offshore wind farm.

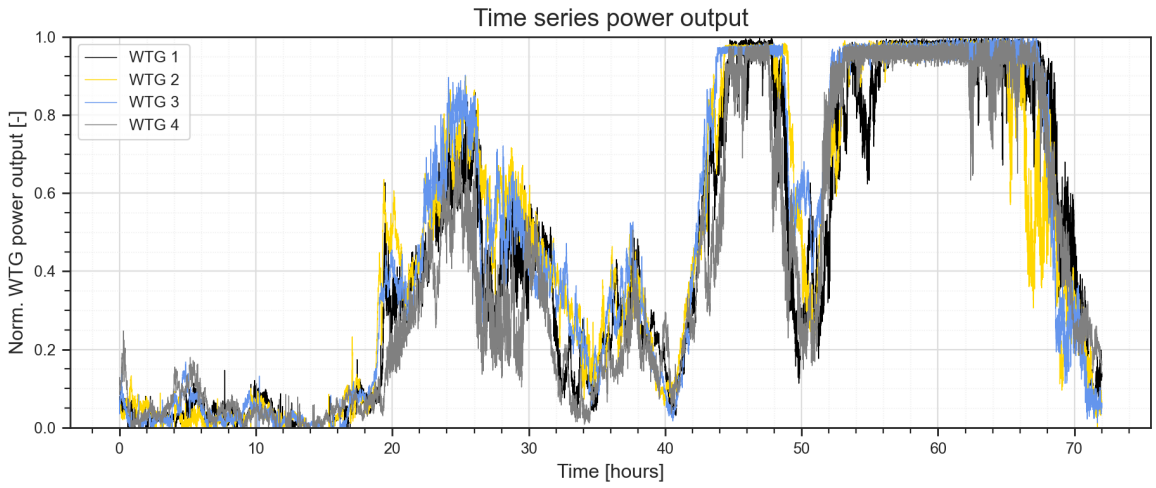

Figure 6.1: Time-series of the individual power output of four wind turbines of the offshore wind farm between 14 and 16 October 2022.

6.3. Time-series data preparation

The data sets obtained from the 59 wind turbines, as received, were not immediately suitable for their intended application. Specifically, measurement errors resulted in missing data points and the power output of the wind turbines was sampled at varying frequencies, resulting in different lengths of the data sets per wind turbine. The procedures employed to rectify these issues and prepare the data set for usage are discussed in the following sections.

6.3.1. Gabs in received data

In each data set, a maximum of 3 data gaps are identified. To fill in these gaps of information, an interpolation method outlined in the study by Lepot et al. [96] is employed. Specifically, once the index of an data gab is located, the value of that index is calculated through linear interpolation of the values from the two nearest indexes that have available data.

6.3.2. Difference in sampling interval

Discrete time-series data of each wind turbine is provided. The data for all wind turbines covers a 72-hour period. However, the sampling intervals for the wind turbines vary, resulting in a different number of data points for each wind turbine, collected at different times. The wind turbine with the highest

sampling frequency is sampled at a frequency of 0.197 Hz (5.072 seconds). The wind turbine with the lowest sampling frequency is sampled at a frequency of 0.165 Hz (6.050 seconds).

To accurately calculate the instantaneous offshore wind farm power production, it is necessary to sum the power production of the individual wind turbines at the same moment in time. However, due to the different sizes of the time-steps, the i-th index of wind turbine x may not be at the same moment in time as the i-th index of wind turbine y. To address this issue, all individual data sets are linearly interpolated and subsequently resampled at an equal sampling rate. This sampling rate should be selected such that no information is lost from the original data set. Sampling the original data set at a too-high sampling frequency results in the peaks in this original data set being shaved off. For this study, these peaks in power output are relevant. Therefore, shaving off the peaks should be minimised.

An appropriate sampling rate would be the Nyquist rate, as established by Nyquist [97], which states that the new sampling rate should be at least twice the original data sampling rate to preserve the information present in the original data set. To have a consistent new sampling rate for all individual wind turbines and to meet the Nyquist criterion for all data sets, the sampling time should be twice the sampling rate of the data set with the lowest sampling rate. The highest sampling rate found is 0.197 Hz. The Nyquist rate is therefore equal to 0.394 Hz. A section of the obtained data set, based on the Nyquist rate, is depicted in Figure 6.2 (left).

However, a visual comparison of the data set created with the Nyquist rate and the original data set reveals that, albeit minimal, some information about the original data set is lost. To mitigate this issue, a higher data sampling rate of 1 Hz is chosen, which corresponds to a sampling interval of 1 second. This data set is presented in Figure 6.2 (right), and is used for the case study. This results in the creation of 59 new data sets, each containing 259.200 data points.

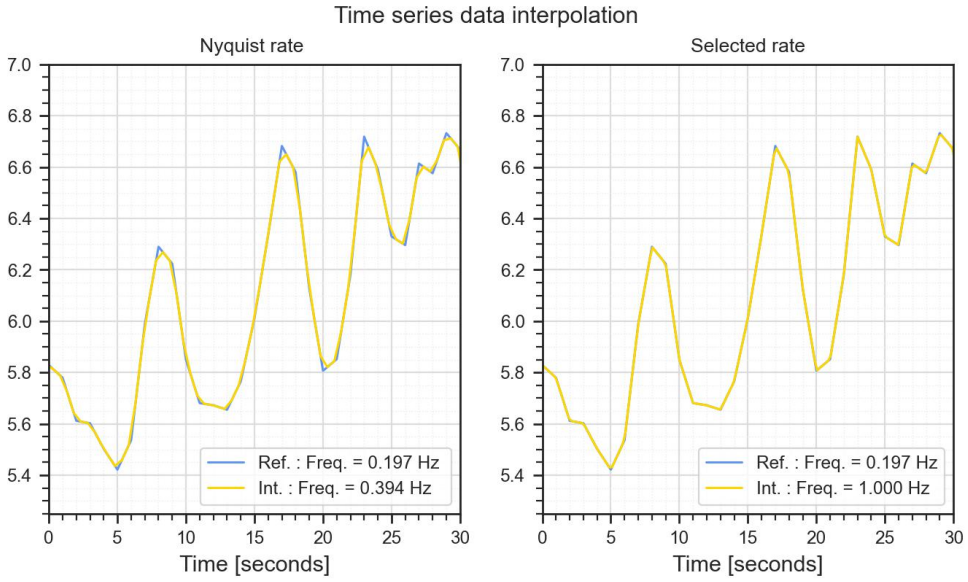

Figure 6.2: Visualisation of sampling at Nyquist rate (left) and the selected rate of 1 Hz. (right)

6.4. Power output analysis

This section analyses the power output of the offshore wind farm and individual wind turbines. Eventually, this power output will serve as the power input for the COHP in the centralised configuration, and for the electrolysers in the decentralised configuration. Since the hydrogen producing system needs to withstand these power fluctuations, it is important to have a thorough understanding of them.

To compare the power output fluctuations, despite the difference in maximum power output between the offshore wind farm and an individual wind turbine, the fluctuations are normalised. Equation 6.1 is used to determine the normalised power fluctuations, $\Delta P_{i,norm}$.

$$\Delta P_{i,norm} = \frac{P_i - P_{i-1}}{P_{max}} \tag{6.1}$$

Here, P_i represents the power output at time-step *i*, and P_{max} the maximum power possibly produced by the power source. The time-step size is variable. The results of this analysis are depicted in Figure 6.3 for fluctuations in the 1-minute average, 5-minute average, and 10-minute average power output of both the offshore wind farm and an individual wind turbine. This methodology enables a quick and intuitive manner to compare and analyse the power fluctuations.

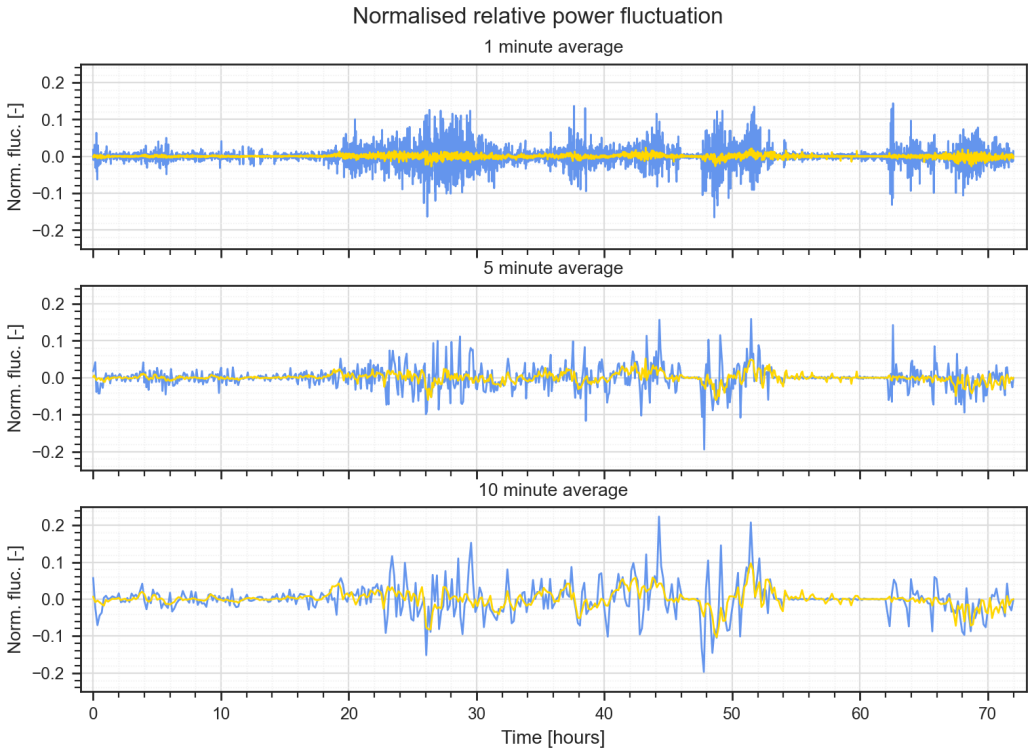

Figure 6.3: Normalised power fluctuation of an individual wind turbine (blue) and the offshore wind farm (yellow) for a 1-minute, 5-minute, and 10-minute average power output. The number of fluctuations decreases as result of increases in averaging time of the output power.

Since only a single random wind turbine is considered, the conclusions drawn based on Figure 6.3 must be with nuance. Nevertheless, it shows, for all time-steps considered, some first examples of the smoothing of the power fluctuations comparing the power output of the offshore wind farm versus an individual wind turbine.

The severity of the fluctuations will differ per wind turbine and depends, amongst others, on the location within the offshore wind farm and the incoming wind direction. Table 6.1 considers all wind turbines present in the offshore wind farm. Here, the maximum normalised power fluctuation of the offshore wind farm and the highest and lowest maximum normalised fluctuation of the population of wind turbines is presented, for the three considered time-steps. The maximum normalised power fluctuations of the remaining wind turbines falls between these two values.

	OWF	WTG	
		Min.	Max.
1 min.	0.041	0.216	0.571
5 min.	0.086	0.244	0.588
10 min.	0.150	0.296	0.674

Table 6.1: Maximum normalised power fluctuation.

The result of this analysis, as presented in Table 6.1, show remarkable differences between the maximum fluctuation of the offshore wind farm and the individual wind turbines. For the data set analysed, the offshore wind farm exhibited a maximum fluctuation in power output of approximately 4% of its maximum power output, while the individual wind turbines showed fluctuations ranging from 22% to 57% of their maximum power output, within a 1-minute interval. Furthermore, the duration of the observed interval influences the magnitude of the maximum fluctuation. Over a 10-minute period, the power output of the offshore wind farm has shown a difference of 15% of its maximum output and the wind turbine maximum output differences between 30% and 67%. The differences between the 1-minute and 10-minute interval power output maximum fluctuation is larger for the offshore wind farm than for the wind turbine.

Further analysis reveals the standard deviation of the normalised power fluctuations, as presented in Table 6.2. The standard deviation reflects the spread of the collection of data points considered. A lower standard deviation implies that the considered data points are closer to the long-term average. Therefore, the standard deviation of a data set of power fluctuations reflects the severity of the power output fluctuations.

	OWF	WTG	
		Min.	Max.
1 min. avg.	0.0044	0.0157	0.0391
5 min. avg.	0.0128	0.0276	0.0785
10 min. avg.	0.0231	0.0371	0.1134

Table 6.2: Standard deviation of the normalised power fluctuation.

From Table 6.2, it becomes evident that the standard deviation of the normalised power fluctuations of the offshore wind farm is significantly lower than those of the individual wind turbines. Even the lowest standard deviation of the normalised power fluctuation of an individual wind turbine is still higher than that of the offshore wind farm. Again, as the considered length of the average power production period increases, the standard deviation of the normalised power fluctuation increases for both the offshore wind farm and the wind turbine.

For a better understanding of after how many wind turbines such power smoothing occurs, a method is adopted to analyse the obtained power output data. As the correlation between the output of wind turbines decreases with increasing distance between the wind turbines [89], it is important to take the distance between the different wind turbines out of the equation when analysing the effect of increasing the number of wind turbines on reducing power fluctuations. A model in Python is written to select a random number of wind turbines from the total wind turbine population and aggregate the power delivered by the respective wind turbine collection. By repeating this program a significant number of times, a certain trend is obtained. This trend converging to the result of the complete offshore wind farm, i.e the case in which all wind turbines are considered. The number of iterations required for this procedure is determined by repeated execution until the observed change in outcome is insignificant. After completing 5,000 iterations, there was no discernible difference in the outcome, leading to the acceptance of this exact number of repetitions.

First, this method is used to evaluate the maximum absolute power fluctuation of a randomly combined set of wind turbines. The results applying this method on the maximum absolute power fluctuations are presented in Figure 6.4. To compare the fluctuations of the randomly generated combinations of wind turbines, the fluctuations are normalised to eliminate the difference in total maximum power output.

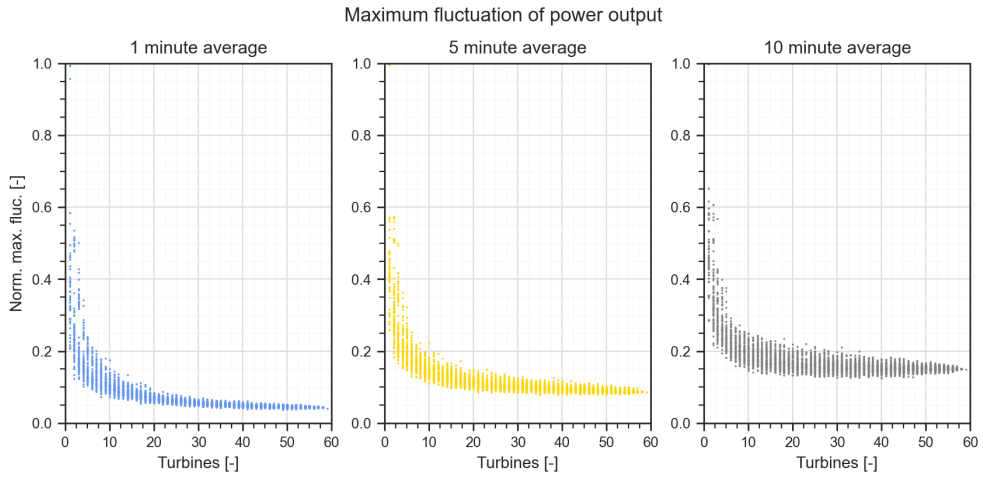

Figure 6.4: Maximum fluctuation versus number of wind turbines for different time-steps. Data created using 5.000 combinations of wind turbines.

Figure 6.4 presents the convergence of the maximum normalised power fluctuation as the number of wind turbines increases, up until all wind turbines are combined, representing the offshore wind farm. This indicates that the number of wind turbine considered, influences the maximum absolute normalised power fluctuation observed. The largest decrease in maximum normalised power fluctuation is observed during the combining of the first 15 wind turbines. Furthermore, the figure present that there exist combinations of wind turbines, with an installed number of wind turbines lower than the maximum uninstallable number of wind turbines, that show a lower maximum fluctuation than the complete offshore wind farm. This is the result of the random coupling of the sets of wind turbine. The power output fluctuations are dampened when wind turbines are combined that are positioned far and downwind from each other, as the output correlation decreases with increasing distance. Conversely, wind turbines located closely and side-by-side, based on the incoming wind direction, demonstrate a high degree of power output correlation and result in low power fluctuation damping effects [98].

Figure 6.5 presents the standard deviation of the normalised power output fluctuations over a 1-minute, 5-minute, and 10-minute average time-step for an increasing number of wind turbines until the complete offshore wind farm is considered. To compare the fluctuations, the fluctuations are normalised to eliminate the difference in total maximum power output.

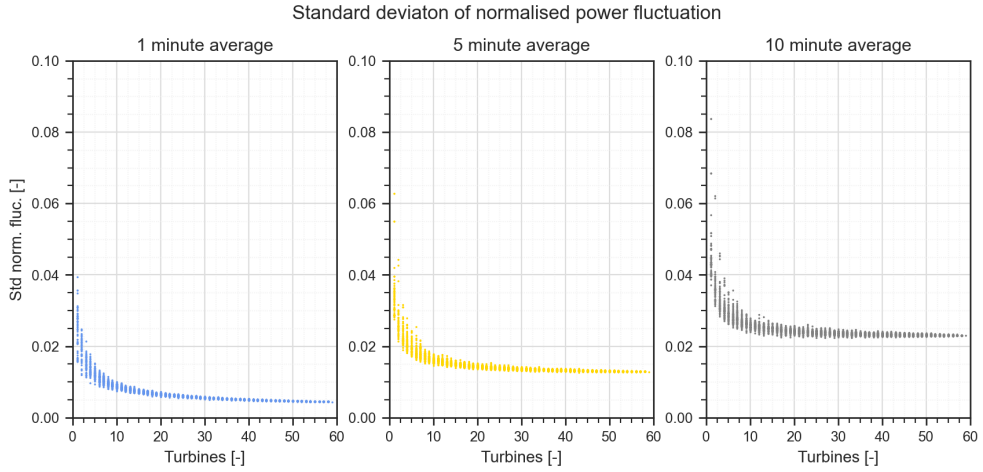

Figure 6.5: Standard deviation of normalised power fluctuations versus number of wind turbines for different time-steps. Data created using 5.000 combinations of wind turbines.

Figure 6.5 presents a downwards converging trend of the standard deviation of the normalised power fluctuations, for all three considered lengths of power output averages, as the number of wind turbines increases. A sharp decrease is observed during the aggregation of the first 15 wind turbines. Hereafter, the change in normalised standard deviation converges slowly to the standard deviation of the normalised fluctuations of the complete offshore wind farm.

The power fluctuations are an important factor to consider since the stacks are only able to withstand a certain ramping. One of the main disadvantages of an AE-based system is the slower dynamics of the system, as presented in Section 2.2. The ramping capabilities of an AE-based system reported in literature show a significant variance, namely between 0.13% per second for older systems and 10.0% per second newer ones [99]. Other newer AE-based systems report a maximum ramping of 1.67% per second [100]. The maximum fluctuation of the complete offshore wind farm is 0.3% per second.

In the centralised configuration, the power fluctuations seem to have decreased sufficiently that an AE-based system is able to withstand them. The power fluctuations of a decentralised configuration however would not suffice for an AE-based system. The results of this section therefore seem to confirm one of the assumptions made in Part I, regarding the assumed capability of the AE-based system to withstand the fluctuations of the incoming power source. Besides, given the high ramping rates of a PEME-based stack, these fluctuations do certainly not form a challenge for a PEME-based system [100].

Concluding this section, this section delved into the difference between power fluctuations between an offshore wind farm, relevant for centralised production, and individual wind turbines, relevant to decentralised production. This section showed that a significant difference between the magnitude of the fluctuation between an offshore wind farm and an individual wind turbine. By means of power aggregation, the power fluctuations are damped resulting in a lower maximum and lower standard deviation of the fluctuations. Furthermore, it was shown that the time-step over which a difference in power output was observed also influenced the magnitude of the fluctuation. With an increasing time-step length, the magnitude of the fluctuation increases. The slope of the increment however decreases as the time-step length increases.

6.5. System operation results

Whether this smoothed power output of the offshore wind farm contributes to the hydrogen production process, is tested by applying the analysed data set to the model. Since literature does not present any benchmark values to compare the centralised configuration with, and because the results of such research are highly dependent on the chosen power input data set and applied control strategy, it was decided to compare the result obtained for a centralised configuration with a decentralised configuration. In a decentralised configuration, all wind turbines are supplied with their own set of electrolysers, eliminating the use of the inter-array cable. A schematic representation of a decentralised configuration is presented in Figure 1.1. To have a representative comparison, both configurations are submitted to similar control strategies.

Anticipated are multiple possible benefits in the centralised configuration. First of all, due to the smoother power input, the thresholds as set as part of the control strategy adopted are less often reached. Therefore, an operation with fewer switches of operational mode might be observed in the centralised configuration. Furthermore, switching operational state requires energy and therefore lowers the total energy available for hydrogen production. This smoother power input might therefore benefit the total amount of hydrogen produced. Nevertheless, the power generated in the wind turbines first has to be transported to the COHP, resulting in inter-array cable losses, as presented in Section 5.5.3. Finally, due to the lower anticipated number of switches, the stacks are assumed to be less time in an idling status.

It was decided to employ four parallel, equally sized, hydrogen producing systems in both configurations. It is anticipated that the use of four parallel stack modules or electrolysers facilitates enough flexibility to operate at an optimal load, while maintaining a sufficiently large size for each individual hydrogen producing system. It must be noted that no further efforts were made in this work to optimise the the number of stack modules or electrolysers.

To ensure a fair comparison between the centralised and decentralised configurations, multiple control strategies are considered as presented in Section 5.6. While the results may not necessarily be indifferent to the control strategy, using multiple strategies helps to account for the possibility that

the optimal strategy may differ between the two configurations.

First, the operational state of the different electrolysers over the entire observed data set is presented, providing a first visual comparison between the centralised and decentralised configurations. Then, the obtained results are further analysed, starting with the total hydrogen produced, the number of switches of operational states, and number of turn-offs. For the centralised configuration, a single result is obtained for each control strategy. For the decentralised configuration, ranges are presented since each wind turbine provides an individual result.

6.5.1. Time-series visualisation

First, a visual representation of the decentralised configuration is presented. It was chosen to present the operation of a random wind turbine. It's important to note that, while the same control strategy is applied to all wind turbines, the incoming power profile differs, leading to varying operations of the wind turbines.

Figure 6.6 presents the operational status of the different electrolysers over the entire duration of the available data set for the decentralised configuration. The figure is based on the results of adapting a control strategy using a 10% turn-to-idle threshold and a 95% turn-on threshold. In the figure, the incoming power profile as supplied by the wind turbine is presented in the top figure. The middle figure presents how this power is distributed among the different operating electrolysers. The bottom figure shows the operational status of the different electrolysers as a result of the applied control strategy on the incoming power profile.

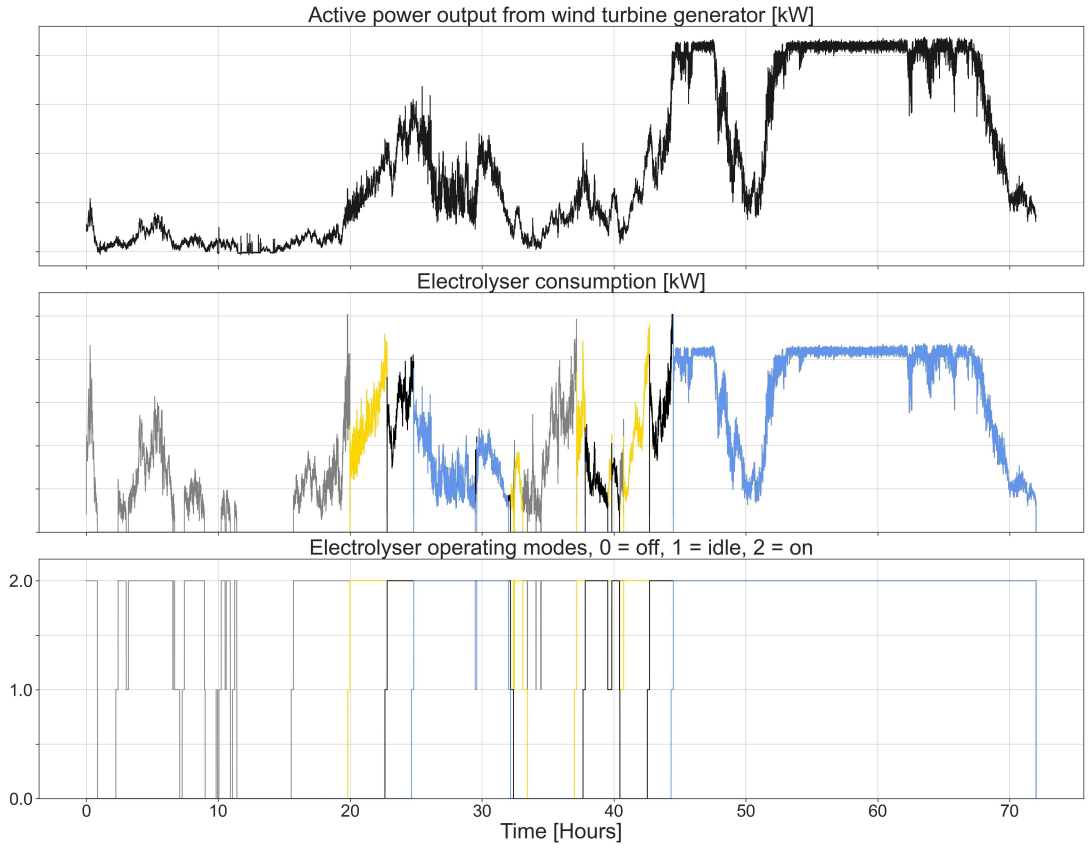

Figure 6.6: Incoming power profile (top), power consumption per electrolyser (middle), and operational mode (bottom) for a decentralised configuration. Power rating on y-axis left out intentionally due to confidentiality.

A value of 0 is subscribed to an offline operation, a value of 1 to idle-mode operation, and 2 to an online status of the electrolysers. Furthermore, the different electrolysers are all presented in their own colour.

At the middle figure in Figure 6.6 a grey colour indicates that only a single electrolyser is operating. Yellow, black, and blue indicate that 2, 3, and 4 electrolysers are in operation, respectively.

The first 15 hours represent a period with a relatively low wind speed and therefore a lower power output by the wind turbine. The control strategy, therefore, summons the single electrolyser in operation to switch operational mode several times. Six times the electrolyser is shut down completely after being in idle mode operation in this segment and three times turned back. These switches often are within short notice of each other, indicating an inefficient use of the available energy.

Following hour 15, a noticeable increase in wind speed was experienced, leading to a corresponding rise in power production from the wind turbine. This, in turn, resulted in turning on an increasing number of electrolysers until all were in operation by hour 25. Then, during the period between hours 30 and 40, a significant number of changes in operational mode as response to the power fluctuations of the incoming power input, was observed. These fluctuations were often characterised by sudden and temporary changes in the power input. Despite the substantial drop in power output by the wind turbine around hour 50, the control strategy demonstrated its robustness by not requiring any changes in the operational mode. Once the wind turbine is operating at rated capacity, it is observed that all electrolysers are operational. Before diving into the exact numbers, it can be observed through visual inspection that the operational mode of the electrolysers changes frequently, particularly during periods of higher power output fluctuations.

Figure 6.7 presents the results for a centralised configuration. Again, a 10% turn-to-idle threshold and a 95% turn-on threshold are adopted. As the centralised configuration is under examination, the terminology changes from wind turbine to offshore wind farm and from electrolyser to stack module.

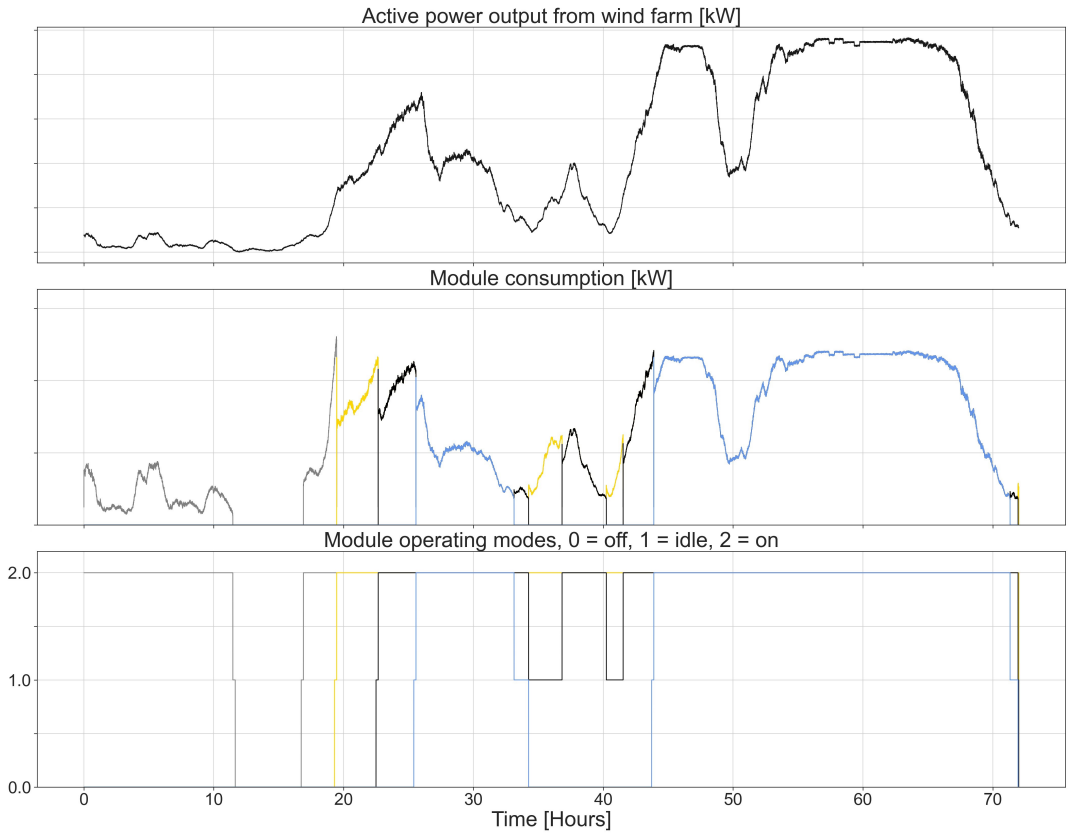

Figure 6.7: Incoming power profile (top), power consumption per module (middle), and operational mode (bottom) for decentralised configuration. Power rating on y-axis left out intentionally due to confidentiality.

The figure presents how the incoming input power influences the operational mode of the stack modules.

A substantial portion of the initial 15 hours of the analysed data set allowed for one stack module to be in an online operational mode. After hour 17, at least one of the stack modules was in operation, similar to the decentralised configuration.

By visual comparison of Figure 6.7 and Figure 6.6, differences in the operational modes between the two configurations are observed. Where in the decentralised configuration multiple switches in operational mode were observed within one hour, the switches of modes in the centralised configuration show a notably longer interval of time between them. The direct cause of switches in operational mode is an significant increase or decrease in delivered power. As concluded in Section 6.4, the magnitude of power output fluctuation within a certain time frame is severely lower in the centralised configuration than in the decentralised configuration. This is reflected by both the time between switches in the control strategy and the total number of switches observed in the analysed data set.

Given the similarities in the outcomes of the various control strategies, it was deemed unnecessary to present them individually. However, a thorough examination of the results obtained for each control strategy is provided in the following subsections.

6.5.2. Hydrogen production

The total hydrogen produced over the 72 hours of simulation, is calculated. In the decentralised configuration, a single quantity per control strategy is obtained since all hydrogen is produced at the COHP. In the decentralised configuration, the total hydrogen production is calculated by summation of the production per wind turbine. Figure 6.8 presents the total hydrogen production of the centralised and decentralised configuration for the four proposed control strategies. Note that the y-axis does not start at zero.

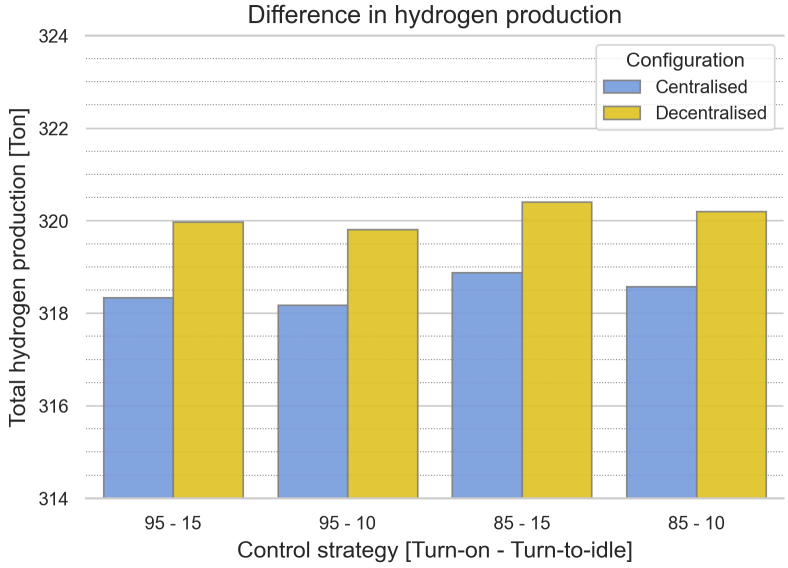

Figure 6.8: Total hydrogen production for the centralised and decentralised configuration for different control strategies.

Both the centralised and decentralised configuration, for all four different control strategies, produce a total of approximately 320 tons of hydrogen in the 72 hours considered. The decentralised configuration shows, for all four control strategies, a marginal benefit in terms of the total produced hydrogen. The chosen control strategy seems to have little effect on the total produced amount of hydrogen. Slightly higher hydrogen production is observed for a strategy adopting a turn-on threshold of 85% compared, to a turn-on threshold of 95%. Due to the lower turn-on threshold, an additional stack module or electrolyser is turned on, dividing the total power over a larger number of stack modules or electrolyser and therefore enabling operating in a more efficient region of the efficiency curve, as seen in Figure 5.4.

Due to the losses in the inter-array cable, 0.87 % less energy is available for hydrogen production in the centralised configuration compared to the decentralised configuration. Furthermore, as a result

of higher losses in the electrical equipment of the centralised configuration, the efficiency curve of the centralised configuration is lower. Nevertheless, the difference in hydrogen production is only 0.47 %, in favour of the decentralised configuration. This indicates that less energy used for processes not contributing directly to hydrogen production, albeit minimal. Anticipated is that this is attributed to the lower number of operational switches. It should be noted that the overall comparison of hydrogen production between the two configurations is so small that it is not possible to determine a clear preference based solely on this factor.

6.5.3. Switching operational modes

The difference in hydrogen production could not give a clear preference for a certain configuration and did not reveal a large benefit from the reduced power fluctuation in the centralised configuration. Hence, the focus has now shifted toward investigating the transitions between operational states. The following subsection relates to the number of switches of the operational modes of the stack modules and electrolysers. For the centralised configuration, a single result is obtained for the number of mode switches and turn-offs. For the decentralised configuration, each wind turbine has its total number of switches and they are varying between the wind turbines. Therefore, the number of switches per wind turbine and their mean are provided. Figure 6.9 presents the number of switches for the centralised and decentralised configuration for four different control strategies.

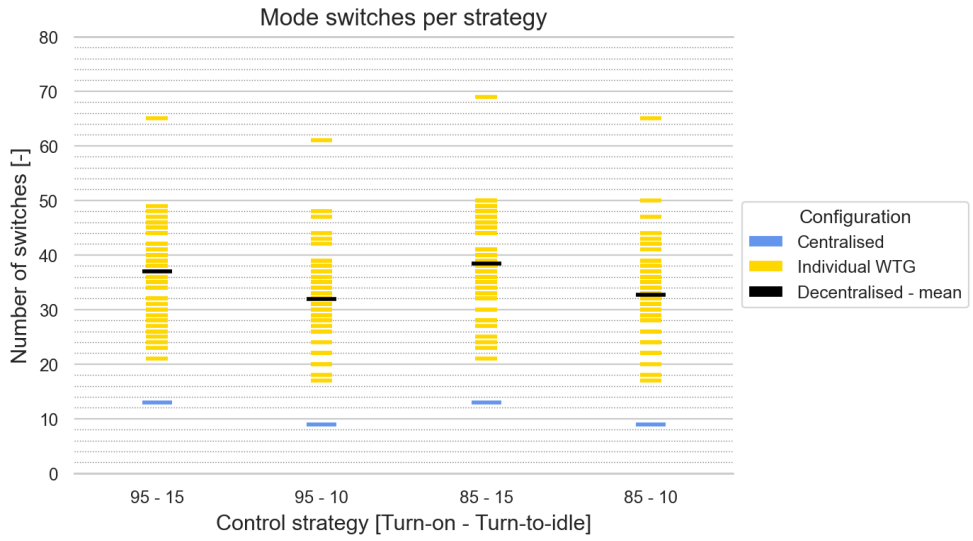

Figure 6.9: Number of operational switches for the centralised and decentralised configuration.

The figure shows a significant difference between the different configurations regarding the number of operational switches. For all four different control strategies, the number of switches of the centralised configuration is significantly lower. The number of switches of operational mode in the centralised configuration is 9 and 13, depending on the applied control strategy. The mean value of the number of switches per wind turbine in the decentralised configuration is between 31 and 39. It is noteworthy that even the wind turbine with the lowest number of operational mode changes, switches more frequently than the centralised configuration. Readers interested in the location of the wind turbines in the offshore wind farm and there respective mean number of switches, are directed to Figure B.4 in the appendix.

For the decentralised configuration, strong outliers are observed. These outliers are caused by unnatural wind turbine operations. The cause of this unnatural operation was not found. There are several potential explanations, both deliberate and accidental, that could be considered. Deliberate causes for such wind turbine operations could be running tests or curtailment because of offshore substation undersizing. If the reason was because of the offshore undersizing, then this would not have been observed if it was a decentralised hydrogen-producing wind turbine because of the absence of an offshore substation.

6.5.4. Turn-offs

Another interesting output of the model is the total turn-offs per strategy. A turn-off implies changing the stack module or electrolyser from an idling mode to an offline status. Figure 6.10 presents the number of turn-offs for both configurations for four different control strategies.

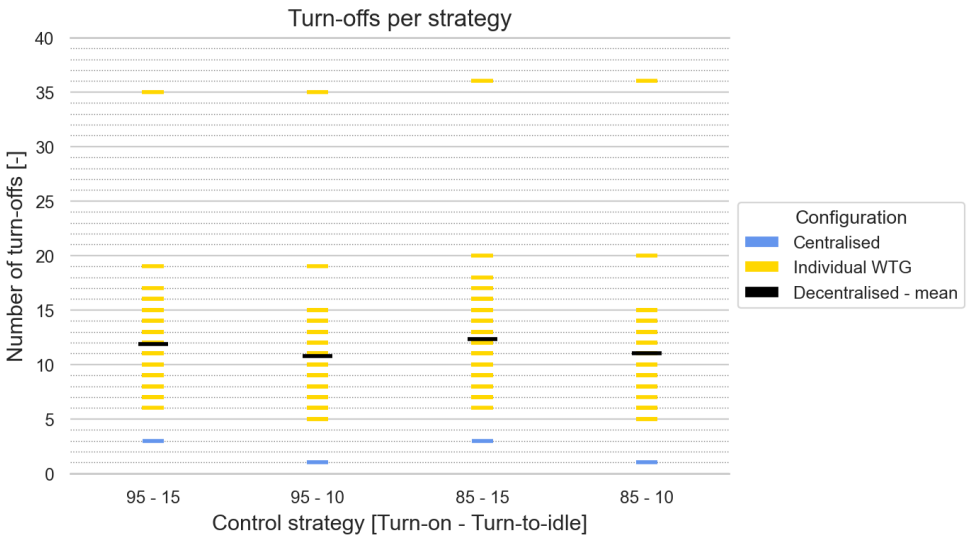

Figure 6.10: Number of turn-offs for the centralised and decentralised configuration.

The figure shows that the number of turn-offs of the centralised configuration is significantly lower than the average number of turn-offs of the decentralised configuration. Furthermore, also the wind turbine with the lowest number of turn-offs still changes to an offline state more frequently than the centralised configuration. The number of turn-offs in the centralised configuration is 1 or 3, depending on the applied control strategy. For the decentralised configuration, for a normal operating wind turbine, the number of turn-offs ranges between 5 and 20, with a mean of approximately 12 occurrences.

To a certain extent, the chosen control strategy has an impact on the number of turn-offs. An increase in the turn-to-idle threshold leads to a decrease in the total number of turn-offs. The number of turn-offs is related to the turn-to-idle threshold since the control strategy allows only one stack module or electrolyser to be in idle mode. When another stack module or electrolyser transitions from an online state to an idle state, the stack module or electrolyser previously in idle mode is forced to switch to an offline state.

What the time-series model does not take into account is the accelerated degradation of the hydrogen-producing equipment. As seen in Figures 6.9 and 6.10, the centralised configuration has a clear advantage in terms of limiting the number of switches of operational modes. The lowered number of switches could over time, as a result of decreased degradation, result in more efficient hydrogen production in the centralised configuration.

6.6. Discussion

A time-series model was used the reflect real-world operations. Due to the limited available power output data and lack of information and knowledge related to the exact design of such systems, assumptions had to be made. The shortcomings of the obtained results of Part II are presented in the following section.

6.6.1. Centralised integrated system

In the centralised configuration, the stack modules were assumed to operate independently of one another. However, during the actual design and implementation of such a system, it is crucial to evaluate whether this independence is achievable. Due to the benefits of scaling individual components, several modules may be connected to a single compressor. This would result in a loss of complete indepen-

dence among the modules and a more complex control strategy would have to be developed. Additionally, the efficiency of hydrogen production would be affected by the compressor's load-dependent efficiency curve. To avoid these complications, a system without additional compressors was chosen in this particular case. The feasibility of this decision depends on factors such as the distance to the customer and the desired hydrogen offtake pressure.

In a centralised configuration, it is assumed that all electrolysers within a module operate in parallel at all times. This parallel operation is most efficient when the power supplied to the module is at least around 30% of its maximum capacity [Figure 5.4]. However, when this 30% power of a single stack module cannot be supplied, it may be more advantageous to operate only some of the electrolysers of a stack module and leave others offline. This would result in a lower minimum load for the module. For example, consider a module that consists of 15 stacks of 10 MW each. If all stacks within the module are operated completely in parallel, the minimum input power required is 15 MW, as this is 10% of 150 MW. However, if the stacks within a module could operate separately, the minimum input power required would be 1 MW, as this is 10% of 10 MW. This would allow for hydrogen production over a wider range of input power.

6.6.2. Energy storage element

The study by Helgason presented that the addition of an energy storage element could lower the number of switches between operational modes in the decentralised configuration. Such energy storage element is used to keep an electrolyser temporarily in idling mode during moments the wind speed is insufficient to meet the requirements for hydrogen production. As a result, when wind conditions are again sufficient to produce hydrogen, there is no start-up time required. Such energy storage element operates in situations the wind speeds are not sufficient for a relatively short period. The length of the period that can be bridged by the storage element depends directly on its installed energy storage capacity. Hence, it is argued that a larger part of the energy is used and that the electrolysers switch fewer times between off and idle mode. The energy provided by the storage element originates from the wind turbine. The use of such a storage element implies that less hydrogen can be produced at times when the storage element is charged than when such storage element is not charged.

For this study, both configurations were assessed without such an additional storage element. This choice was made since this would require research into the installed capacity of the additional storage element and this was beyond the scope of this work. However, it can be noted that in the case of the centralised configuration, short periods when the wind speed is not enough to produce hydrogen are less frequent and the use of such a storage element may not be necessary.

6.6.3. Data set choice

The data set used covers a total of three days in October and influences the results obtained. As presented in Section 5.2 the power varies both on a short-term and long-term period. Measurements taken close to the location of the offshore wind farm over a 50-year period, present strong variations of average wind speed per month. Here, it was found that the average wind speeds were around 5 m/s during summer, while being around 8 m/s during the winter. This difference in average wind speed directly influences the amount of hydrogen produced. Furthermore, these higher wind speeds are likely paired with operations happening more often in the steeper part of the wind turbine power curve, hence larger power fluctuations are observed influencing the number of switches and turn-offs.

Therefore, the obtained results are not representative for the entire year. However, since the centralised and decentralised configurations were tested using the same data set, the results provide a benchmark to compare the two configurations during periods characterised by a higher average wind speeds. Operation during the summer could result in lower power output fluctuation, decreasing the difference in the number of switches and turn-offs for the two configurations. It is suggested that a data set spanning more than 3 days is used to perform a comprehensive comparison between different configurations.

6.7. Summary Part II

For readers who have just read this chapter, this summary is superfluous. In Part II, the focus was shifted towards a closer examination of hydrogen production, utilising time-series power output data. Since there are no benchmark values for the performance of such system, regarding hydrogen pro-

duction and switching of operational modes, the centralised configuration was compared to a decentralised configuration. The main interest of this part was whether aggregating power, as observed in a centralised configuration, would have a positive effect on hydrogen production and the state of performance of the equipment.

First, the obtained power output data was analysed in Section 6.4. This section showed large reductions in the observed normalised power fluctuations comparing an offshore wind farm to an individual wind turbine. This was concluded by analysing the maximum and standard deviation of the normalised fluctuations, occurring in 1-minute, 5-minute, and 10-minute intervals. The observed offshore wind farm's maximum normalised fluctuations halved the magnitude of the normalised fluctuation of the least fluctuating wind turbine. Compared to the wind turbine which showed the largest maximum fluctuations for a given time interval, a fluctuation four times larger than that of the offshore wind farm was observed.

In Section 6.5, the model as presented in Chapter 5 was used to gain insight into the effects of this damped power fluctuations on hydrogen production and the number of switches of operational modes. With regard to total hydrogen production, it was observed that there is no clear preference for either centralised or decentralised production. While there may be slight tendencies towards decentralised production, the available data does not allow for a definitive conclusion to be drawn in favour of one configuration over the other. It was found that the centralised configuration produces hydrogen more efficiently per available unit of energy. However, due to the inter-array cable losses, the total available energy destined for hydrogen production is lower compared to the decentralised configuration. With regard to the number of switches of operational mode and turn-offs, a clear preference for the centralised configuration was found. The number of switches of operational mode and turn-offs was found to be three times lower for the centralised configuration, compared to the average of the decentralised configuration. Also, the best-performing wind turbine of the decentralised configuration had around twice as many changes in operational mode and turn-offs. Since frequent changing of operational mode influences degradation and system performance, over time this could result in a benefit in hydrogen production for the centralised configuration.

Note to reader: This was the final section of Part II. Hereafter, the conclusion on both Part I and Part II starts.

7

Conclusion and recommendations

The following chapter presents the conclusion derived from the findings obtained in Part I and Part II, and the recommendations for future studies. In case readers have not perused either of the parts or wish to revisit the content, they are directed to the part-specific summaries provided in Section 4.8 for Part I and Section 6.7 for Part II. The conclusion is presented in Section 7.1 and the recommendations in Section 7.2.

7.1. Conclusion

The primary objective of this study was to have a thorough understanding of centralised offshore hydrogen production, under the condition of using a single platform in island mode operation, connected to a 1-gigawatt OWF, based on projected performances and costs of the year 2030. To accomplish this objective, both a techno-economic analysis and an assessment of the benefit of power aggregation were conducted on this configuration. The research question of this study was formulated as follows:

> "What is the techno-economic viability of centralised offshore green hydrogen production for projected performances and costs of 2030, and how beneficial is its smoother power input on electrolyser dynamics?"

The main conclusion of this study is that the centralised offshore hydrogen production configuration facilitates the possibility to produce hydrogen at a competitive levelised cost of hydrogen. Furthermore, the reduction in power fluctuations due to power aggregation of the spatially distributed wind turbines provides partial benefits. The reasoning behind this conclusion is provided below.

Based on a qualitative assessment of the available electrolysis technologies, alkaline electrolysis (AE) and proton exchange membrane electrolysis (PEME) are concluded to be feasible for centralised offshore hydrogen production for the year 2030, as was presented in Section 2.2.7.

For both technologies, an undersizing of the hydrogen production unit capacity in comparison to the offshore wind farm capacity results in a more cost-efficient production of hydrogen, as presented in Section 4.2.4. The main drivers for this optimal installed hydrogen production unit capacity are the decreasing performance of the offshore wind farm and the relative cost of the centralised offshore hydrogen platform to the offshore wind farm, in reference to the diminishing marginal hydrogen production. The optimal installed hydrogen production unit capacity is influenced by the choice between optimising for the minimum levelised cost of hydrogen or maximising the net present value, as the hydrogen selling price has an impact on the latter. An optimal installed hydrogen production unit capacity undersizing ranging from 5% to 9% was found.

Moreover, it was concluded that increasing the hydrogen pressure at the platform above the required minimum pressure to overcome the pressure drop in the hydrogen transmission system, facilitates the possibility to reduce the production costs of hydrogen, as presented in Section 4.3. Nevertheless, given the relatively small distance to shore used in the case study of this work, the benefits of this reduction were marginal.

The PEME-based system is capable of delivering slightly more cost-competitive hydrogen, at a rate of 2.83 €/kg in comparison to 2.92 €/kg for an AE-based system. Multiple factors lead to this outcome.

The hydrogen yield of the PEME-based system is slightly higher, mainly due to the smaller hydrogen compression requirements, as was found in Section 4.4.1. Additionally, the smaller physical footprint of the PEME-based system translates into less expensive transportation, installation, and commissioning procedures, thus compensating for the higher stack capital expenditure, as was found in Section 4.4.2. Moreover, the larger compression step and higher stack operational expenditure resulted in a higher operational expenditure of the AE-based system. Despite, the lower number of stack replacements as a result of the lower degradation rate of the AE-based system, this benefit could not offset the lower hydrogen yield, and higher capital and operational expenditure. Nevertheless, as demonstrated in the sensitivity analysis in Section 4.5, and uncertainty analysis in Section 4.6, there are possibilities in which the AE-based system produces hydrogen at a more competitive levelised cost. Therefore, it is advised to consider both technologies for further concepts from a production cost perspective. From a mass perspective, however, both technologies could encounter significant challenges due to their high topside masses.

Furthermore, the effects of the aggregation of the power output of the individual wind turbines, benefit the hydrogen-producing system partially. It was found that the short-term normalised fluctuations of the power output of an offshore wind farm are significantly reduced compared to the normalised power fluctuations of an individual wind turbine. Depending on the time step and wind turbine observed, a decrease of maximum normalised power fluctuation of 50% to 90% was observed in the centralised configuration, as presented in Section 6.4. The significant reduction in the standard deviation of the normalised power fluctuation showed that aggregation affect the total severity of the power fluctuations, not only the maximum normalised fluctuation.

However, the more constant power supply had a limited effect on the total produced hydrogen. This is attributed to the additional inter-array cable and converter losses in the centralised configuration, as presented in Section 6.5. The more constant power supply had however a significant result on the number of switches of operational mode and the number of turn-offs of the stack modules. The number of switches was reduced by approximately 70% on average and the number of turn-offs by approximately 80% on average, compared to the decentralised configuration, as presented in Subsection 6.5.3 and Subsection 6.5.4. This reduction in the number of switches of operational mode and reduced number of turn-offs decelerates the degradation of the stacks and therefore benefit hydrogen production.

7.2. Recommendations

Interesting issues and the need for further research regarding centralised offshore hydrogen production emerged during this study. Although the current study does not specifically address these topics, they are presented here to generate interest and encourage future research.

- *Multiple platforms:* For this study, the use of a single platform was assumed. However, the mass of both the PEME- and AE-based COHP is in the range of the largest installed offshore structures. Further research should point out the technical and economical feasibility of such large structures. An alternative could be to use multiple medium-size platforms. Dividing the total mass over multiple platforms could realise the use of cheaper transport, installation, and commissioning methods. This raises the need for new location optimisation. Placing the platforms next to one another and linking them results in maximising the economies of scale and could increase availability. On the other hand, spreading the platforms across the OWF could lower the cost of IAC and spread risk.
- *Alternative design choices:* To narrow down the scope, a certain base design was assumed. However, there are also alternative designs potentially delivering a cost-competitive LCOH. These alternative design options include utilising a gravity-based or floating substructure, and float-over installation as a potential method of transport, installation, and commissioning method.
- *Availability:* Further research should be carried out to find the exact COHP availability. Since all the power produced by the OWF needs to be processed at the COHP, this forms a bottleneck in terms of availability. If the complete COHP is offline, this is disastrous for the availability of the total system, since all the power potentially produced by the OWF is not useful. However, if for example, one of the four modules is offline (25% offline) while the power supplied by the OWF is less than 75% of the total HPU capacity, this does not reduce the amount of hydrogen produced. The platform must be designed with this in mind. During the process of creating advanced designs of the COHP, incorporating redundancy should be paramount. Components with a high individual capacity, such as compressors, but that require regular maintenance, should have a

spare component available to provide increased system availability. Also, cross-connections between the different modules could increase the total system availability but it should be assessed whether this is cost-effective.

- *Synergies:* Due to the limited available knowledge and information, the COHP was designed as an add-on to the OWF. Further research should be carried out to maximise the synergies between the OWF and the COHP. Earlier studies pointed out that the use of conventional WTGs would also be most beneficial when combined with centralised offshore hydrogen production. Nevertheless, no work pointed out the possible benefit for the OWF. The COHP could be used as storage or close access point to the OWF, to increase the OWF's availability. Furthermore, during the construction and transport, installation, and commissioning phase, synergies between the OWF and the COHP must be maximised.
- *Control strategies:* A relatively simple but robust control strategy was applied both in the centralised and decentralised configuration. It was found that the fluctuations per WTG vary particularly, caused by the relative placement in the OWF. In the decentralised configuration, these differences in occurring power fluctuations might demand for a WTG-specific control strategy. Such a WTG-specific control strategy might increase hydrogen production and the electrolyser's lifetime.
- *Replacement strategies:* During the lifetime of the project, the stacks need to be replaced. Such replacement is a logistically challenging and costly process. Furthermore, it influences the availability of the system. A sound replacement strategy could benefit the overall performance of the system in terms of produced hydrogen and incurred costs. During the design of the platform, the replacement should already be anticipated.

References

[1] Investable Universe. *Dutch government to subsidize world first offshore green hydrogen plant*. 2021. URL: https://investableuniverse.com/2021/07/22/dutch-government-grants-subsidy-to-poshydon-offshore-hydrogen-project/.

[2] United Nations. *Paris Agreement*. Tech. rep. 2015. URL: https://unfccc.int/sites/default/files/english_paris_agreement.pdf.

[3] DNV. *HYDROGEN FORECAST TO 2050*. Tech. rep. 2022. URL: https://www.dnv.com/focus-areas/hydrogen/forecast-to-2050.html.

[4] Siemens Gamesa. *Unlocking the Green Hydrogen Revolution*. Tech. rep. 2021. URL: https://www.siemensgamesa.com/en-int/-/media/whitepaper-unlocking-green-hydrogen-revolution.pdf.

[5] IRENA. *Renewable Power Generation Costs in 2021*. Tech. rep. ISBN 978-92-9260-452-3. 2022. URL: https://www.irena.org/mwg-internal/2535425/progress?id=7Se3N3Q4y3PcXAmy0x7fnA-BY2G6LMca_NKTWT31m1w,&dl.

[6] Alessandro Singlitico, Jacob Østergaard, and Spyros Chatzivasileiadis. "Onshore, offshore or in-turbine electrolysis? Techno-economic overview of alternative integration designs for green hydrogen production into Offshore Wind Power Hubs". In: *Renewable and Sustainable Energy Transition* 1 (2021), p. 100005. DOI: 10.1016/j.rset.2021.100005.

[7] Poshydon. URL: %7Bhttps://poshydon.com/en/home-en/%7D.

[8] *Brande Hydrogen: Wind to hydrogen production for the future*. Aug. 2022. URL: https://stateofgreen.com/en/solutions/brande-hydrogen/.

[9] Vattenfall. *Hydrogen Turbine 1*. 2022. URL: https://group.vattenfall.com/uk/what-we-do/our-projects/european-offshore-wind-deployment-centre/aberdeen-hydrogen.

[10] IRENA. *Global hydrogen trade to meet the 1.5°C climate goal: Part II – Technology review of hydrogen carriers*. Tech. rep. 2022. URL: https://www.irena.org/mwg-internal/2535425/progress?id=NEfgVo9dYdQLIFVXDuwKLCGbXVa1BrT5JykHbKRSS0s,&dl.

[11] G. Calado and R. Castro. "Hydrogen Production from Offshore Wind Parks: Current Situation and Future Perspectives". In: *Applied Sciences* 11 (2021), p. 5561.

[12] E. Morgan, J. Manwell, and J. McGowal. "Opportunities for economies of scale with alkaline electrolyzers". In: *International Journal of Hydrogen Energy* 38.36 (2013), pp. 15903–15909.

[13] IRENA. *Green Hydrogen Cost Reduction: scaling up electrolysers to meet thee 1.5° climate goal*. Tech. rep. 2020. URL: https://irena.org/-/media/Files/IRENA/Agency/Publication/2020/Dec/IRENA_Green_hydrogen_cost_2020.pdf.

[14] Omar S. Ibrahim et al. "Dedicated large-scale floating offshore wind to hydrogen: Assessing design variables in proposed typologies". In: *Renewable and Sustainable Energy Reviews* 160 (2022), p. 112310. DOI: 10.1016/j.rser.2022.112310.

[15] Toshiya Nanahara et al. "Smoothing effects of distributed wind turbines. Part 1. Coherence and smoothing effects at a wind farm". In: *Wind Energy* 7.2 (Apr. 2004), pp. 61–74. DOI: 10.1002/we.109. URL: http://dx.doi.org/10.1002/we.109.

[16] World Energy Council, EPRI, and PwC. *Working Paper | Hydrogen Demand and Cost Dynamics*. Tech. rep. 2021. URL: https://www.worldenergy.org/assets/downloads/Working_Paper_-_Hydrogen_Demand_And_Cost_Dynamics_-_September_2021.pdf?v=1658324860.

[17] Shell. *Shell to start building Europe's largest renewable hydrogen plant*. 2022. URL: https://www.shell.com/media/news-and-media-releases/2022/shell-to-start-building-europes-largest-renewable-hydrogen-plant.html.

[18] P. Lozada Ayala et al. “Modeling and Analysis of a Novel Grid Connection Topology for Offshore Wind Farms using MMC-HVDC Transmission”. In: *2019 IEEE Power amp; Energy Society General Meeting (PESGM)* (Aug. 2019). DOI: 10.1109/pesgm40551.2019.8973767. URL: http://dx.doi.org/10.1109/pesgm40551.2019.8973767.

[19] F. González-Longatt, P. Wall, and V. Terzija. “Wake effect in wind farm performance: Steady-state and dynamic behavior”. In: *Renewable Energy* 39.1 (Mar. 2012), pp. 329–338. DOI: 10.1016/j.renene.2011.08.053. URL: http://dx.doi.org/10.1016/j.renene.2011.08.053.

[20] Iain Staffell and Richard Green. “How does wind farm performance decline with age?” In: *Renewable Energy* 66 (June 2014), pp. 775–786. DOI: 10.1016/j.renene.2013.10.041. URL: http://dx.doi.org/10.1016/j.renene.2013.10.041.

[21] R. Vermeij. Conversation, expert view. Oct. 2022.

[22] M. Davida, C. Ocampo-Martínez, and R. Sánchez-Peña. “Advances in alkaline water electrolyzers: A review”. In: *Journal of Energy Storage* 23 (2019), pp. 392–403.

[23] I. Vincent and D. Bessarabov. “Low cost hydrogen production by anion exchange membrane electrolysis: A review”. In: *Renewable and Sustainable Energy Reviews* 81.2 (2018), pp. 1690–1704.

[24] M. Kopp et al. “Energiepark Mainz: Technical and economic analysis of the worldwide largest Power-to-Gas plant with PEM electrolysis”. In: *International Journal of Hydrogen Energy* 42.19 (May 2017), pp. 13311–13320. DOI: 10.1016/j.ijhydene.2016.12.145. URL: http://dx.doi.org/10.1016/j.ijhydene.2016.12.145.

[25] G. Guandilini et al. “Simulation of a 2 MW PEM Fuel Cell Plant for Hydrogen Recovery from Chlor-Alkali Industry”. In: *Energy Procedia* 105 (2017), pp. 1839–1846.

[26] S. Dresp et al. “Direct Electrolytic Splitting of Seawater: Opportunities and Challenges”. In: *ACS Energy Lett.* 4 (2019), pp. 933–942.

[27] Hussam Khasawneh, Motasem N Saidan, and Mohammad Al-Addous. “Utilization of hydrogen as clean energy resource in chlor-alkali process”. In: *Energy Exploration amp; Exploitation* 37.3 (Mar. 2019), pp. 1053–1072. DOI: 10.1177/0144598719839767. URL: http://dx.doi.org/10.1177/0144598719839767.

[28] J. Niklas Hausmann et al. “Is direct seawater splitting economically meaningful?” In: *Energy Environmental Science* 14 (2021), pp. 3679–3685.

[29] R. d’Amore-Domenech, O. Santiago, and T. Leo. “Multicriteria analysis of seawater electrolysis technologies for green hydrogen production at sea”. In: *Renewable and Sustainable Energy Reviews* 133 (2020), p. 110166.

[30] Alfredo Ursua, Luis M. Gandia, and Pablo Sanchis. “Hydrogen Production From Water Electrolysis: Current Status and Future Trends”. In: *Proceedings of the IEEE* 100.2 (Feb. 2012), pp. 410–426. DOI: 10.1109/jproc.2011.2156750. URL: http://dx.doi.org/10.1109/jproc.2011.2156750.

[31] Ester López-Fernández et al. “Recent Advances in Alkaline Exchange Membrane Water Electrolysis and Electrode Manufacturing”. In: *Molecules* 26.21 (2021), p. 6326. DOI: 10.3390/molecules26216326.

[32] Enapter. *Anion exchange membrane water electrolysis: How it works*. 2022. URL: https://www.enapter.com/newsroom/aem-water-electrolysis-how-it-works.

[33] DNV-GL. *Power-to-Hydrogen IJmuiden Ver*. Tech. rep. 2018. URL: https://tennet-drupal.s3.eu-central-1.amazonaws.com/default/2022-07/P2H_IJmuiden_Ver_-_Final_Report_-_Public.pdf.

[34] Offshore Renewable Energy Catapult. *Guide to an offshore wind farm*. Tech. rep. 2019. URL: https://ore.catapult.org.uk/app/uploads/2019/04/BVGA-5238-Guide-r2.pdf.

[35] Institute for Sustainable Process Technology. *A One-GigaWatt Green-Hydrogen Plant: Advanced Design and Total Installed-Capital Costs*. Tech. rep. 2022. URL: https://ispt.eu/media/Public-report-gigawatt-advanced-green-electrolyser-design.pdf.

[36] Sofia G. Simoes et al. “Water availability and water usage solutions for electrolysis in hydrogen production”. In: *Journal of Cleaner Production* 315 (Sept. 2021), p. 128124. DOI: 10.1016/j.jclepro.2021.128124. URL: http://dx.doi.org/10.1016/j.jclepro.2021.128124.

[37] Krzysztof Mitko, Adam R. Rosiński, and Marian Turek. “Energy consumption in membrane capacitive deionization and electrodialysis of low salinity water”. In: *DESALINATION AND WATER TREATMENT* 214 (2021), pp. 294–301. DOI: 10.5004/dwt.2021.26701. URL: http://dx.doi.org/10.5004/dwt.2021.26701.

[38] Clean Hydrogen Partnership. *Strategic Research and Innovation Agenda 2021 - 2027: Clean hydrogen joint undertaking*. Tech. rep. 2022. URL: https://www.clean-hydrogen.europa.eu/about-us/key-documents/strategic-research-and-innovation-agenda_en.

[39] M.A Khan et al. *The Techno-Economics of Hydrogen Compression*. Tech. rep. ISSN 2564-1379. 2021. URL: https://transitionaccelerator.ca/wp-content/uploads/2021/12/1_TA-Brief_-TEEA-Hydrogen-Compression-PUBLISHED-print-UST-THIS-ONE-Dec-2021.pdf.

[40] Mohammad-Reza Tahan. “Recent advances in hydrogen compressors for use in large-scale renewable energy integration”. In: *International Journal of Hydrogen Energy* 47.83 (Oct. 2022), pp. 35275–35292. DOI: 10.1016/j.ijhydene.2022.08.128. URL: http://dx.doi.org/10.1016/j.ijhydene.2022.08.128.

[41] O. Partenie. Mail contact, expert view. 2022.

[42] Liu and Li. *Offshore Platform Integration and Floatover Technology*. Amsterdam, Netherlands: Amsterdam University Press, 2017. DOI: 10.1007/978-981-10-3617-0. URL: https://link.springer.com/content/pdf/10.1007/978-981-10-3617-0.pdf.

[43] North Sea Energy. *HAZID - Offshore Hydrogen Production*. Tech. rep. NSE3-DO 00-HAZID 4 3. 2019. URL: https://north-sea-energy.eu/static/6bbd76649713672208ea6cd31703e4c1/10b.-FINAL-NSE3_D4.2-Appendix-A_HAZID.pdf.

[44] North Sea Energy. *Report on offshore structural integrity and safety performance of H2 production, processing, storage and transport*. Tech. rep. NSE3-D4.2. 2020. URL: https://north-sea-energy.eu/static/84050b605af439a07d9806c763618802/10a.-FINAL-NSE3_D4.2-Report-on-offshore-structural-integrity-and-safety-performance-of-H2-production-processing-storage-and-transport.pdf.

[45] Subrata Chakrabarti, John Halkyard, and Cuneyt Capanoglu. “Historical Development of Offshore Structures”. In: *Handbook of Offshore Engineering* (2005), pp. 1–38. DOI: 10.1016/b978-008044381-2.50004-7. URL: http://dx.doi.org/10.1016/b978-008044381-2.50004-7.

[46] James A. Schneider and Marc Senders. “Foundation Design: A Comparison of Oil and Gas Platforms with Offshore Wind Turbines”. In: *Marine Technology Society Journal* 44.1 (Jan. 2010), pp. 32–51. DOI: 10.4031/mtsj.44.1.5. URL: http://dx.doi.org/10.4031/mtsj.44.1.5.

[47] Magued Iskander, Sherif El-Gharbawy, and Roy Olson. “Performance of suction caissons in sand and clay”. In: *Canadian Geotechnical Journal* 39.3 (June 2002), pp. 576–584. DOI: 10.1139/t02-030. URL: http://dx.doi.org/10.1139/t02-030.

[48] G. Kaloritis. Conversation, expert view. Sept. 2022.

[49] IRENA. *Global hydrogen trade to meet the 1.5°C climate goal: Part II – Technology review of hydrogen carriers*. Tech. rep. 2022. URL: https://www.irena.org/-/media/Files/IRENA/Agency/Publication/2022/Apr/IRENA_Global_Trade_Hydrogen_2022.pdf.

[50] International Energy Agency. *The Future of Hydrogen*. Tech. rep. 2019. URL: https://iea.blob.core.windows.net/assets/9e3a3493-b9a6-4b7d-b499-7ca48e357561/The_Future_of_Hydrogen.pdf.

[51] Chiemela Victor Amaechi et al. “Review on Fixed and Floating Offshore Structures. Part II: Sustainable Design Approaches and Project Management”. In: *Journal of Marine Science and Engineering* 10.7 (July 2022), p. 973. DOI: 10.3390/jmse10070973. URL: http://dx.doi.org/10.3390/jmse10070973.

[52] S. Chakrabarti. “Handbook of offshore engineering”. In: Elsevier, 2005. Chap. 14. ISBN: 9780080443812.

[53] P. Spies. Conversation, expert view. Sept. 2022.

[54] Litty Dani Cherian, P. K. Suresh, and Oussama Halim Takieddine. “Topside Installation by Float over – Engineering Challenges”. In: *Day 3 Wed, November 12, 2014* (Nov. 2014). DOI: 10.2118/171736-ms. URL: http://dx.doi.org/10.2118/171736-ms.

[55] M.A. Tribe and R.L.W. Alpine. “Scale economies and the “0.6 rule””. In: *Engineering Costs and Production Economics* 10.4 (Dec. 1986), pp. 271–278. DOI: 10.1016/s0167-188x(86)80025-8. URL: http://dx.doi.org/10.1016/s0167-188x(86)80025-8.

[56] Giulio Guandalini and Stefano Campanari. “Wind Power Plant and Power-to-Gas System Coupled With Natural Gas Grid Infrastructure: Techno-Economic Optimization of Operation”. In: *Volume 9: Oil and Gas Applications; Supercritical CO2 Power Cycles; Wind Energy* (June 2015). DOI: 10.1115/gt2015-42229. URL: http://dx.doi.org/10.1115/gt2015-42229.

[57] M. Krogsgaard. Conversation, expert view. July 2022.

[58] Agora Energywende. *The Future Costs of Electricity-Based Synthetic Fuels*. Tech. rep. 133/06-S-2018/EN 09-2018-EN. 2018. URL: https://www.renewableh2.org/wp-content/uploads/2018/11/2018-09-Agora_SynKost_Study_EN_WEB.pdf.

[59] Christoph Rakousky et al. “An analysis of degradation phenomena in polymer electrolyte membrane water electrolysis”. In: *Journal of Power Sources* 326 (Sept. 2016), pp. 120–128. DOI: 10.1016/j.jpowsour.2016.06.082. URL: http://dx.doi.org/10.1016/j.jpowsour.2016.06.082.

[60] energy Industrial Strategy Department for Business. *Hydrogen Production Costs 2021*. Tech. rep. 2021. URL: https://assets.publishing.service.gov.uk/government/uploads/system/uploads/attachment_data/file/1011506/Hydrogen_Production_Costs_2021.pdf.

[61] O. Schmidt et al. “Future cost and performance of water electrolysis: An expert elicitation study”. In: *International Journal of Hydrogen Energy* 42.52 (Dec. 2017), pp. 30470–30492. DOI: 10.1016/j.ijhydene.2017.10.045. URL: http://dx.doi.org/10.1016/j.ijhydene.2017.10.045.

[62] Hans Böhm et al. “Projecting cost development for future large-scale power-to-gas implementations by scaling effects”. In: *Applied Energy* 264 (Apr. 2020), p. 114780. DOI: 10.1016/j.apenergy.2020.114780. URL: http://dx.doi.org/10.1016/j.apenergy.2020.114780.

[63] Yujing Guo et al. “Comparison between hydrogen production by alkaline water electrolysis and hydrogen production by PEM electrolysis”. In: *IOP Conference Series: Earth and Environmental Science* 371.4 (Dec. 2019), p. 042022. DOI: 10.1088/1755-1315/371/4/042022. URL: http://dx.doi.org/10.1088/1755-1315/371/4/042022.

[64] Araceli Martin-Candilejo, David Santillán, and Luis Garrote. “Pump Efficiency Analysis for Proper Energy Assessment in Optimization of Water Supply Systems”. In: *Water* 12.1 (Dec. 2019), p. 132. DOI: 10.3390/w12010132. URL: http://dx.doi.org/10.3390/w12010132.

[65] Paul Webb. *6.3 Density – Introduction to Oceanography*. URL: https://rwu.pressbooks.pub/webboceanography/chapter/6-3-density/.

[66] *Capacitive Deionization (CDI)*. URL: https://www.lenntech.com/processes/capacitive-deionization-cdi-.htm.

[67] Institute for Sustainable Process Technology. *Integration of Hydrohub GigaWatt Electrolysis Facilities in Five Industrial Clusters in The Netherlands*. Tech. rep. 2020. URL: https://ispt.eu/media/Final-report-ISPT-GW-Water-Electrolysis-Project-Integration-in-Five-Industrial-Clusters-Final-Report.pdf.

[68] M Holst et al. *Cost forecast for low-temperature electrolysis - technology driven bottom-up prognosis for PEM and alkaline water electrolysis systems*. Tech. rep. 2021. URL: https://www.ise.fraunhofer.de/content/dam/ise/de/documents/publications/studies/cost-forecast-for-low-temperature-electrolysis.pdf.

[69] Díez et al. *Technical assessment of Hydrogen transport, compression, processing offshore*. Tech. rep. 2020. URL: https://north-sea-energy.eu/static/7ffd23ec69b9d82a7a982b828be04c50/FINAL-NSE3-D3.1-Final-report-technical-assessment-of-Hydrogen-transport-compression-processing-offshore.pdf.

[70] Ian H. Bell et al. “Pure and Pseudo-pure Fluid Thermophysical Property Evaluation and the Open-Source Thermophysical Property Library CoolProp”. In: *Industrial & Engineering Chemistry Research* 53.6 (2014), pp. 2498–2508. DOI: 10.1021/ie4033999. eprint: http://pubs.acs.org/doi/pdf/10.1021/ie4033999. URL: http://pubs.acs.org/doi/abs/10.1021/ie4033999.

[71] *EUR Inflation Calculator - Euro (2018-2022)*. URL: https://www.inflationtool.com/euro?amount=100&year1=2018&year2=2022&period1=6&period2=1&frequency=monthly.

[72] M. Bussemakers. Conversation. 2022.

[73] A Van der Stap and J Hoving. *Substructure Design: Geometry and configuration*. Tech. rep. 2021.

[74] National Renewable Energy Laboratory. *NREL Offshore Balance-of-System Model*. Tech. rep. NREL/TP-6A20-66874. 2017. URL: https://www.nrel.gov/mwg-internal/2535425/progress?id=9yDTylMskCPbjrVyQc4y9__cCNme5xErjig1zVKAZLQ,.

[75] E Craye. *The Sizing and Costing of Hydrogen Pipelines for Offshore Wind Farms*. Tech. rep. 2022.

[76] Jean André et al. “Time development of new hydrogen transmission pipeline networks for France”. In: *International Journal of Hydrogen Energy* 39.20 (July 2014), pp. 10323–10337. DOI: 10.1016/j.ijhydene.2014.04.190. URL: http://dx.doi.org/10.1016/j.ijhydene.2014.04.190.

[77] Dr. Uchenna O. Ajator. “Costing of Oil and Gas Projects for Efficient Management and Sustainability”. In: *IOSR Journal of Environmental Science, Toxicology and Food Technology* 8.12 (2014), pp. 70–84. DOI: 10.9790/2402-081217084. URL: http://dx.doi.org/10.9790/2402-081217084.

[78] M. Fog Thoisen. Mail conversation, expert view. Jan. 2023.

[79] DNV Energy Systems. *Lifetime Extension and Optimal Lifecycle Offshore Wind Turbines*. Tech. rep. 2022. URL: https://www.topsectorenergie.nl/sites/default/files/uploads/20220414_RAP_DNV_Lifetime%5C%20extension%5C%20and%5C%20optimal%5C%20lifecycle%5C%20offshore%5C%20wind%5C%20turbines_LBA_V01.pdf.

[80] IEA. *The cost of capital in clean energy transitions – Analysis*. 2021. URL: https://www.iea.org/articles/the-cost-of-capital-in-clean-energy-transitions.

[81] Dohyung Jang et al. “Techno-economic analysis and Monte Carlo simulation for green hydrogen production using offshore wind power plant”. In: *Energy Conversion and Management* 263 (July 2022), p. 115695. DOI: 10.1016/j.enconman.2022.115695. URL: http://dx.doi.org/10.1016/j.enconman.2022.115695.

[82] Hirokazu Kojima et al. “Influence of renewable energy power fluctuations on water electrolysis for green hydrogen production”. In: *International Journal of Hydrogen Energy* (Nov. 2022). DOI: 10.1016/j.ijhydene.2022.11.018. URL: http://dx.doi.org/10.1016/j.ijhydene.2022.11.018.

[83] Wolfgang Schlez and David Infield. “Horizontal, Two Point Coherence for Separations Greater Than the Measurement Height”. In: *Boundary-Layer Meteorology* 87.3 (June 1998), pp. 459–480. DOI: 10.1023/a:1000997610233. URL: http://dx.doi.org/10.1023/a:1000997610233.

[84] R Bos. *Extreme gusts and their role in wind turbine design*. Tech. rep. 2017. URL: https://doi.org/10.4233/uuid:d6097e3a-%201cdd-4845-a71c-90f469d28b7a.

[85] Claire L. Vincent and Pierre-Julien Trombe. “Forecasting intrahourly variability of wind generation”. In: *Renewable Energy Forecasting* (2017), pp. 219–233. DOI: 10.1016/b978-0-08-100504-0.00008-1. URL: http://dx.doi.org/10.1016/b978-0-08-100504-0.00008-1.

[86] Peter Brugger, Fernando Porté-Agel, and Fernando Porté-Agel. “Field measurements of wake meandering at a utility-scale wind turbine with nacelle-mounted Doppler lidars”. In: *Wind energy science* 7.1 (Feb. 2022), pp. 185–199. DOI: 10.5194/wes-7-185-2022. URL: https://wes.copernicus.org/articles/7/185/2022/wes-7-185-2022.pdf.

[87] Robert Braunbehrens and Antonio Segalini. “A statistical model for wake meandering behind wind turbines”. In: *Journal of Wind Engineering and Industrial Aerodynamics* 193 (Oct. 2019), p. 103954. DOI: 10.1016/j.jweia.2019.103954.

[88] Sara C. Pryor, Rebecca J. Barthelmie, and Tristan J. Shepherd. “Wind power production from very large offshore wind farms”. In: *Joule* 5.10 (Oct. 2021), pp. 2663–2686. DOI: 10.1016/j.joule.2021.09.002. URL: http://dx.doi.org/10.1016/j.joule.2021.09.002.

[89] A G DAVENPORT. “THE RESPONSE OF SLENDER, LINE-LIKE STRUCTURES TO A GUSTY WIND.” In: *Proceedings of the Institution of Civil Engineers* 23.3 (Nov. 1962), pp. 389–408. DOI: 10.1680/iicep.1962.10876. URL: http://dx.doi.org/10.1680/iicep.1962.10876.

[90] Juliaan Bossuyt, Charles Meneveau, and Johan Meyers. “Wind farm power fluctuations and spatial sampling of turbulent boundary layers”. In: *Journal of Fluid Mechanics* 823 (June 2017), pp. 329–344. DOI: 10.1017/jfm.2017.328. URL: http://dx.doi.org/10.1017/jfm.2017.328.

[91] Joaquin Mur-Amada and Jess Salln-Arasanz. “Power Fluctuations in a Wind Farm Compared to a Single Turbine”. In: *From Turbine to Wind Farms - Technical Requirements and Spin-Off Products* (Apr. 2011). DOI: 10.5772/15957. URL: http://dx.doi.org/10.5772/15957.

[92] Jay Apt. “The spectrum of power from wind turbines”. In: *Journal of Power Sources* 169.2 (June 2007), pp. 369–374. DOI: 10.1016/j.jpowsour.2007.02.077. URL: http://dx.doi.org/10.1016/j.jpowsour.2007.02.077.

[93] Þ. Helgason. *System Design and Advisory Control Strategy For an Offshore Stand-Alone Hydrogen-Only Wind Turbine*. Thesis. 2022.

[94] Markus Lerch, Mikel De-Prada-Gil, and Climent Molins. “Collection Grid Optimization of a Floating Offshore Wind Farm Using Particle Swarm Theory”. In: *Journal of Physics: Conference Series* 1356.1 (Oct. 2019), p. 012012. DOI: 10.1088/1742-6596/1356/1/012012. URL: http://dx.doi.org/10.1088/1742-6596/1356/1/012012.

[95] K. Skaug. Expert view. Jan. 2023.

[96] Mathieu Lepot, Jean-Baptiste Aubin, and François Clemens. “Interpolation in Time Series: An Introductive Overview of Existing Methods, Their Performance Criteria and Uncertainty Assessment”. In: *Water* 9.10 (Oct. 2017), p. 796. DOI: 10.3390/w9100796. URL: http://dx.doi.org/10.3390/w9100796.

[97] H. Nyquist. “Certain Topics in Telegraph Transmission Theory”. In: *Transactions of the American Institute of Electrical Engineers* 47.2 (Apr. 1928), pp. 617–644. DOI: 10.1109/t-aiee.1928.5055024. URL: http://dx.doi.org/10.1109/t-aiee.1928.5055024.

[98] Janna Kristina Seifert et al. “Correlations of power output fluctuations in an offshore wind farm using high-resolution SCADA data”. In: *Wind Energy Science* 6.4 (July 2021), pp. 997–1014. DOI: 10.5194/wes-6-997-2021. URL: http://dx.doi.org/10.5194/wes-6-997-2021.

[99] Mahin Basha Syed. “Technologies for renewable hydrogen production”. In: *Bioenergy Resources and Technologies* (2021), pp. 157–198. DOI: 10.1016/b978-0-12-822525-7.00013-5. URL: http://dx.doi.org/10.1016/b978-0-12-822525-7.00013-5.

[100] Christian Schnuelle et al. “Dynamic hydrogen production from PV amp; wind direct electricity supply – Modeling and techno-economic assessment”. In: *International Journal of Hydrogen Energy* 45.55 (Nov. 2020), pp. 29938–29952. DOI: 10.1016/j.ijhydene.2020.08.044.

A

Appendix Techno-economic analysis

A.1. Cost modelling superstructure

The following section presents the relations found and used. The relations are taken from the DNV report unless state otherwise [33]. The topside structure is a steel structure, often consisting of several decks, that supports and houses all the equipment. It also consists of the gratings and claddings. The gratings act as floors, and the claddings act as walls for the rooms. This includes the control rooms and their equipment mass.

A.1.1. Topside primary steel

The mass of the topside steel structure depends on the weight of the equipment for which it is designed, as presented in equation A.1.

$$m_{PS} = k_{PS,1} \cdot m_{Equipment} \tag{A.1}$$

Where $k_{PS,1}$ is primary steel constant. The total topside primary steel CAPEX is determined by multiplying the primary steel mass by the price per fabricated ton primary steel, as presented in equation A.2.

$$C_{PS} = m_{PS} \cdot p_{PS} \tag{A.2}$$

Where p_{PS} is the price per fabricated ton primary steel.

A.1.2. Topside grating

The total area to be grated is related volume of the topside. The topside volume dependent on the installed electrolyser capacity and is estimated according to equation A.3.

$$V_{Topside} = k_{volume,1} \cdot P_e \tag{A.3}$$

Where $k_{volume,1}$ is the volume constant and P_e the installed electrolyser capacity. The grating area is subsequently estimated according to equation A.3.

$$A_{Grating} = k_{Grating,1} \cdot V_{Topside} \tag{A.4}$$

Where $k_{Grating,1}$ is the grating area constant. The CAPEX related to the gratings is determined according to equation A.5.

$$C_{Grating} = A_{Grating} \cdot p_{Grating} \tag{A.5}$$

Where $p_{Grating}$ is the price per square meter grating

A.1.3. Cladding

The mass of the cladding is related to the installed electrolyser capacity, and estimated using equation A.6.

$$m_{cladding} = k_{cladding,1} \cdot P_e \tag{A.6}$$

Where $k_{Cladding,1}$ is the cladding mass constant. The total cladding costs are calculated using equation A.7.

$$C_{Cladding} = m_{Cladding} \cdot p_{Cladding} \tag{A.7}$$

Where $C_{Cladding}$ is the cladding CAPEX and $P_{Cladding}$ the cladding price per ton.

A.1.4. Topside coating

The area to be coated of the topside is dependent on the primary steel mass and the mass of the auxiliary equipment, and estimated according to equation A.8.

$$A_{Coating} = k_{Coating,1} \cdot (m_{PS} + m_{Cladding}) \tag{A.8}$$

Where $k_{Coating,1}$ is the coating area constant. The total coating CAPEX is determined according to equation A.9.

$$C_{Coating} = A_{Coating} \cdot p_{Coating} \tag{A.9}$$

Where $p_{Coating}$ is the coating price per square meter.

A.1.5. Total topside structure

The total CAPEX of the topside structure is determined according to equation A.10.

$$C_{Topsidestructure} = C_{PS} + C_{Grating} + C_{Coating} \tag{A.10}$$

The total topside mass is calculated according to equation A.11.

$$m_{Topside} = m_{PS} + m_{PS} + m_{Equipment} \tag{A.11}$$

Where $C_{Topsidestructure}$ is the total CAPEX of the topside structure.

A.1.6. Data input

This section presents the constants and prices[1] used to determine the weight and costs of the topside structure.

Constant	Value	Unit
$k_{PS,1}$	1.035	ton/ton
p_{PS}	3722	€$/ton$
$k_{Volume,1}$	193.55	m^3/MW
$k_{Grating,1}$	0.11	m^2/m^3
$p_{Grating}$	191	€$/m^2$
$k_{Coating,1}$	12.74	m^2/ton
$p_{Coating}$	128	€/ ton

Table A.1: Topside structure constants and prices

[1] Prices are expressed in January 2022 Euro's. Converted according to: €$_{2018}$ = 1.0635 €$_{2022}$ [71]

A.2. Total CAPEX and OPEX curves

Figure A.1 present the total CAPEX and OPEX curves for the PEME- and AE-based system.

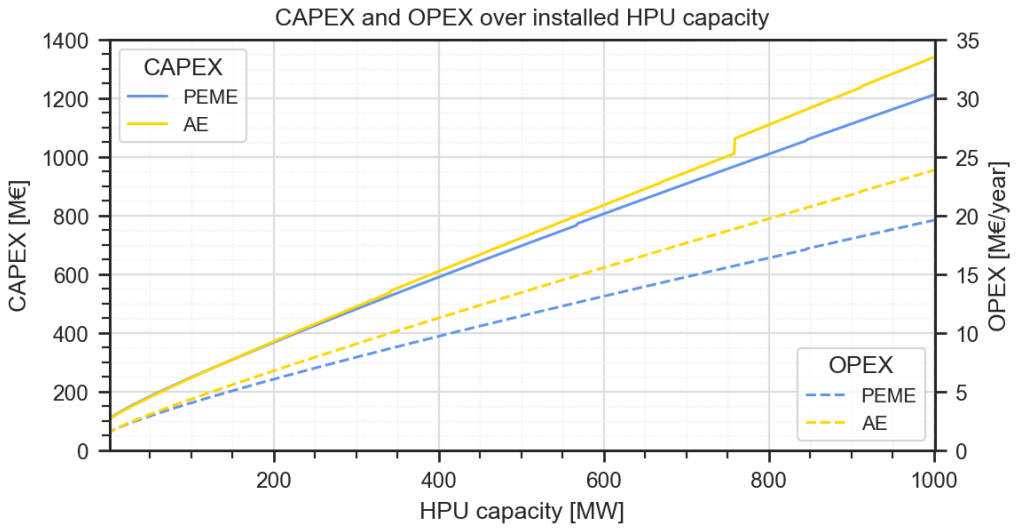

Figure A.1: CAPEX and OPEX for PEME-based and AE-based system

A.3. LCOH curve per technology

Figure A.2 presents the LCOH curve solely for the PEME-based system. The figure shows the LCOH versus both the installed HPU capacity and stack capacity.

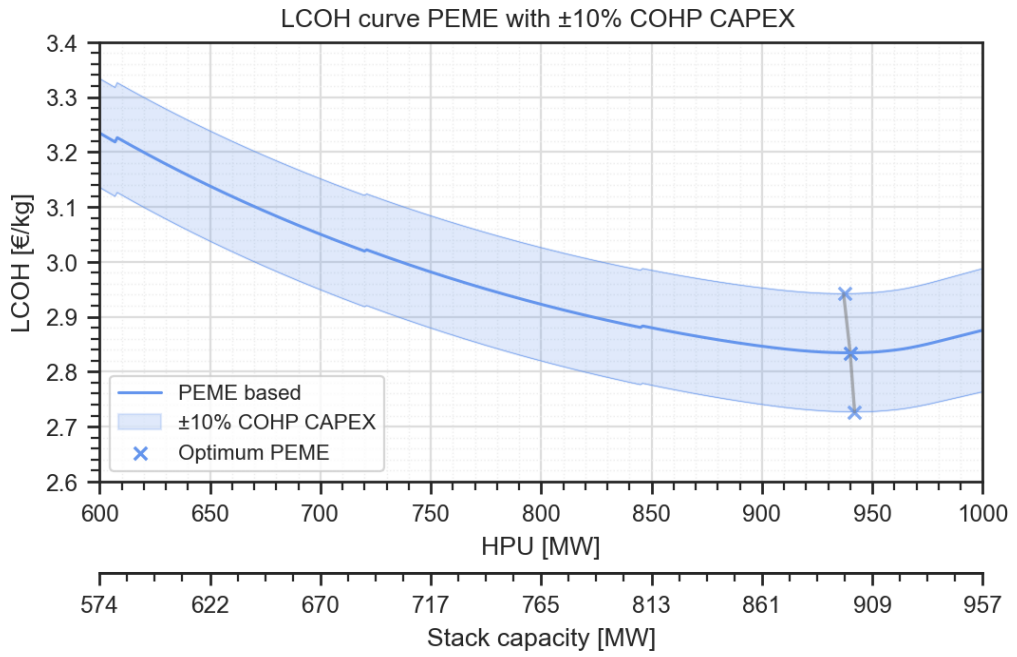

Figure A.2: LCOH for the PEME-based system.

The trend of the LCOH curve for the PEME-based system demonstrates a downward slope until reaching an optimal installed HPU capacity of 940 MW, after which it rises again, indicating the optimal

installed HPU capacity when the lowest LCOH is the objective. This corresponds to an installed stack capacity of 899 MW. Here, an LCOH of 2.84 €/kg is found. The small jumps in the PEME-based LCOH curve are the result of the jumps in the CAPEX curve. These were caused by the increasing required pipeline diameter as a result of the increasing hydrogen mass flow. The difference between the HPU capacity and the stack capacity is attributed to the electrical losses and power consumption of auxiliary equipment.

Figure A.3 presents the LCOH curve solely for the AE-based system. Again, showing both the LCOH versus the installed HPU capacity and stack capacity.

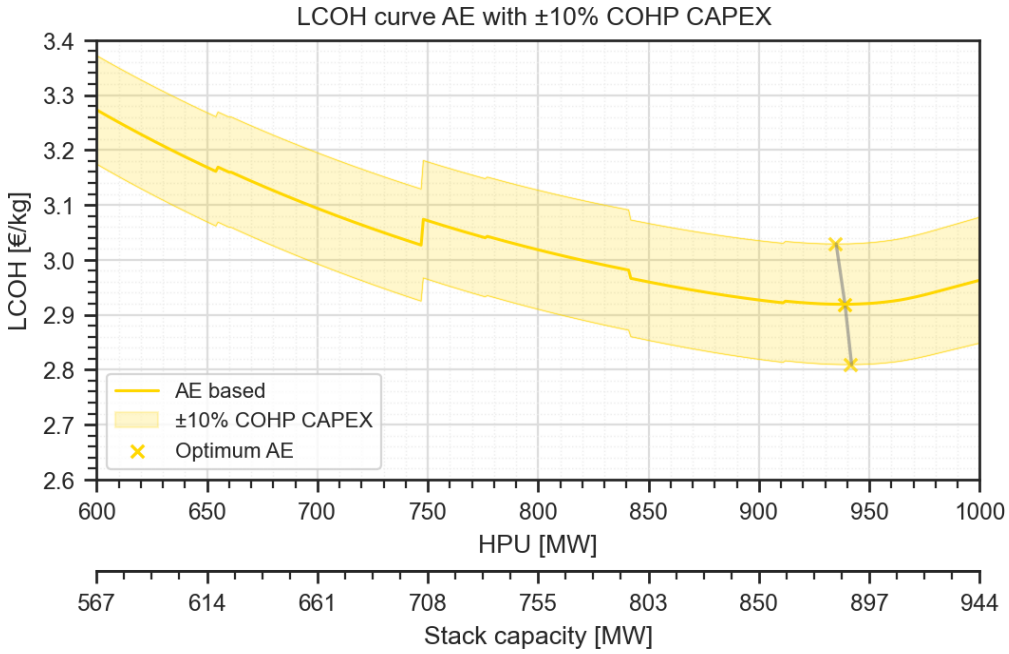

Figure A.3: LCOH curve for the AE-based system.

The trend of the LCOH curve for the AE-based system demonstrates overall a similar shape as the LCOH curve of the AE-based system. The optimal HPU capacity when the objective is to find the lowest LCOH occurs at an HPU capacity of 939 MW This corresponds to an installed stack capacity of 886 MW. Here, an LCOH of 2.93 €/kg is obtained. The lower optimal installed HPU capacity is in line with previously made statements related to the negative effect of COHP CAPEX on the optimal HPU capacity.

For the AE-based system, more jumps are observed in the LCOH curve, both upwards and downwards. The smaller jumps are the result of the increasing required pipeline diameter causing an increase in the CAPEX curve. The larger jump upwards is the result of the different required installation method, increasing the CAPEX curve significantly [Figure 4.6].

The only decrease in LCOH is observed at an installed HPU capacity of 841 MW. This decrease in LCOH is dedicated to the number of stack replacements required. The increasing HPU capacity decreases the number of operational hours of the stacks from 841 MW onwards, only a single stack replacement is required [Figure 4.5]. Since replacing the stacks is a cost-intensive procedure, a decrease in the number of replacements has a positive effect on the LCOH curve. The difference between the HPU capacity and the stack capacity is attributed to the electrical losses and power consumption of auxiliary equipment.

A.4. Monte-Carlo method

Table A.2 present the input parameters covered by the uncertainty analysis of the Monte Carlo method.

Performance	CAPEX	OPEX	Mass	Others
Stack efficiency	OWF	OWF	Stacks	WACC
Stack lifetime	Stacks	Stacks	Electrical	Project lifetime
Stack degradation	Electrical	Electrical	Compressors	Water depth
Availability	Gas conditioning	Gas conditioning	Superstructure	In-deck height
IAC losses	Water treatment	Water treatment	Substructure	
Electrical losses	Compressors	Compressors		
Gas conditioning	Superstructure	Superstructure		
Compressor efficiency	Substructure	Substructure		
RO Recovery factor	Foundation	Foundation		
DI Recovery factor	Transmission	Transmission		
RO consumption	Transport			
DI consumption	Installation			
Pump efficiency	Commissioning			
OWF initial availability	Decommissioning			
OWF availability loss	EPCm			
OWF degradation	Owner costs			
	Contingencies			

Table A.2: Input parameters or categories covered by the Monte-Carlo uncertainty analysis

B

Times series appendix

B.1. Original lay-out offshore wind farm

Figure B.1 presents the original lay-out of the offshore wind farm.

Figure B.1: Original layout of the offshore wind farm.[*Confidential*]

B.2. Distance inter-array cable sections

Table B.1 present the distances between the different wind turbines.

Section	Distance [m]	Section	Distance [m]

Table B.1: Distance per cable section. [*Confidential*]

B.3. Output per wind turbine

Figure B.2, Figure B.3, and Figure B.4 present the standard deviation, maximum fluctuation and number of switches per wind turbine of the wind farm.

Figure B.2: Standard deviation of power fluctuation over 5 minutes per WTG.[*Confidential*]

Figure B.3: Maximum power fluctuation over 5 minutes per WTG.[*Confidential*]

Figure B.4: Number of switches of operational state per WTG.[*Confidential*]